The Dissertation Committee for Karthik Raghavan Certifies that this is the approved version of the following dissertation:

Design of a wireless bio-telemetric device for measurement of left ventricular pressure-volume loops using the admittance technique in conscious, ambulatory rats

Committee:

John A. Pearce, Supervisor

Jonathan W. Valvano, Co - supervisor

Marc D. Feldman

Ranjit Gharpurey

H Grady Rylander III

Design of a wireless bio-telemetric device for measurement of left ventricular pressure-volume loops using the admittance technique in conscious, ambulatory rats

by

Karthik Raghavan, B.E. ; M.S.E.

Dissertation

Presented to the Faculty of the Graduate School of

The University of Texas at Austin

in Partial Fulfillment

of the Requirements

for the Degree of

Doctor of Philosophy

The University of Texas at Austin

May 2009

Dedication

To my dad and my mom for their never-ending support

and

To all my family members and friends for their help and encouragement.

Acknowledgements

I was widely criticized for my extremely long acknowledgement section in my master's thesis that covered only 2 years of my life at UT, Austin. Now, having spent a total of nearly 6 years here for my PhD studies, that list is only going to get bigger.

First, I was extremely grateful to have three of the finest professors as my supervisors. Each of them had contrasting styles towards approaching problems. Together, they made the perfect research group.

Dr. John A. Pearce was my principal supervisor. His main interests involve instrumentation, analog circuit design and electromagnetics. He is an extremely insightful person with great ideas at all the times. I was always able to get concise and extremely accurate answers to most of my problems when I approached him. At the same time, he had a caring nature which cannot be described in words. I also got an opportunity to be a TA for him for a couple of classes including the Circuit Theory course. Always a great person to work with.

Dr. Jonathan W. Valvano was my co-supervisor. His main interests involve instrumentation and microcontroller programming. He is a very hands-on person giving very practical solutions to somewhat sticky problems. He has this ability to boost your spirits when you are down and out like no other professor I know. I have also heard that he was a great teacher and extremely patient with students' problems. This was evident from the extremely long lines of students outside of his office at most of the times.

Dr. Marc D. Feldman is always fun to be around. He is extremely resourceful and knowledgeable. However, when you get a chance to be around Dr. Feldman, you can never make out the extreme depths of knowledge this cardiologist possesses. He is

always behind your back driving you to write a paper, or a grant, or perform an experiment. He tends to keep you motivated at all times. We had some extremely good experiments down in his animal studies lab at The University of Texas Health Sciences Center at San Antonio.

Apart from this great group of professors, I was blessed with the most awesome research mates: Anil G.T. Kottam, John E. Porterfield and Erik R. Larson. Again, a group of fine gentlemen with a great knowledge pool amongst them. Anil and Erik are the analog – gurus, with great experience in building instruments, circuits and pretty much anything analog. If I had any question during the analog design process, I could just reach back and get help almost immediately. John completed the package with extreme intuition in software and related topics. Not only was this group as extremely knowledgeable and competent, but also was the most fun guys to spend your time with regular activities including but not limited to poker nights, football games, Friday lunches etc., etc.,

I would like to give special thanks to Mr. Daniel Escobedo, our chief animal surgeon at University of Texas Health Sciences Center at San Antonio. His dexterity and skill with the small animal surgery is unmatched. At many times, I was left awed by the outcome of a particular procedure or surgery. Without Danny, it would have been impossible to perform any experiment, especially, the chronic rat experiments, where the catheter had to be placed into the LV with minimal surgery and the rat had to live the entire duration of the experiment. He was also a great guy to hang out with. We had many energetic football discussions.

I would like to thank James (Travis) Jenkins for his help with the rat experiments. An extremely resourceful guy and always ready to help me out when I needed it the most. He had to stay up for the entire night for 2 out of the 6 chronic rat experiments.

I would also like to thank Rudy J. Trevino for his help with the mouse studies. A cool guy and extremely helpful and cheerful at all times.

I would like to thank my committee members Dr. Grady Rylander III and Dr. Ranjit Gharpurey for accepting to be in my PhD committee and with the help I received over the years. I also had the privilege of taking 2 courses with Dr. Rylander, who is not only a great teacher but is also a practicing doctor.

I would like to extend my thanks to Dr. David Brown, Dr. Benito Fernandez, Dr. Lizy John, and Dr. Brian Evans for providing me with TA jobs at critical junctions during my graduate studies. I enjoyed teaching and loved the interaction with both the professors and the students.

A great round of applause goes to the truly great and awesome ECE support staff: Ms. Melanie Gullick, Ms. Michelle Belisle, Mr. Perry Durkee, Ms. Lupe Perez, Ms. Diana Vega, Ms. Diana Perez, Ms. Carole Bearden, Mr. Steven Moore, Mr. Kendrick Weld, Mr. Paul Landers, Mr. Daryl Goodnight, Ms. Mary Matejka, Mr. Fred Kirby and Mr. Merydith Turner. It is hard to describe the help and encouragement I received from each one of them.

I have a long list of friends here to thank starting from the group in Austin: Nachiket Kharalkar, Jignesh Shah, John Slater, Chris Flesher, Geethapriya Raghavan, Smriti Ramakrishnan, Sowmya Ramachandran, Meenakshi Venkataraman, Sathish Jothikumar, Larbi Boughaleb, Eric Lasmana, Robin Tsang, Srinivasan Venkataraman *et al*. Then, the group in San Diego: Muralidharan Murugan, Ramkumar Nagarajan, Swaminathan Ganesan. All of these friends played a crucial part in my graduate school. Many thanks to mentors at Qualcomm, namely, Mr. Junyan Bei, Mr. Michael Castelloe and Mr. Kuntal Sampat for their constant support.

Finally, last but definitely not the least, my dad: Mr. Venkataraman Raghavan and my mom Mrs. Hema Raghavan. Without them, none of this would have been possible. A never ending source of motivation, encouragement and most importantly love. I can never write enough to bring out the total and unselfish help and love that my parents have provided throughout my life, especially, during my graduate school. I am extremely fortunate to have them as my parents. Same goes to my extended family here in San Diego: Devan Nguyen, mom Tam and Viet Tran for all their support, love and providing me a home away from home.

Design of a wireless bio-telemetric device for measurement of left ventricular pressure-volume loops using the admittance technique in conscious, ambulatory rats

Publication No._____

Karthik Raghavan, PhD

The University of Texas at Austin, 2009

Supervisor: John A. Pearce

Left ventricular (LV) volume analysis in small animals has proven difficult because of the small size of the hearts and the rapid heart rate. Furthermore, there is a substantial contribution to the signal from both the blood as well as the muscle. Admittance - based measurement techniques has been proven effective in eliminating the muscular component and estimating the blood component accurately. The key factor that makes this measurement effective is the fact that the measurement is made in the complex plane, which measures both the magnitude as well as the phase of the complex phasor. This dissertation presents the design of a wireless telemetric device that measures impedance magnitude and phase measurements along with pressure from conscious, ambulatory rats. Using this impedance data along with other calibration data such as blood resistivity, stroke volume etc., volume is determined.

Table of Contents

List of Tables

List of Figures

CHAPTER 1

Introduction

1.1 MOTIVATION

Simultaneous measurement of left ventricular (LV) pressure and volume (P-V) yields a quantitative assessment of the hemodynamic status of the heart. A real time technique that measures the contractility of the heart would be valuable for evaluation of new drugs and gene therapy. [1] The LV P-V relationship generated on a beat-by-beat basis during transient occlusion of the inferior vena cava allows hemodynamic characterization of LV systolic and diastolic functions independent of loading conditions. [2]

The main challenges that are posed in the accurate estimation of volume in small animals, such as mice and rats, are their small heart sizes and their rapid heart rates. In addition, anesthesia has adverse effects on the hemodynamic of small animals. The benefits of chronic studies are that they involve minimal anesthesia (beginning of the experiment). They would also be useful for long term studies on drug evaluation and disease progression.

1.1.1 An application of P-V loop analysis – Early detection of CHF

P-V loop analysis has a variety of applications in small and large animals as well as in humans. An example application of P-V loop analysis used in a clinical setting is the early detection of heart failure.

Amidst other applications, P-V loop analysis could be used for the early detection of heart failure (HF). As of 2004, 5.2 million Americans suffer from heart failure with 550,000 new cases reported every year. The estimated direct and indirect cost of heart failure in the United States for 2007 is $33.2 billion. [3]

Heart failure (HF) is a chronic condition in which the heart muscle gets progressively weaker and is unable to pump effectively to meet the body's need for blood and oxygen. It usually leads to an enlarged heart and often causes shortness of breath, tiredness and swelling of the legs and feet. The primary causes for heart failure may be due to coronary artery disease (clogged arteries), myocardial infarction (heart attack), hypertension (high blood pressure), abnormal heart valves (valvular disease), cardiomyopathy (heart muscle disease), and congenital heart disease (heart defects from birth).

Congestive heart failure (CHF) is similar to HF but with additional features of circulatory congestion such as jugular venous distention, rales (an abnormal sound heard accompanying the normal respiratory sounds on auscultation of the chest), peripheral edema, and ascites (accumulation of serous fluid in the spaces between tissues and organs in the cavity of the abdomen).

Two different kinds of CHF exist with varying symptoms. In systolic dysfunction, the ventricles are enlarged, and thus when they pump blood, it is less than 40 to 50% of the volume of a normal heart output volume. It manifests itself as an increase in the end-systolic volume and a reduction in the stroke volume. The diastolic portion of the P-V loop has simply shifted to the right. Figure 1-1 shows an example P-V loop of systolic failure. [4] The other kind of CHF is diastolic failure, which refers to a thickened, small – cavity ventricle in which the filling is limited. This condition often coexists with poorly controlled systemic hypertension and systolic hypertension found commonly in the

elderly. The LVEDP (left ventricular end diastolic pressure) is the same as the normal heart but there is an upward shift of the LV diastolic pressure-volume relationship, which indicates a decrease in LV diastolic distensibility such that a higher diastolic pressure is required to achieve the same diastolic volume. Figure 1-2 shows an example P-V loop of diastolic failure. [4]

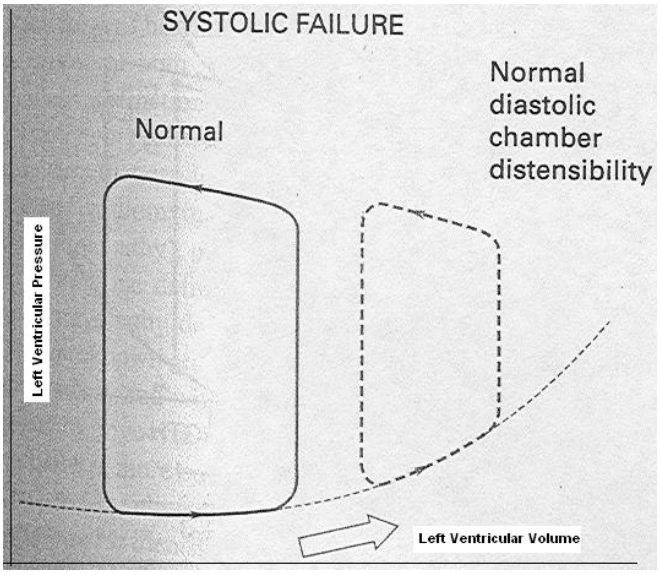

Figure 1-1: P – V loop comparison of a normal heart and a systolic failure heart

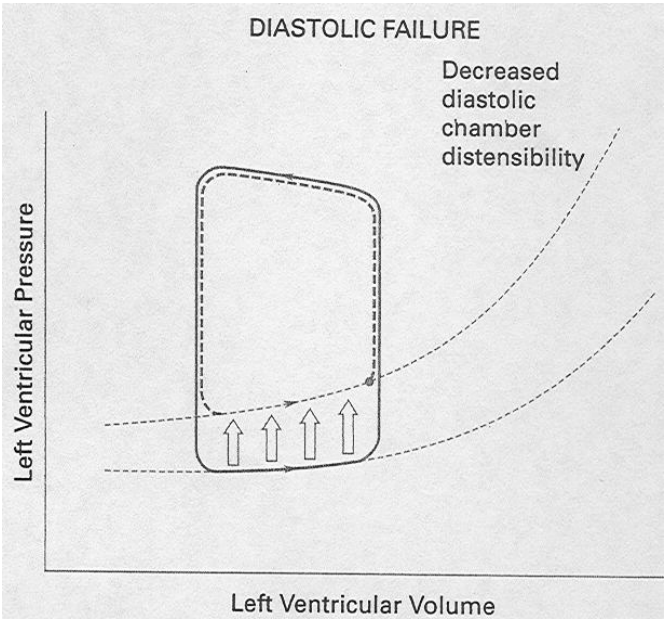

Figure 1-2: P – V loop comparison of a normal heart and a diastolic failure heart

From the above motivation, it can be seen that that real-time P-V loops are a vital tool for a cardiologist.

1.2 BACKGROUND

The tetrapolar conductance - catheter technique has been used to estimate LV volume for almost 27 years. This technique involves the introduction of a four-electrode catheter inside the LV of the heart. Experiments have this catheter introduces via the apex of the heart, in open-chest experiments or via the carotid artery and the aorta into the LV, in closed-chest experiments. Fig. 1-3 shows an example of a tetrapolar catheter placed in the LV via the apex of the heart.

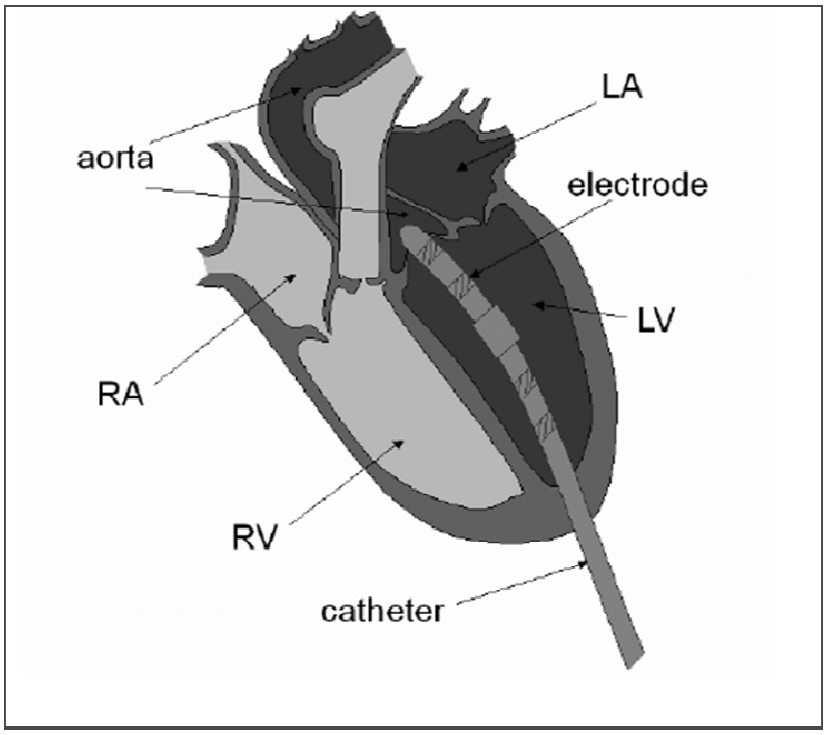

Figure 1-3: Tetrapolar catheter placed in the LV of the heart

When the outer two electrodes are stimulated using a constant AC current source, the voltage sensed by the inner two electrodes would depend on the conductance of the medium present. This conductance would then be mapped to LV volume.

However, the field lines stretch between the outer two electrodes pass through the blood and the surrounding myocardium. Therefore, the voltage signal that is sensed is a combination of the contributions due to the myocardium and the blood itself. However, only the blood contribution is useful for the determination of LV volume. The myocardial contribution needs to be determined and removed from this combined signal.

In 1981, Baan *et al*. [8] derived the original conductance (G)-volume equation (Equation 1). They, however, assumed that the myocardial contribution is a constant and can be lumped as one parameter – the parallel conductance (G_p) (S) derived from other

techniques such as hypertonic saline method. α was a stroke – volume gain calibration constant, dependent on the field geometry. They assumed it to be a constant (α = 1), ρ is the resistivity of blood (Ω-m) and L (m) was the length between the voltage sensing electrodes in the tetrapolar catheter.

$$Volume = \frac{\rho L^2}{\alpha}(G - Gp) \qquad (1)$$

Investigators have applied the hypertonic saline technique developed for larger mammals to determine a single value of steady state parallel (cardiac muscle) conductance and used it for the derivation of absolute LV volume [17]. The saline technique, however, is problematic in small animals such as mice and rats since administration of even small volumes of hypertonic saline significantly alters both blood resistivity and hemodynamics (i.e., blood volume) [13], violating the framework of the governing assumptions [14]. Simultaneous measurement at two frequencies combined with the hypertonic saline technique has been proposed by other investigators [18, 19, 20]. However, in all cases these methods determine only a single value of steady state parallel conductance. It is evident that as the heart beats, the myocardium gets closer to the catheter during end-systole and further away from the catheter during end-diastole. Therefore, the assumption that the myocardial contribution can be lumped as one parallel conductance parameter is incorrect. This leads us to the admittance technique.

Briefly, the admittance technique includes time varying contribution from the blood and the myocardium. Fig. 1-4 is an illustrative example of the electrical model of the blood and the LV myocardium.

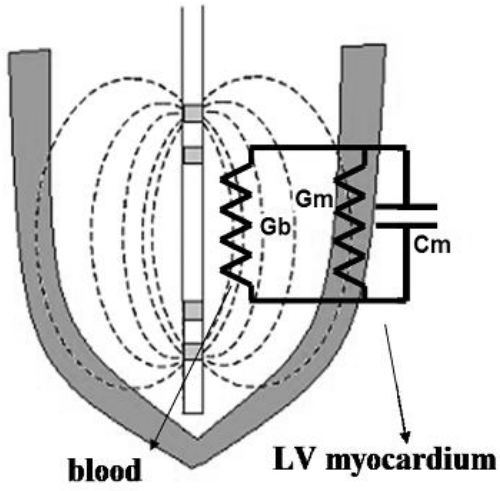

Figure 1-4: Electrical property of the blood and the LV myocardium

In Fig. 1-4, it can be seen that, under homogenous conditions, the blood can be assumed to be purely conductive (modeled as a resistor) while the surrounding myocardium can be modeled as a parallel combination of resistor and a capacitor. This yields an admittance equation (Equation 2).

$$Y_{meas} = Y_b + Y_m = G_b + G_m + j\omega C_m \qquad (2)$$

Where Y_b is the admittance of the blood (S), Y_m is the admittance of the myocardium (S), Y_{meas} is the combined measured admittance (S), G_b is the conductance of blood (S), G_m is the conductance of the myocardium (S) and C_m is the capacitance of the myocardium (F).

Fig. 1-5 and Fig. 1-6 further illustrate this point by representing the admittance as a triangle in the complex plane. It can be seen that the contributions due to the blood and the myocardium are continually changing during the course of a heart cycle. Also shown are sample Admittance magnitude (X-axis) vs. pressure (Y-axis) and Admittance phase (X-axis) vs. pressure (Y-axis) plots, obtained from a murine experiment.

Thus, measuring the magnitude and the phase is critical for estimation of the admittance accurately. When the measurement is made *in vivo*, the catheter contribution is also added to this combined admittance signal caused due to inter-wire catheter capacitance. Thus, equation 2 modifies into equation 3.

$$Y_{meas} = Y_b + Y_m + Y_{catheter} = G_b + G_m + j\omega C_m + j\omega C_{catheter} \quad (3)$$

The catheter contribution could be estimated using a saline calibration technique, which involves estimating the magnitude and phase contributions when a catheter is immersed in vials of saline solutions of different conductivities. Since, the saline itself does not contribute to the phase; the entire imaginary component arises from the catheter.

The myocardial contribution is estimated using a separate epicardial probe experiment. This is explained in detail in Chapter 3.

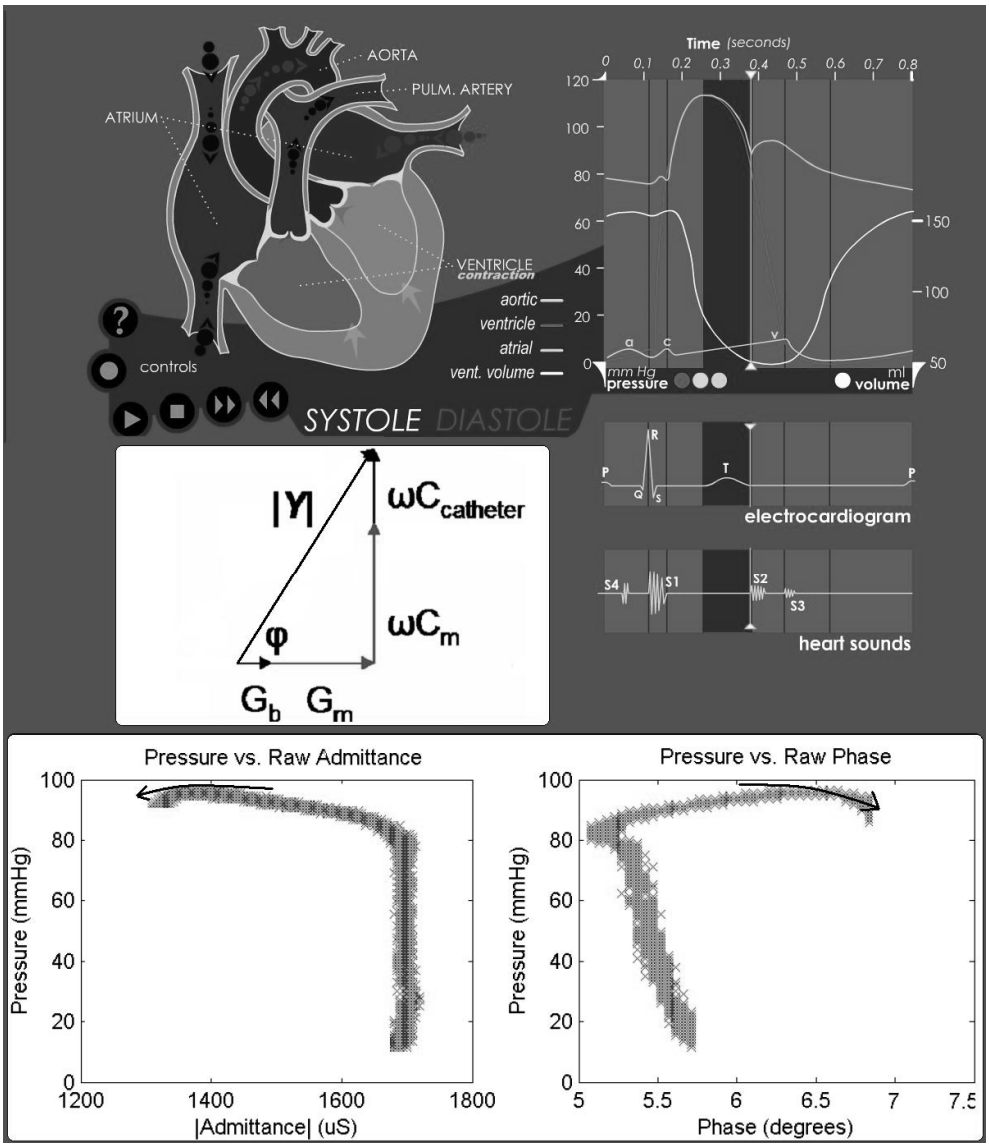

Figure 1-5: Admittance triangle, Pressure-Magnitude and Pressure-Phase plots at end-systole.

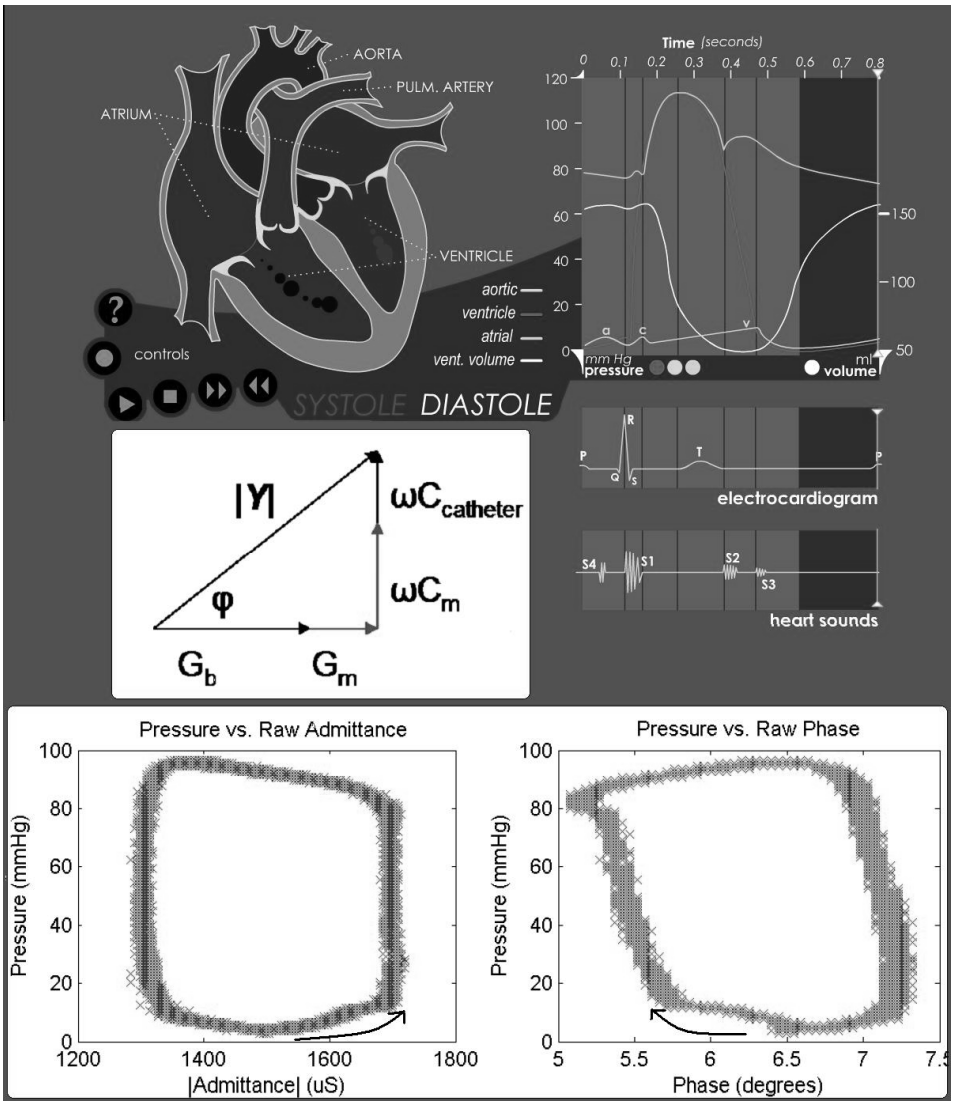

Figure 1-6: Admittance triangle, Pressure-Magnitude and Pressure-Phase plots at end-diastole.

The other limitation of Baan's equation is the static α term. As the heart beats, the electric field lines are modified as the myocardium gets closer and further away from the catheter. In order to include a dynamically changing α term, Baan's original equation was then modified by Wei *et al.* [2]

$$Vol(t) = \frac{1}{\alpha(G_B)} \rho L^2 \cdot G_B \qquad (2)$$

$$\alpha(G_B) = 1 - \frac{G_B}{\gamma} \qquad (3)$$

Where γ is a constant described as

$$\gamma = \frac{-b \pm \sqrt{b^2 - 4ac}}{2a}$$, where $a = SV - \rho L^2 (G_{B-ED} - G_{B-ES})$, $b = -SV \cdot (G_{B-ED} + G_{B-ES})$, $c = SV \cdot G_{B-ED} \cdot G_{B-ES}$. (4)

The larger positive solution for γ is used in all calculations. $G_{B\text{-}ED}$ is the steady state end – diastolic conductance (S), $G_{B\text{-}ES}$ is the steady state end – systolic conductance (S), and SV is the stroke volume (m^3) obtained by an independent method such as a flow meter or 2-D echo. γ is a constant, while $\alpha(G_B)$ is dependent on G_B, which changes as the heart beats, contrary to the constant α in Baan's equation. [7]

Thus, when admittance equations are used in conjunction with Wei's equation, the benefits of both dynamically changing α (t) and myocardial contribution Gp (t) can be obtained, thus, leading to a better estimate of LV volume.

1.3 PREVIOUS WORK – CHRONIC STUDIES

In their experiment, Uemura *et al*. [5] designed a self-calibrating telemetry system for LV P-V loops in conscious rats. They, however, used a dual – frequency (2 and 20 kHz) method for obtaining the parallel conductance (myocardial contribution). However, it has been shown by a study conducted by our research group [6] that the myocardial electrical permittivity (ε_r) estimated from dual – frequency magnitude only measurements

can cause a large source of uncertainty at low frequencies arising from the subtraction of large numbers. Instead, a time varying myocardial contribution can be estimated during the experiment using both the magnitude and phase information using the admittance technique.

They (Uemura *et al*.) also assumed that the calibration factor (α) in Baan's equation to be equal to 1. However, in another study performed by our research group, it has been shown that this calibration factor (α), in fact, is time varying and is dynamically changing as the heart beats and the moving wall changes the shape of the electric field. [7]. This point has been highlighted in the "Limitations" section of their paper.

This dissertation pioneers a wireless telemetric backpack device that measures both magnitude and phase of impedance, thus, obtaining admittance derived LV volume *in vivo* from conscious ambulatory rats. Measurement of both magnitude and phase has been included in the circuitry, all performed at a single frequency. Thus, this eliminates the need for additional circuitry for two different frequencies. In addition, due to the nature of complex plane measurements, we obtain a continuous measurement of a time-varying myocardial contribution (G_p (t)). This method also enjoys the benefits of time-varying calibration factor (α (t)) by application of Wei's equation. [2, 7].

1.4 OBJECTIVE – CHRONIC STUDY

Obtain pressure and admittance derived volume from conscious, ambulatory rats for a period of at least 24 hours.

Sub Objectives – Acute Studies:

1) Obtain electrical properties of the myocardium;

2) Validate closed chest (CC) and open chest (OC) admittance derived volume vs. volume standard using CC 2-D echo and OC 2-D echo respectively;

3) Compare OC echo SV vs. OC SV flow meter standard.

4) Compare and contrast CC admittance derived volumes with established techniques such as cuvette volume and hypertonic saline methods.

5) Prove that admittance scales from mice to rats.

Specific Aim 1: Design and build instrumentation capable of measuring impedance magnitude, phase and pressure with low power and low area; Instrument should be interfacable with a tetrapolar LV catheter.

Specific Aim 2: Design and build a backpack complete with above low power instrument, low power microcontroller, low power transmitter and lithium ion cell. Measure, sample and transmit data wirelessly to a receiver nearby. Receiver collects data and post-processes it to obtain pressure, admittance magnitude and phase data, which will later be converted to pressure-volume loops. The backpack must sample at a sampling frequency of fs=100 Hz and transmit at least 5 heart cycles of data every 2 minutes. The battery must last at least 24 hours.

Specific Aim 3: Perform chronic LV P-V studies on rats. Rats must be concious and freely moving in a cage. Rats should have the tetrapolar LV catheter surgically placed into their LV and must be devoid of anesthesia (fully conscious) during the experiment.

CHAPTER 2

Design of instrumentation for LV catheter and epicardial surface probe measurements

2.1 INTRODUCTION

Two different measurement techniques that involve complex measurement (both magnitude and phase) of the admittance were designed and built: the "digital" and "analog" approaches to distinguish the two admittance measurement techniques.

2.2 ADMITTANCE MAGNITUDE AND PHASE MEASUREMENT BY THE DIGITAL METHOD:

A function generator board (Data Translation, Inc., Marlboro, MA) was used to produce sinusoidal voltages at the desired excitation frequency. The function generator output was converted into a current signal (10 μA rms) that was applied to the two outer electrodes, 1 and 4 of the LV catheter / surface probe (depending on the experiment). The instantaneous voltage signal between the inner electrodes, 2 and 3 was: 1) amplified with an instrumentation amplifier (AD624, Analog Devices, Norwood, MA), 2) rectified and inverted with a divider chip (MPY100, Texas Instruments, Inc., Dallas, TX) and 3) scaled to + 5V to represent the conductance signal over the range of expected values. The output was sampled at a sampling rate of 1 kHz using Powerlab (AD Instruments Pty Ltd., Bella Vista, NSW, Australia) data acquisition hardware and analyzed using Chart Acquisition Software (AD Instruments Pty Ltd., Bella Vista, NSW, Australia).

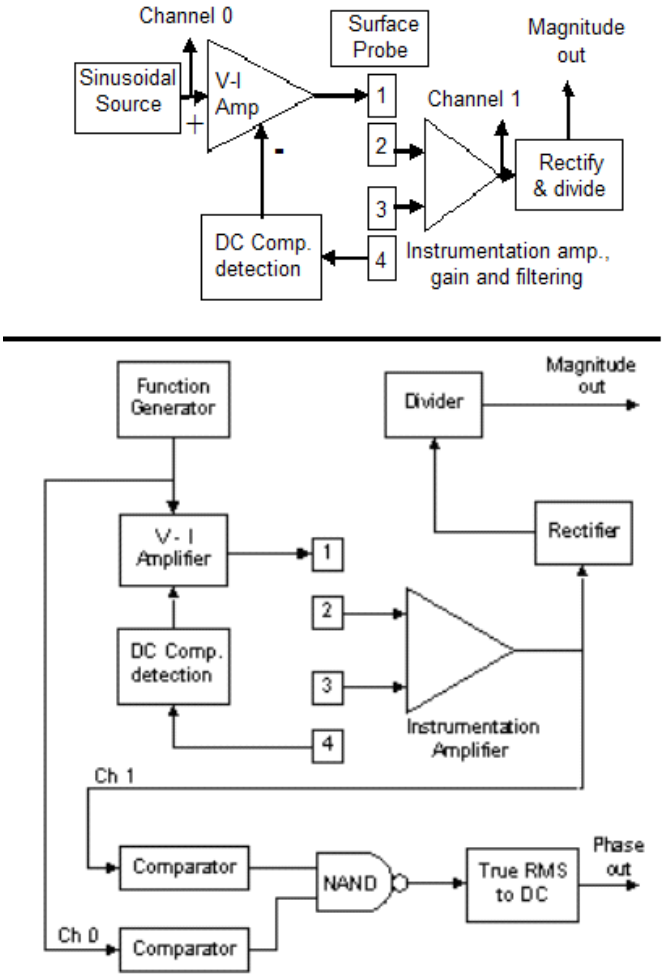

Figure. 2-1-a (Top figure): Block diagram of instrumentation used for admittance measurements. The magnitude output is the rectified DC amplitude signal. Figure. 2-1-b (Bottom figure): Block diagram of instrumentation used for complex plane (magnitude and phase) admittance measurements (analog method) [36, 37].

2.3 ADMITTANCE MAGNITUDE AND PHASE MEASUREMENT BY THE ANALOG METHOD:

The "analog" technique measures admittance magnitude and phase in hardware. This instrument is described by Kottam *et al*. elsewhere [37] and Fig. 2-1-b is a block diagram for this instrument. The phase difference is determined using the reference voltage signal and the filtered output voltage signal. These signals are converted to square

waves and applied through NAND logic to generate pulses whose duty cycle varies according to the phase difference between the signals. The relative duty cycle is converted to a DC signal using a true RMS detector [37]. This instrument has a sensitivity of 100 mV/degree for the phase measurement.

Simultaneous admittance magnitude and phase measurements were made using this device in real-time. The outputs were sampled at a sampling rate of 1 kHz and acquired using Powerlab.

CHAPTER 3

Study of frequency – dependent properties of murine myocardium

3.1 INTRODUCTION

In LV catheter based measurements, the signal obtained is a combination of the contributions from the blood and the surrounding myocardium. This necessitates the need for estimation of myocardial electrical properties so that the signal contribution of the myocardium can be determined and removed from the combined signal, thus, yielding only the blood contribution.

This chapter concerns with the *in vivo* epicardial surface probe measurements of electrical properties in murine myocardium using two different techniques (a digital and an analog approach). These methods exploit the capacitive properties of the myocardium. The instrumentation design has been described in Chapter 2.

Measurements of the permittivity of muscle by Gabriel *et al*. [21, 22] suggest that the relative permittivity of cardiac muscle exceeds 15,000 at 20 kHz. The hypothesis is that the electric permittivity of muscle *in vivo* is high enough that the admittance in the LV at frequencies in this range can be used to identify and separate the cardiac muscle component from the combined admittance measurement.

Equation 2 from Chapter 1 introduces the admittance technique used in LV volume measurement. In this equation, the C_m is the myocardial capacitance (F) and G_m is the myocardial conductance (S).

For any electric field spatial distribution, E, in a homogeneous medium:

$$G = \frac{I}{V} = \sigma \frac{\iint E \bullet dA}{-\int E \bullet dl} = \sigma F \qquad (1\text{-a})$$

$$C = \frac{Q}{V} = \varepsilon \frac{\iint E \bullet dA}{-\int E \bullet dl} = \varepsilon F \qquad (1\text{-b})$$

Where: I = current (A), V = potential (V), σ = electrical conductivity (S/m), Q = charge (C), ε = electric permittivity (F/m), and F is the electric field form factor, or "cell constant", common to both relations (m). The symmetry in the relationships of equations (1-a) and (1-b) leads to the familiar "conductance-capacitance" analogy. The symmetry is also the feature that allows identification and elimination of the cardiac muscle from the combined admittance signal: if C_m is measured, then G_m can be calculated:

$$G_m = C_m \frac{\sigma_m}{\varepsilon_m} \qquad (1\text{-c})$$

An accurate value for the σ_m/ε_m ratio is required to apply this new method for eliminating the parallel admittance of cardiac muscle.

Complex admittivity (ψ) has been used in impedance tomography research [31, 32] and is the formulation of choice over complex resistivity.

Equation 2 from Chapter 1 describes the admittance relationship when a catheter is placed within the LV of the heart. This relationship involves contributions from both the blood and the myocardium. However, this equation modifies into a simpler form when a surface probe is placed on the epicardium to measure the properties of the myocardium alone.

$$Y_m = G_m + j\omega C_m \qquad (2\text{-a})$$

Thus, the measured myocardial admittivity ψ_m (S/m) is:

$$\psi_m = \frac{Y_m}{F} = \frac{G_m + j\omega C_m}{F} = \sigma_m + j\omega\varepsilon_m \qquad (2\text{-b})$$

Where Y_m is the admittance of the myocardium (S), F is the cell constant described in equations (1-a) and (1-b). This definition for admittivity is clearly harmonious with Ampere's Law in point form:

$$\nabla \times \boldsymbol{H} = \boldsymbol{J} + j\omega\boldsymbol{D} = (\sigma + j\omega\varepsilon)\boldsymbol{E} = \psi\boldsymbol{E} \qquad (3)$$

3.2 METHODS

In this study, the electrical properties of the murine myocardium (permittivity, ε_m and conductivity, σ_m) are measured in order to estimate and eliminate the myocardial contribution (Y_m, Equation 3-a) from the combined contribution (Y_{meas}, Equation 1, Chapter 1) in the LV, thus, yielding the blood contribution alone in real time throughout the cardiac cycle.

3.2.1 Epicardial Surface Probe

A miniature tetrapolar surface probe was applied to the epicardial surface of the beating murine heart *in vivo* [Fig. 3-1]. It was custom fabricated by The University of Texas Health Science Center at San Antonio (UTHSCSA), San Antonio, TX. The probe contains four parallel platinum electrodes aligned with an intra-electrode spacing of 0.25,

0.4, and 0.25 mm between electrodes 1 and 2, 2 and 3, and 3 and 4, respectively. In the standard tetrapolar technique electrodes 1 and 4 are driven with a current source and electrodes 2 and 3 are used for potential measurement at negligible current (due to the high input impedance of the voltage sensing differential amplifier). The tetrapolar method is thus essentially insensitive to the series electrode-electrolyte interface impedance of the measurement electrodes.

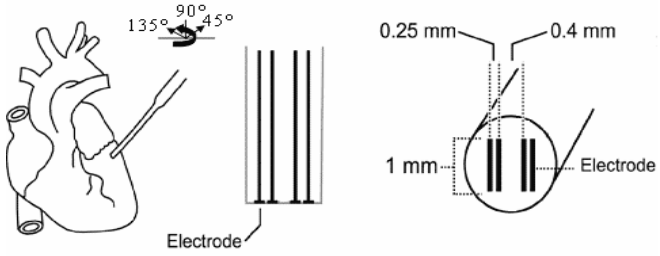

Figure. 3-1. Epicardial admittivity surface probe consists of four electrodes 1mm long spaced at 0.25 mm (typical) and 0.4 mm center to center between electrodes 2 and 3. Suction ports permit application of a mild vacuum to assist in securing the electrode.

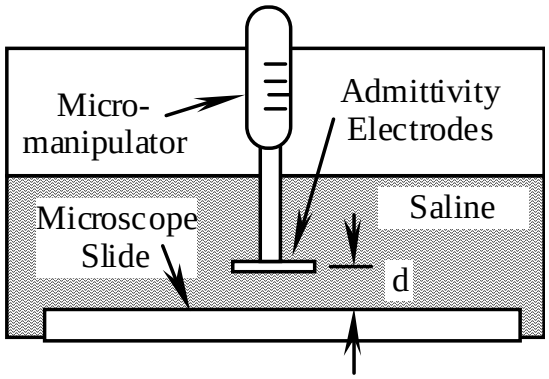

Figure. 3-2. Experimental setup to measure field penetration depth of the surface probe

The electrode design was modeled after an electrode developed for the canine heart by Steendijk *et al.* [23]. However, their electrode spacing was designed to sample only the epicardium. Wider electrode spacings relative to the myocardial thickness were

used to gain a greater depth of penetration by the electric field. This minimizes the effect of tissue anisotropy in the "longitudinal plane", as it were, by measuring over a substantial fraction of the ventricular free wall thickness. Consequently, the effect of anisotropy due to fiber orientation within layers of myocardium is averaged. The substantial anisotropy between longitudinal (to the fiber) and transverse measurements is not addressed by this approach. In a parallel study [32], it was confirmed (by measurement at four different orientations of 0, 45, 90 and 135 degrees) that probe orientation effects showed no variation more significant than intra-measurement and inter-animal variability.

3.2.2 Surface Probe Depth of Penetration

The effective measuring depth of the surface probe [Fig. 3-1] was determined experimentally in a saline bath by advancing the probe normally toward an insulating glass surface with a micro-manipulator [Fig. 3-2]. The "effective depth" was defined as the depth at which the measured conductance decreased 5% from the value at large depth. [33, 34]

This measurement determines the thickness of myocardium at which a substrate material affects the probe current field sufficiently to be reflected as a measurable change at the voltage electrodes. Separate FEM numerical studies (not included here) confirm that the effective depth over an insulator is essentially the same as the effective depth over a blood substrate.

3.2.3 Calibration

Calibration of the conductance (magnitude of admittance) measurement device was accomplished with 1% metal film resistors between 267 Ω (3,750 μS) and 5.33 kΩ (188 μS). The calibration resistors were tested on an Agilent Inc. Model 4194A

Impedance / Gain-Phase Analyzer to ensure that no inductive or capacitive behavior was observable in them over the frequency range of interest, 2 to 50 kHz. This method was employed for the calibration of the magnitude of admittance of all three instruments mentioned above.

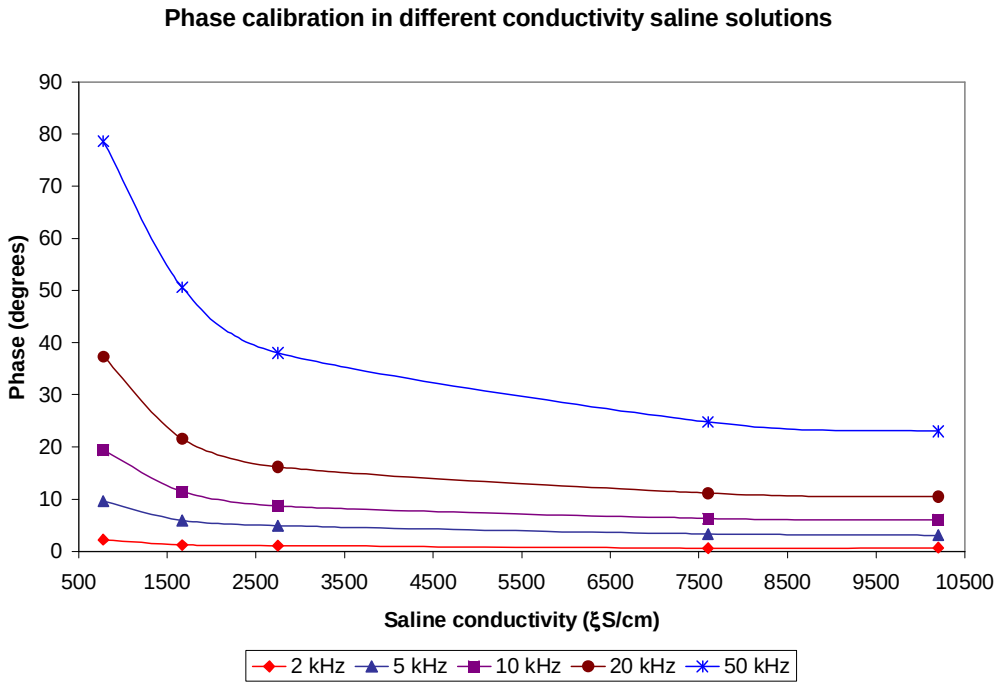

Figure. 3-3: Sample saline calibration curves measured using the digital method. The graph shows measured admittance phase as a function of saline conductivity for various frequencies. These curves would be used in the estimation of myocardial electrical properties to calibrate the capacitance of the epicardial probe [34].

The small epicardial surface probe cable has substantial inter-wire capacitance: there are six inter-electrode parallel capacitances among the four lead wires. The net effect of these capacitances was studied using a relatively large volume of saline of known electrical conductivity. Different conductivity saline solutions were prepared in the range of 800 to 10200 μS/cm, or 0.08 to 1.02 S/m at 37^{o}C. This range of conductivities includes the range of effective conductivities of blood and myocardium.

The conductivity of the saline solutions was measured with a Hanna Model HI 8033 conductivity meter (Hanna Instruments, Woonsocket, RI). The saline solutions were placed in large plastic vials, and the epicardial surface probe was advanced just enough to touch the surface of the saline solution. Admittance magnitude and phase measurements were made using both the digital and analog admittance instruments. Calibration curves (measured admittance phase vs conductivity) were constructed at each measurement frequency. Fig 3-3. is a representative sample saline calibration curve performed with the epicardial surface probe using the digital method. Because saline is semiconducting, the phase responses in Fig. 2-4 only occur because of the capacitances of the lead wires. The net effect of these capacitances was compensated by this calibration.

3.2.4 Murine studies

The Institutional Animal Care and Use Committee (IACUC) at the University of Texas Health Science at San Antonio and at The University of Texas at Austin approved all experiments. Ten CD-1 mice were studied by the digital admittance magnitude and phase measurements. Seven additional C57BlkS mice were studied by the analog admittance magnitude and phase measurement.

Mice were anesthetized by administration of urethane (1000 mg/kg ip) and etomidate (25 mg/kg ip), and mechanically ventilated with a rodent ventilator set at 150 breaths/min (100% O2). Mice were placed on a heated, temperature-controlled operating table for small animals (Vestavia Scientific, Birmingham, AL). Experiments were performed at a murine body temperature of 37 ^{o}C. The chest was entered via an anterior thoracotomy. The tetra-polar surface probe, mounted on a micro-manipulator, was placed on the LV epicardium of the intact beating mouse heart. Verification was done to make sure that the surface probe made complete contact with the myocardium by checking the quality of the signal.

3.3 RESULTS

3.3.1 Surface Probe Effective Depth

In Fig. 3-4, the measured response at large depth is 249 μS, which decreases to 237 μS at a depth of 0.6 mm. The 0.6 mm effective depth is less than the average thickness of the murine myocardium in the left ventricular free wall - approximately 1.2 mm at end-systole and 0.8 mm at end-diastole.

Blood is approximately 4 times more conductive than cardiac muscle — around 0.5 S/m compared to a range of 0.11 to 0.17 S/m, respectively [32]. As mentioned, numerical models show that the effective depth over an insulator is essentially the same as over a blood substrate (i.e. within 15%). Therefore, the surface probe measurement is not significantly affected by the LV blood pool.

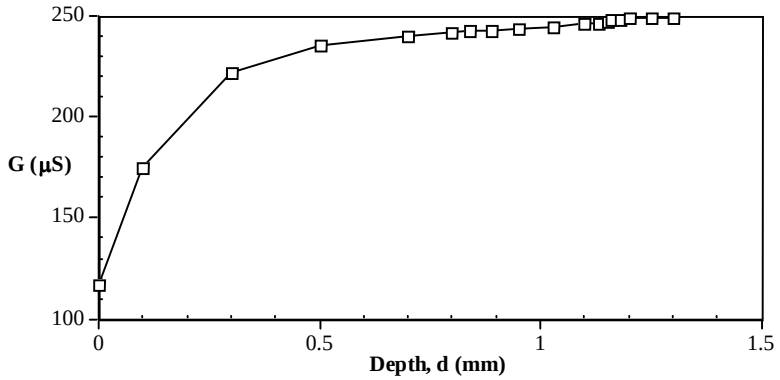

Figure. 3-4: Experimental measurements of the effective measurement depth of the surface probe.

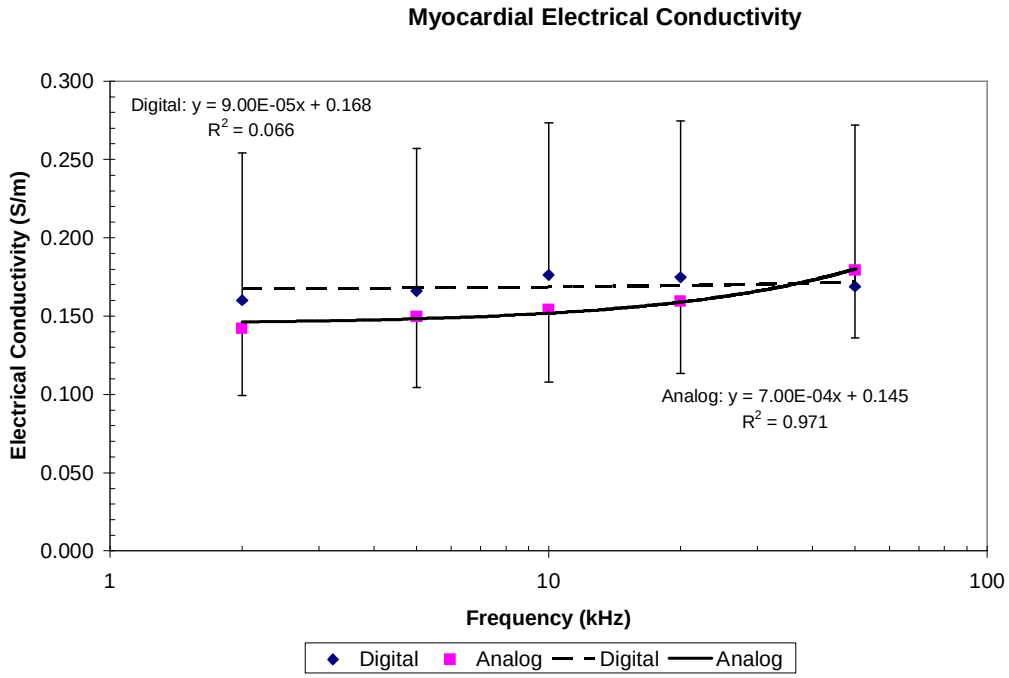

Figure. 3-5: Estimate of mouse-to-mouse variations in the electrical conductivity of mouse left ventricular myocardium from the real part of the complex admittivity for CD-1 mice using the digital method [N=10] and C57BlkS mice using the analog method [N=7]. Error bars are one standard deviation.

3.3.2 Estimation of myocardial conductivity from admittance magnitude and phase measurements

When the surface probe is placed on the epicardium, the admittance measured is a combination of the contributions from the myocardium and the probe itself, so:

$$Y_{meas} = Y_m + j\omega C_{probe} = G_m + j\omega C_m + j\omega C_{probe} \quad (4)$$

Where Y_m is the admittance contribution from the myocardium and the C_{probe} is the capacitance of the probe.

The real part of equation (4) yields the myocardial conductance (G_m, S).

$$G_m = | Y_{meas} | \cos(\theta_{meas}) \quad \text{(5-a)}$$

Where $|Y_{meas}|$ is the measured admittance magnitude and θ_{meas} is the measured phase angle. The field form factor, F, is then estimated using known conductivity saline solutions. Then, using Equations (1-a) and (5-a), the myocardial electrical conductivity is estimated (σ_m, S/m).

Table 2-1 lists the determination of myocardial electrical conductivity from admittance magnitude and phase measurements (N=10 for digital method, N=7 for analog method).

The individual mouse data mean values were combined to obtain the overall estimates across all mice. These values are plotted in Fig. 3-5 for both the digital and analog methods.

The slopes of the linear fits (presented in Fig. 3-5) are very small indicating that the conductivity is essentially independent of frequency. Also, a repeated measures ANOVA between the digital and analog estimates of the electrical conductivity gave a p=0.772 (for "between subjects" effects) indicating that the two sets of data are not statistically different from each other.

Frequency (kHz)	Electrical Conductivity (S/m) (Digital Method) (N=10)		Electrical Conductivity (S/m) (Analog Method) (N=7)	
	Mean	Standard Deviation (%)	Mean	Standard Deviation (%)
2	0.160	0.099 (62)	0.142	0.043 (30)
5	0.166	0.095 (57)	0.150	0.046 (30)
10	0.176	0.103 (58)	0.154	0.046 (30)
20	0.175	0.106 (60)	0.159	0.046 (29)
50	0.169	0.109 (65)	0.179	0.043 (24)

Table 2-1: Myocardial electrical conductivity

3.3.3 Estimation of myocardial relative permittivity from admittance magnitude and phase measurements

Some of the imaginary part of Equation (4) is due to the probe and wires. This can be estimated using the saline calibration curves (Fig. 3-3). Once compensated, the myocardial capacitance, C_m (F) can be calculated from:

$$C_m = (|Y_{meas}| \sin(\theta_{meas}) - |Y_{saline}| \sin(\theta_{saline}))/\omega \quad \text{(5-b)}$$

Where $|Y_{meas}|$ is the measured admittance magnitude and θ_{meas} is the measured phase angle, $|Y_{saline}|$ is the interpolated (spline interpolation) admittance magnitude signal in saline and θ_{saline} is the interpolated (spline interpolation) phase signal in saline. The interpolation is done to estimate $|Y_{saline}|$ and θ_{saline} accurately in conductances in the vicinity of $|Y_{meas}|$, using the saline calibration curves generated in the methods section. Finally, using Equations (1-b) and (5-b), the myocardial permittivity, ε_m (F/m) is calculated.

Frequency (kHz)	Relative permittivity:Complex		Relative permittivity: Complex plane analog	
	Mean	Std. Dev. (%)	Mean	Std. Dev. (%)
2	114,000	33500 (29)	80,600	25100 (31)
5	47,500	13700 (29)	34,900	8000 (23)
10	27,900	7170 (26)	20,300	3310 (16)
20	14,900	4800 (32)	11,800	2690 (23)
50	5,010	2680 (53)	4,970	2500 (50)

Table 2-2: Myocardial electrical permittivity

Table 2-2 lists the estimates of myocardial relative permittivity (ε_r) from both the complex admittance methods (N = 10 CD-1 mice for digital method, N=7 C57BlkS mice for analog method).

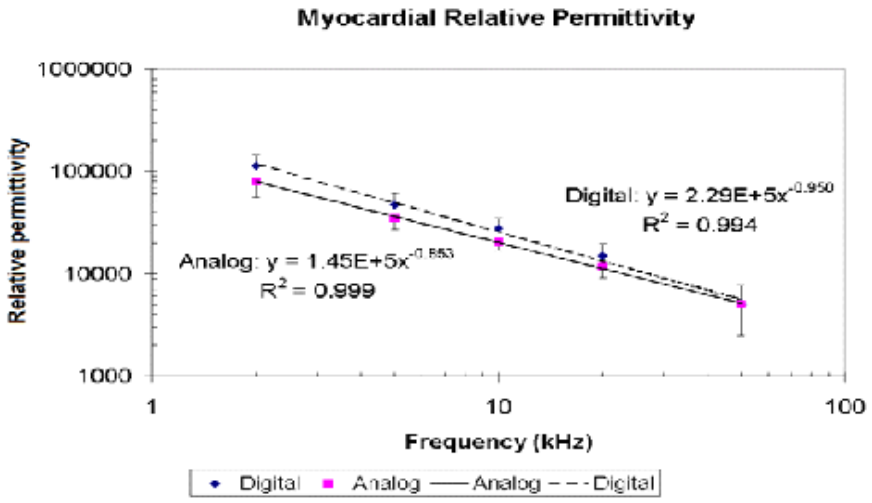

Figure. 3-6: Estimate of the mean relative permittivity of mouse left ventricular myocardium from the imaginary part of the complex admittivity showing mouse-to-mouse variations. Combined data are for the same 10 additional CD-1 mice as Fig. 3-5 for the digital method and the same 7 additional C57BlkS mice as Fig. 3-5 for the analog method.

The individual mouse data mean values were combined to obtain the overall estimates across all mice. These values are plotted in Fig. 3-6 for both the digital and the analog methods.

The results show that the relative permittivity decreases with frequency in a logarithmic sense. Also, repeated measures ANOVA with three different post-hoc results indicate that the two complex measurements (the digital and analog approach) are not statistically different from each other ($p=0.606$, $p=0.345$ and $p=1.0$).

3.4 DISCUSSION

3.4.1 Effect of myocardial anisotropy

The primary application for these results involves the measurement of P-V loops inside the murine LV using a tetrapolar catheter. The catheter measurement has

contributions from both the blood and the myocardium. Myocardium is known to be highly anisotropic: the electrical conductivity in the longitudinal direction has been shown to be approximately twice that in the direction transverse to the fibers [23, 24]. Further, the fibers transition as much as 160 degrees in the various "longitudinal planes" that make up the thickness of the myocardium, from epicardium to endocardium [38, 39]. Like the LV conductance catheter, the surface probe measurement is dominated by the longitudinal components; however, there is some contribution from the transverse direction. Surface measurements in the mouse have been shown to be essentially insensitive to probe rotation relative to the longitudinal planes [32] owing to the depth of penetration of the surface probe. Some transverse / longitudinal anisotropy is always included in the lumped measurement provided by the surface probe. Needle electrodes, like the ones used by Salazar *et al.* [40] in their study of porcine myocardial tissue, would provide a longitudinal measurement alone; but, needle electrodes are not practical in the extremely thin murine ventricular free wall due to the relative amount of tissue trauma they would cause.

3.4.2 Electrical permittivity

Previously, Gabriel *et al.* [22] reported electrical permittivity values that range from approximately 200,000 at 2 kHz to about 20,000 at 50 kHz. They suggested that the high permittivity most likely originates in the cardiac myocyte trans-membrane charge distribution. However, they had lumped the relative permittivity and conductivity into a complex permittivity. Salazar *et al.* [40] reported *in-situ* complex resistivity measurements on porcine myocardium using needle electrodes. These data were re-analyzed to obtain the relative permittivity. The relative permittivity varied from about 190,000 at 2 kHz to about 23,000 at 50 kHz in their measurements and the electrical conductivity was about 0.4 (S/m). These relative permittivity measurements varied from

approximately 100,000 at 2 kHz to about 5,000 at 50 kHz. The epicardial surface probe measurements also include some transverse component, which accounts for the differences between measurements. As mentioned, it is impractical for us to use needle electrodes on the murine myocardium due to the extremely thin nature of the ventricular free wall (approximately 1.2 mm at end-systole and 0.8 mm at end-diastole). I suggest, however, that since our goal is to determine the σ/ε ratio for the myocardium, our estimate of this ratio – $1.8*10^5$ (S/F) at 2 kHz compared to Salazar *et al*, at $2.3*10^5$ (S/F) – is useful for the intended purpose in spite of this limitation.

3.4.3 Choice of optimal frequency for LV P-V experiments

As the frequency increases, the relative permittivity decreases while the conductivity remains relatively constant. The $\omega\varepsilon_m$ term (the imaginary component of the admittivity formulation) at the different frequencies (see Table 2-3) has a local maximum near 20 kHz, which is comparable to the measurements by Epstein *et al.* [41]. This observation is a key point in LV P-V analysis because this frequency will give the maximum resolvable imaginary cardiac muscle component.

Frequency (kHz)	ε_r	$\omega\varepsilon_m$
2	114,000	0.013
5	47,500	0.013
10	27,900	0.016
20	14,900	0.017
50	5,010	0.014

Table 2-3: $\omega\varepsilon_m$ terms obtained from digital permittivity data

3.4.4 Implications: Real time parallel myocardial contribution estimation and removal in LV volume analysis

The complex measurement technique presented in this chapter is a progression of the initial formulation of Wei *et al*. [42] and can be used to estimate the electrical properties of myocardium in real time. The results of this chapter have an important application during catheter based LV P-V analysis in murine hearts, where the myocardial contribution to the measured admittance is changing instantaneously and needs to be estimated and removed from the combined signal during the cardiac cycle. This is particularly important when, for example, transient occlusion of the inferior *vena cava* is performed to generate more complex measures of left ventricular function available in the pressure volume plane such as end-systolic elastance, diastolic chamber compliance, and effective arterial elastance. Without true left ventricular volume, absolute determination of these measures of ventricular function would not be available, but are desired by investigators of whole - heart mechanics.

The application of admittance to determine instantaneous LV volume allows comparison of measures of ventricular function between mice, and in a given mouse to itself over time. Current methods in determination of murine LV P-V suffer from a major limitation in that they fail to estimate a time – varying myocardial contribution within a heart cycle. However, this can be overcome by using real-time admittance which utilizes the capacitive component of muscle to remove the myocardium from the combined blood/myocardial signal, thus providing a broader application of this technology to invasive hemodynamic murine studies.

CHAPTER 4

IC Design Details

4.1 OVERVIEW

The initial design plan was to design a System on a chip (SOC) which would consist of the sinusoidal generator, constant current source, interface with the catheter, impedance magnitude generation, phase estimation and the pressure amplifier stages.

This IC was designed using the AMI C5N process (0.5 μ). This technology featured 2 poly layers, 3 metal layers, and offers a precision poly-poly capacitor. It also supports an operating voltage from 2.5V to 5V. Thus, a +/- 2.5V bipolar design was chosen.

The PDK files (amis500cx) were obtained via Europractice (IMEC, Hevelee, Belgium), after signing a license agreement with the company. These files were integrated into the Cadence suite of IC Design tools (Cadence Design Systems Inc., San Jose, CA). The Cadence tools were used for schematic editing, layout editing, and simulation. Design Rule Checks (DRC), and Layout Vs Schematic (LVS), and Parasitic Extraction (PEX) were performed using Calibre (Mentor Graphics Corporation, Wilsonville, OR) suite of tools, which was also integrated into the Cadence Analog Design Environment. The University of Texas at Austin has licenses for each of these tools intended for academic/research purposes (non-commercial uses).

4.2 AREA AND POWER ESTIMATES

The overall layout area (not including the ESD pads) turned out to be 1742.4 μ x 2286.9 μ = 1.74 mm x 2.29 mm = 3.98 mm^2. Table 4-1 lists the summary of the active (ON) power consumption estimation.

Opamp count	Current consumption (μA)	Total Current (μA)	Total Current (mA)	Power (mW)
27	135	3645	3.65	
1	890	890	0.89	
3	120	360	0.36	
	Total	**4895**	**4.90**	**24.5**

Table 4-1: Summary of overall active (ON) power consumption

4.3 DESIGN, SCHEMATICS, LAYOUT AND SIMULATION

After going through design, schematics, layout of the various blocks and simulation, DRC, LVS, and PEX, it was determined that the chip could not be taped out because of budgetary constraints. However, I would like to share some of the key blocks' design thoughts, schematics and layout screen shots from Cadence.

The design itself had 5 blocks. The overall block diagram was very similar to the one depicted in Fig. 4-1. Fig. 4-1 shows the overall top module schematic (connections). Block 1 is the sinusoidal generator. Block 2 is the constant current source. Block 3 is the filtering and gain stages after differential voltage sensing from the catheter. Block 4 is the magnitude and phase estimation. Block 5 is the pressure amplifier. It also shows the DC

biasing circuit as a separate block supplying the bias currents for the various operational amplifiers in each of the 5 blocks.

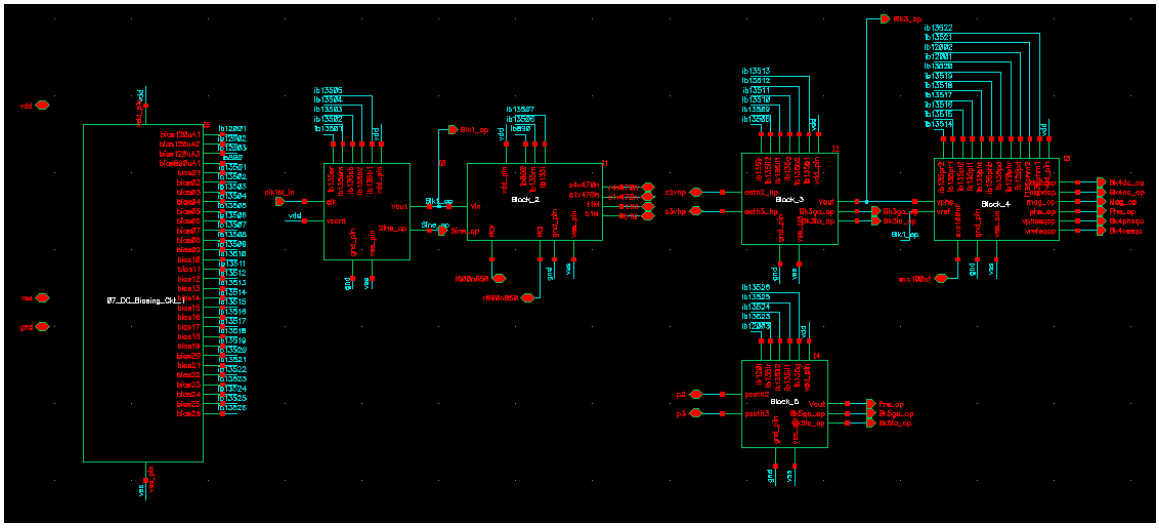

Figure 4-1: Top module schematic

Fig. 4-2 shows the overall top module along with the ESD pad logic in place. Fig. 4-3 shows the top module complete layout (without the ESD pads). Also shown is the ruler to show the actual silicon area of the top module (without ESD pads).

The DC biasing circuit biases the entire circuit which included 26 “opamp1”s drawing 135 μA each, 3 “opmap2”s drawing 120 μA each and 1 opamp3 drawing 890 μA. The three kinds of opamps were designed to support different capacitive loads without running into instability. The DC biasing circuit itself contains an opamp0 drawing 135 μA, but is self-biased (using a resistor). Fig. 4-4 shows part of the DC biasing circuit schematic. The schematic itself is a repetition of the same basic module and is based on precision current mirrors to obtain the exact current needed.

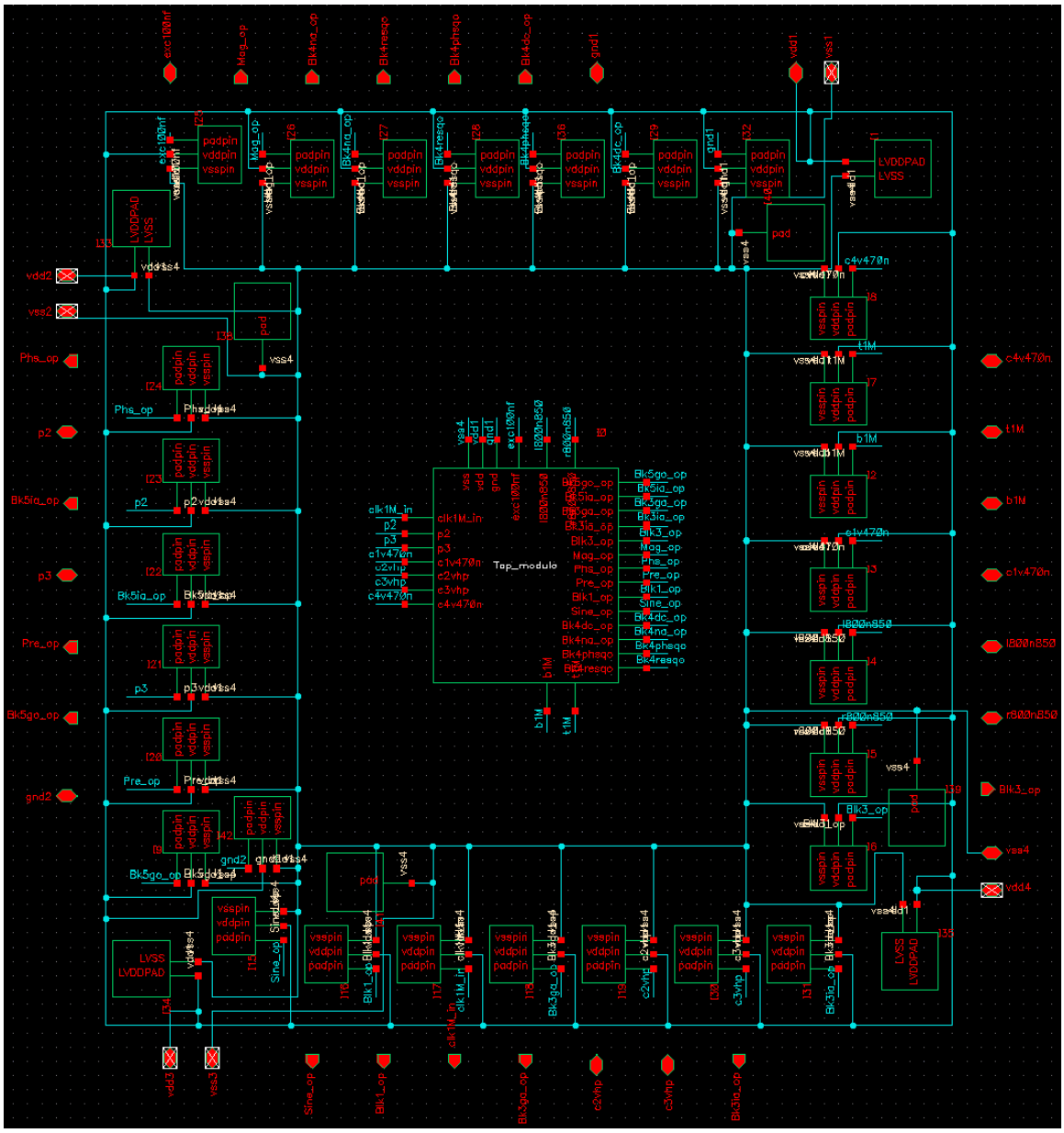

Figure 4-2: Top module schematic with ESD pads and logic

Fig. 4-5 shows the layout of the complete DC biasing circuit. The layout has been designed keeping in mind that there would be variations along the X- and Y- axes. Therefore, careful matching was performed to ensure that the variations are canceled out.

Also, similar modules were routed from similar positions on the layout. Thereby, achieving a better current biasing circuit.

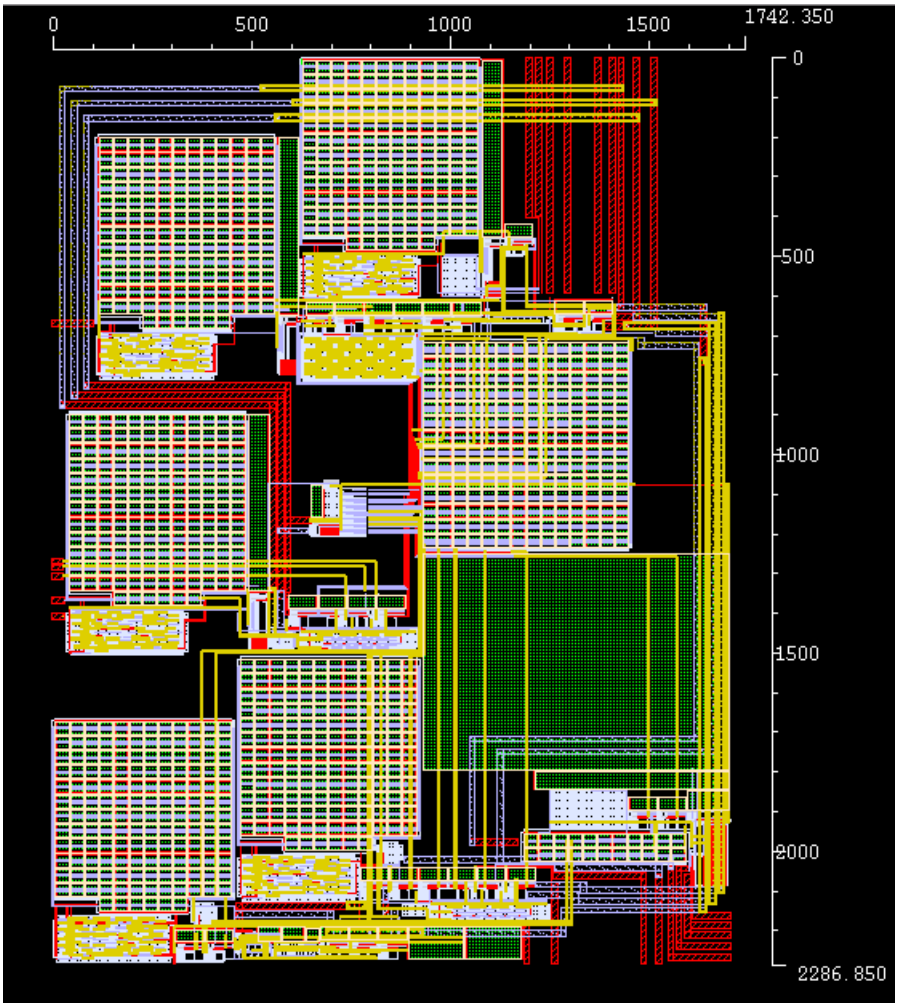

Figure 4-3: Top module layout (excluding ESD pads)

Fig. 4-6 and Fig. 4-7 show the schematic and layout (respectively) of the basic operational amplifier used in most of the cases (designated "opamp1"). The design was based on a 2-stage opamp [43]. This opamp has a bandwidth of about 1 MHz and was stable in the unity – gain configuration. Again, since the opamp is the basic building block of the entire design, careful matching was performed. Even the input stage was

designed to be symmetric so that there is very little variation between the two inputs. Dummy transistors were also used for matching the surrounding environment of transistors. Better matching and better symmetry lead to more accurate results.

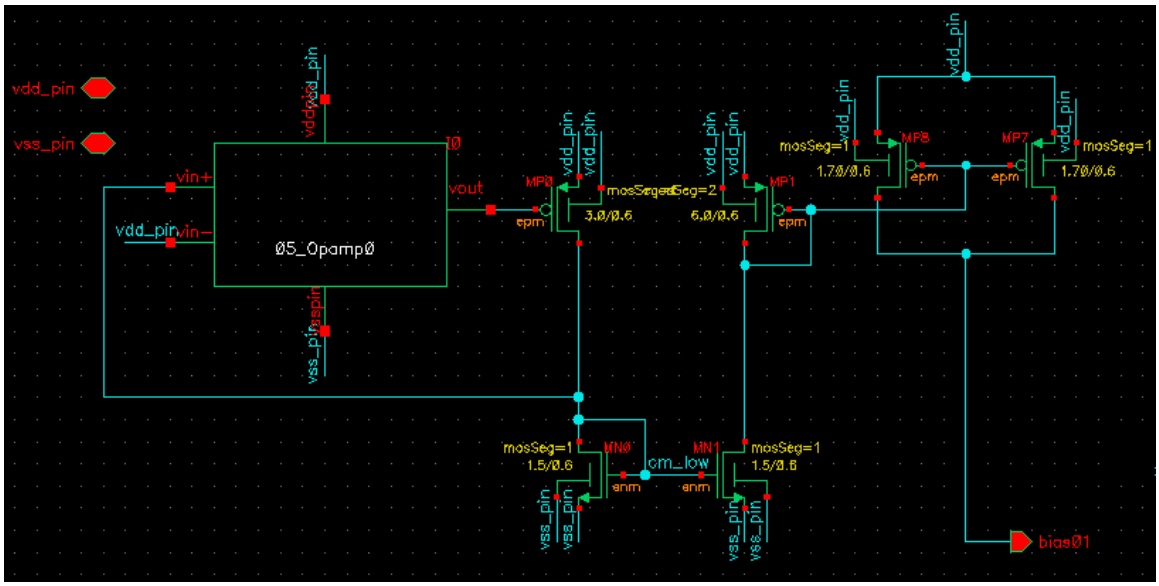

Figure 4-4: Part of the schematic of the DC biasing circuit

The sinusoidal constant current source design was broken down into two parts. The first part generates a 30 kHz sinusoidal voltage. (The earlier epicardial probe studies prove that the 20 kHz gave the maximum resolvable imaginary component. However, at the time the IC was designed, 30 kHz was chosen because that study had not been completed at that point in time). This is a switched-capacitor implementation. An external clock source at 1 MHz feeds the network. In turn, the sinusoidal generator is based on a square wave relaxation oscillator followed by high Q band pass biquad filter. [44]

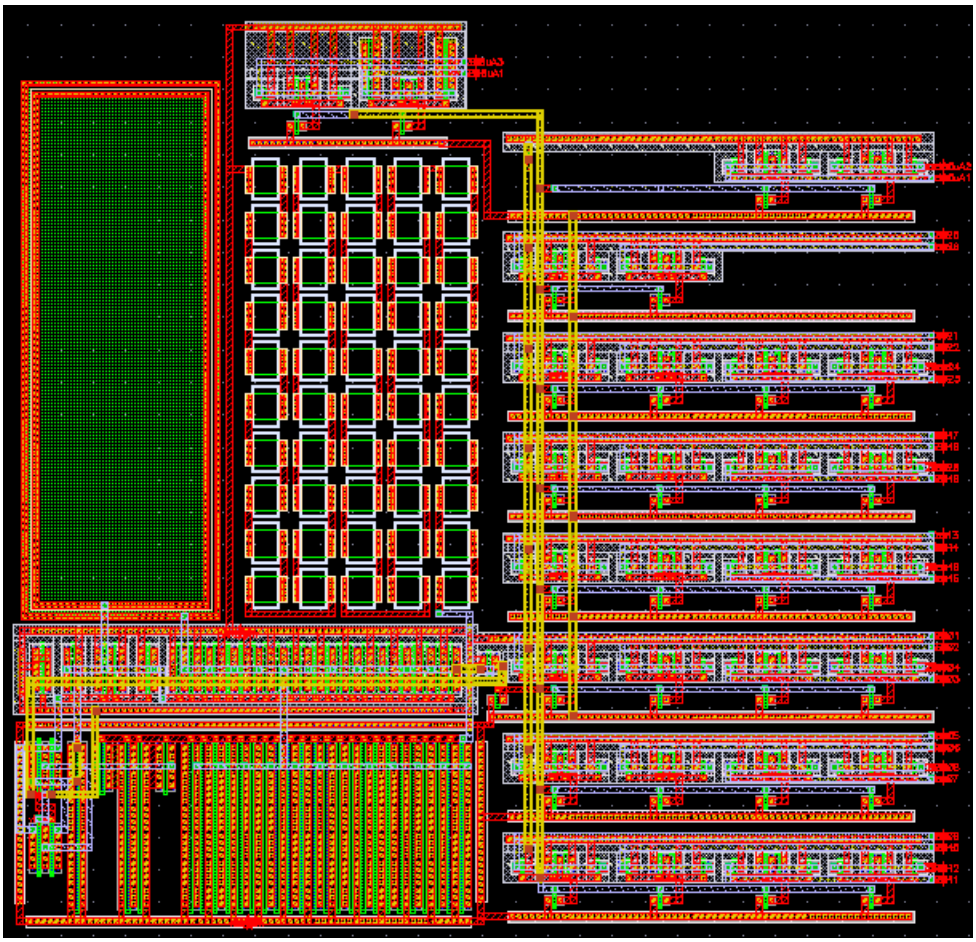

Figure 4-5: Complete layout of the DC biasing circuit

Using basic digital logic elements, two non-overlapping clocks were obtained from the input clock. Choice of the values of k1, k2 and switch transistor sizes are described in the reference text. [44] For my design, $k_1 = 0.4$, $k_2 = 0.2$, C = 100pF. [44]

Fig. 4-8 and Fig. 4-9 show the overall schematic and layout (respectively) of the sinusoidal voltage source.

This was followed by the constant current source. Fig. 4-10 shows the block level schematic of the constant current source. The resistors have been broken down into 1k resistors for ease with LVS matching. Also, breaking down large resistors into smaller

chunks enables a better-matched layout. Long resistive fingers can lead to mismatches along the direction of elongation. Fig. 4-11 shows the simulation output of a parametric sweep of different resistive loads to test the constant current source.

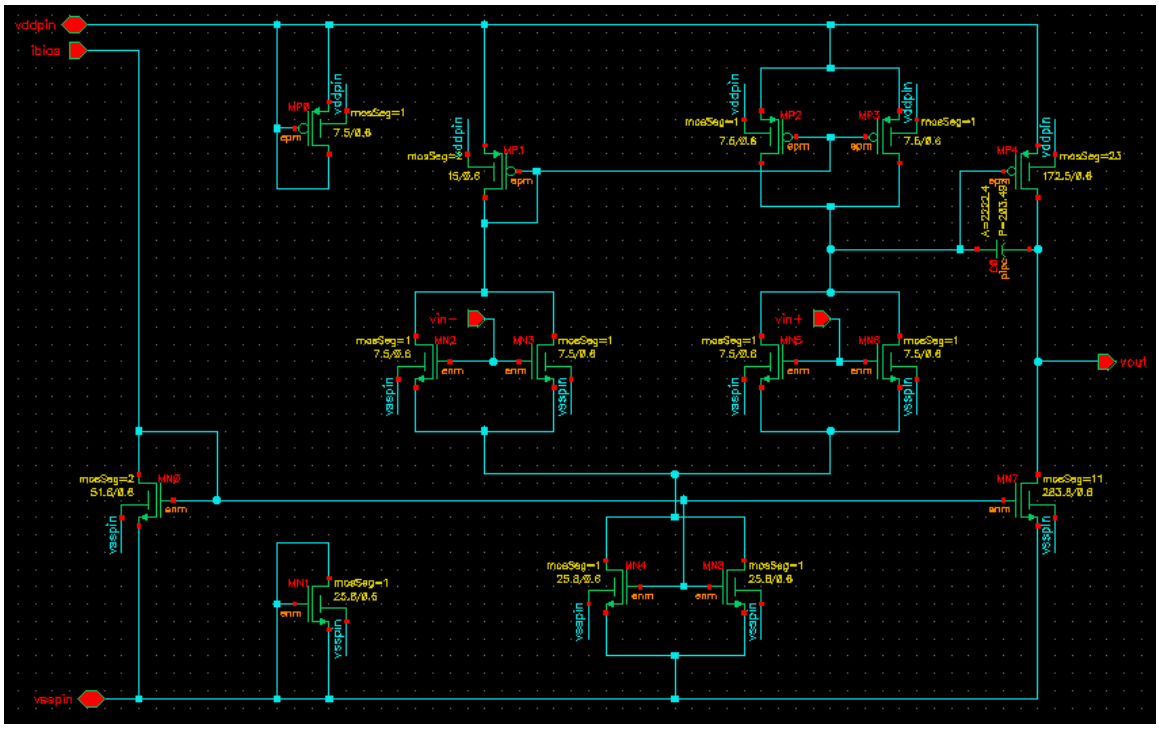

Figure 4-6: Schematic of opamp1

Blocks 3 and 5 are standard configurations consisting of a differential amplifier stage (3 – stage opamp based instrumentation amplifier), followed by gain and filtering.

The magnitude estimation block, depicted in Fig. 4-12, is based on a simple peak detector circuit.

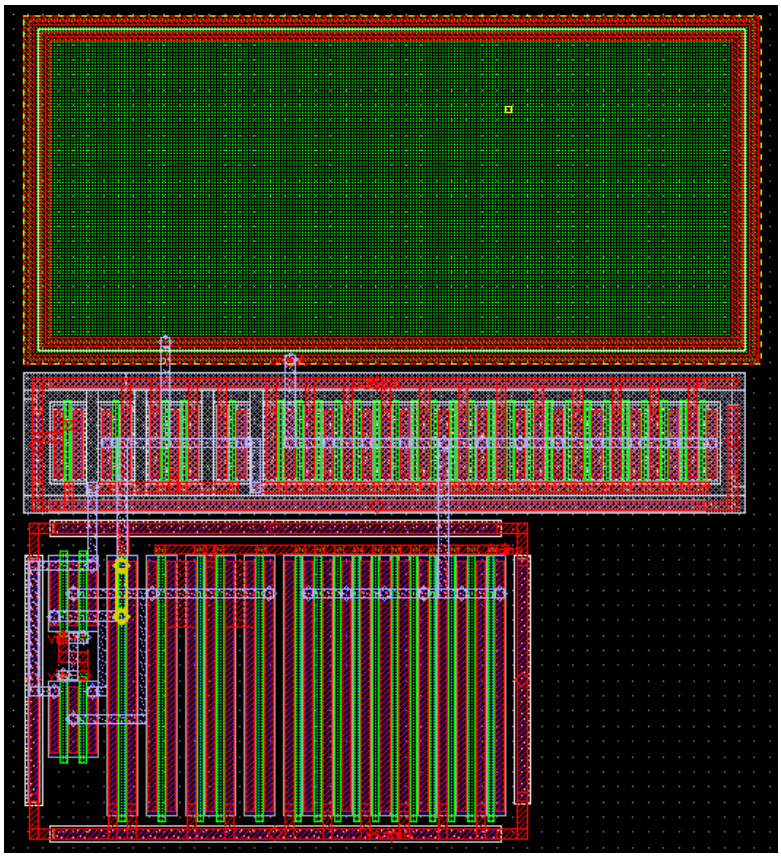

Figure 4-7: Layout of opamp1

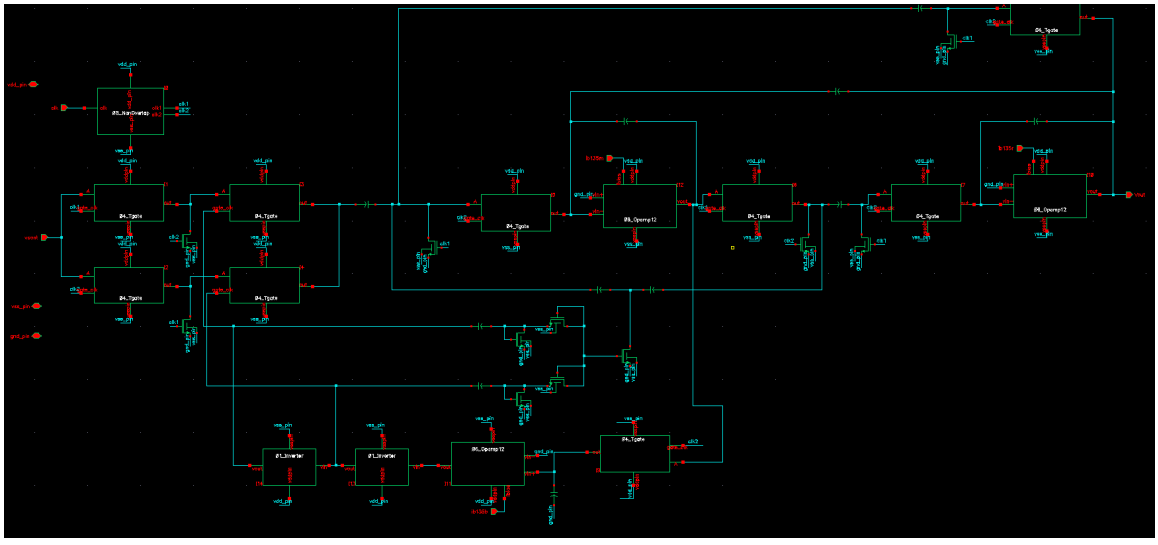

Figure 4-8: Schematic of sinusoidal generator

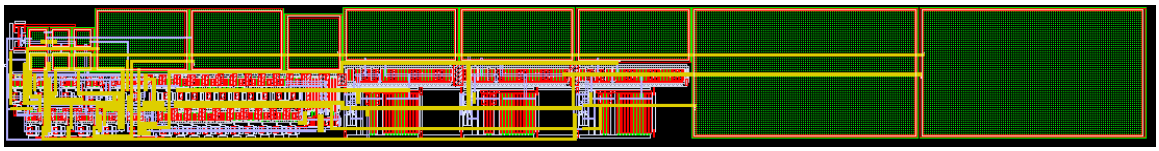

Figure 4-9: Layout of sinusoidal generator

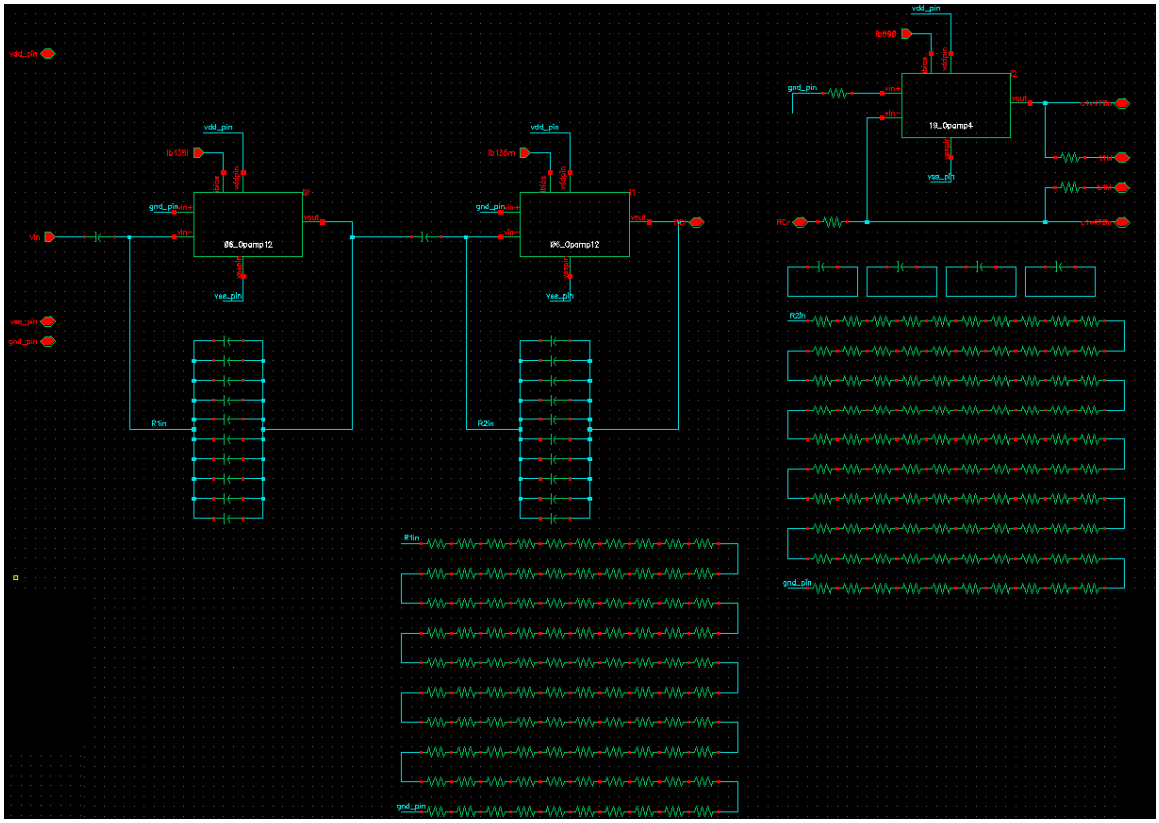

Figure 4-10: Schematics of the constant current source

The phase estimation is based on an initial design by Kottam *et al.* [37]. For a constant frequency application like this one, the reference signal and the phase-shifted signal are converted to square waves, followed by NAND logic, whose duty cycle varies according to the phase shift. After this, a duty cycle to DC voltage logic, based on R-C time constants, outputs a DC voltage based on the phase difference. Fig. 4-13 is the schematic of the phase detection block.

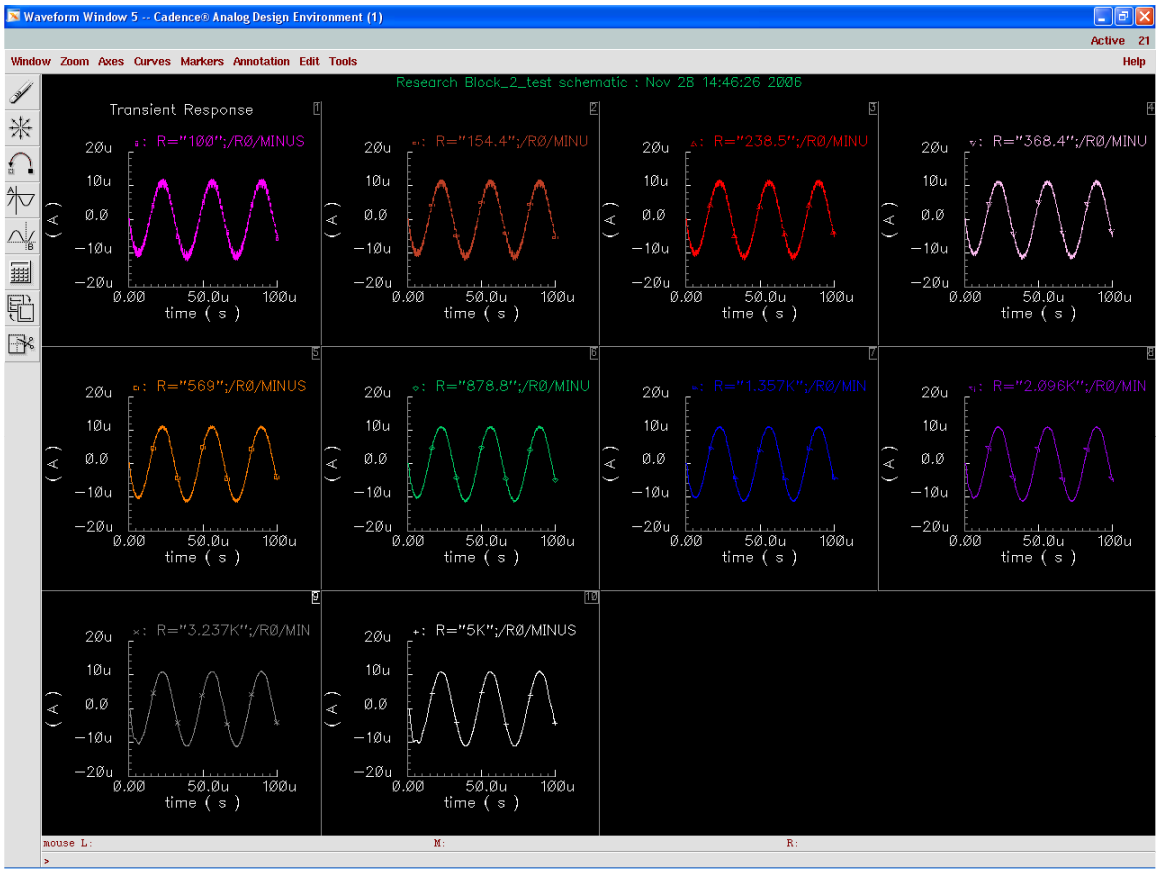

Figure 4-11: Simulation output of the constant current source (10μA peak, 30 kHz)

Finally, the sensitivity plots of the three channels: impedance magnitude, phase and pressure outputs have been summarized in Fig. 4-14. The output sensitivities are 500mV/kΩ for the impedance magnitude, 35mV/deg for the impedance phase and 2.5mV/mmHg for the pressure.

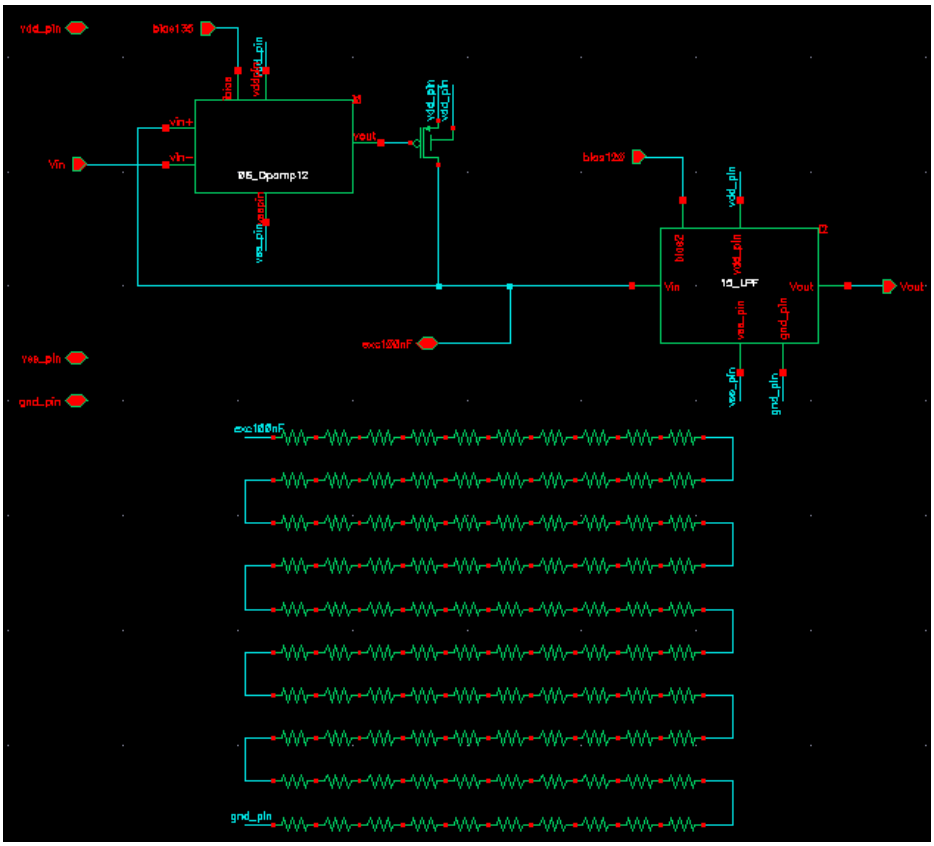

Figure 4-12: Impedance magnitude generation schematic

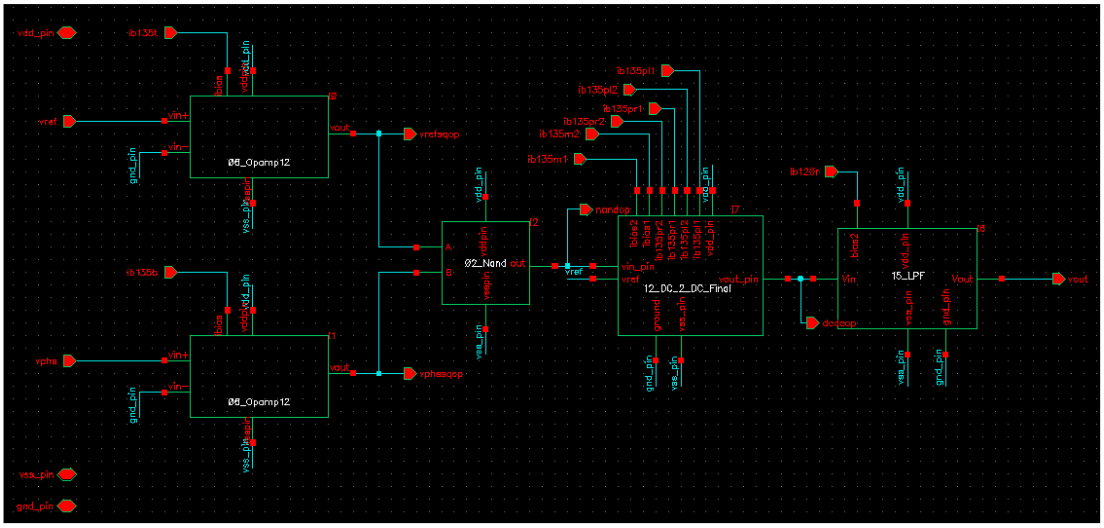

Figure 4-13: Impedance phase generation schematic

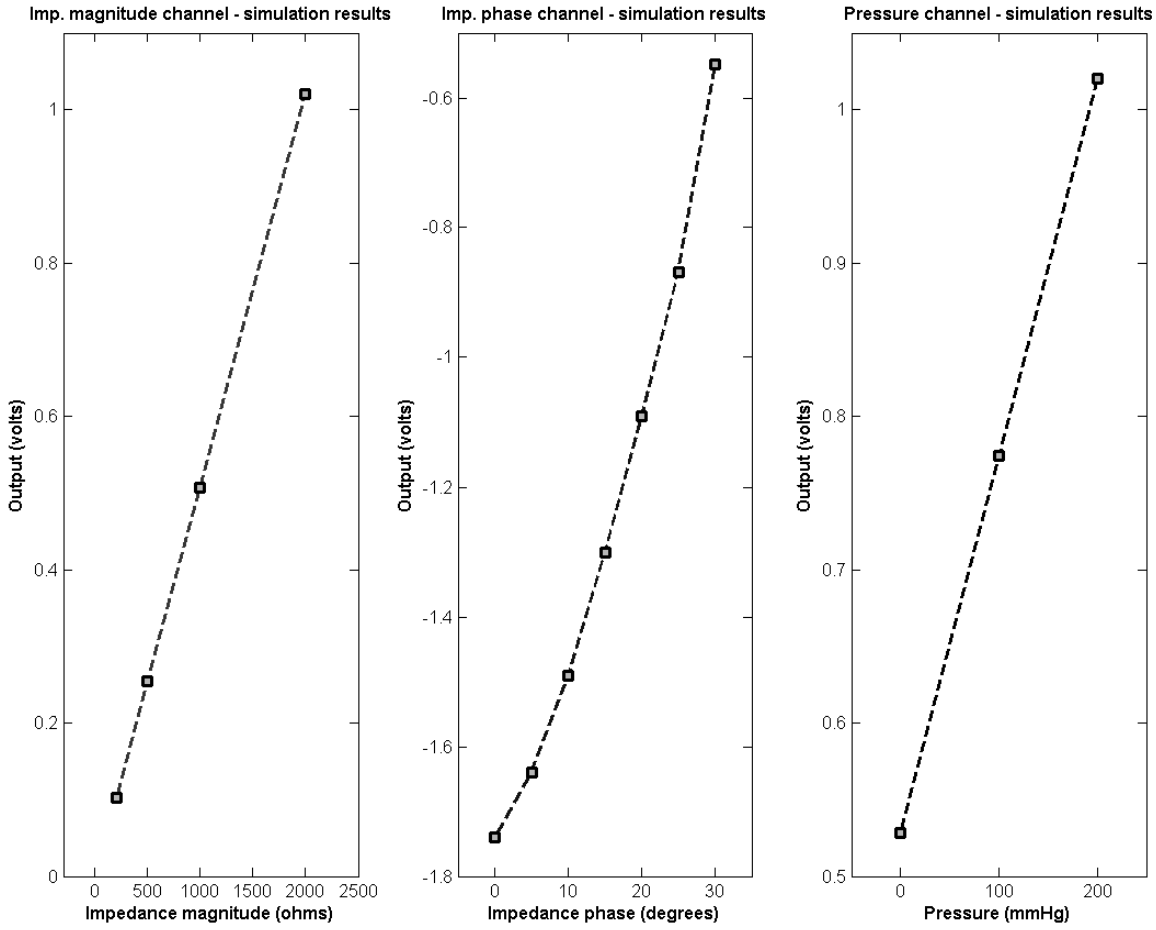

Figure 4-14: Sensitivity plots of the impedance magnitude, phase and pressure outputs

CHAPTER 5

Design of the wireless telemetry based backpack instrumentation

5.1 OVERVIEW

This chapter describes the instrumentation design for the backpack. These backpacks were tested on rats for the 24-hour chronic studies. Rats were chosen because they are larger than mice and can carry the backpack of this size. The design of the backpack was done with two main constraints (in the order of preference): Low power and low area. It was absolutely critical for the backpack to last at least the 24 hour experiment time frame for the chronic studies on the rats. In addition, a low area meant a lower volume and subsequently lower weight. This was critical too because the rat would be carrying this backpack for the entire period of the experiment. A lower weight meant that the rat would be more comfortable with the backpack and would be able to perform its regular activities and more importantly, it would not try to remove the backpack from its back.

5.2 CIRCUIT DESCRIPTION

5.2.1 Top level design description

Fig. 5-1 is the overall block diagram of the backpack. A 3.7V, 625 mAh lithium ion-cell is used to power the circuit. The circuit is based on a single-supply design with the clock generator, phase detector chip, operational amplifiers and differential amplifiers operating on a single 3.6V supply. All the components were chosen with the lowest power possible while meeting the required voltage swings, bandwidth and slew-rate. To

save area, quad – package low power operational amplifiers (LM6134) were used, wherever possible.

The backpack consisted of three different components. The instrumentation (indicated by the grey block in Fig. 5-1) on a surface mount PCB, the lithium – ion cell and the microcontroller/transceiver on a separate surface mount PCB.

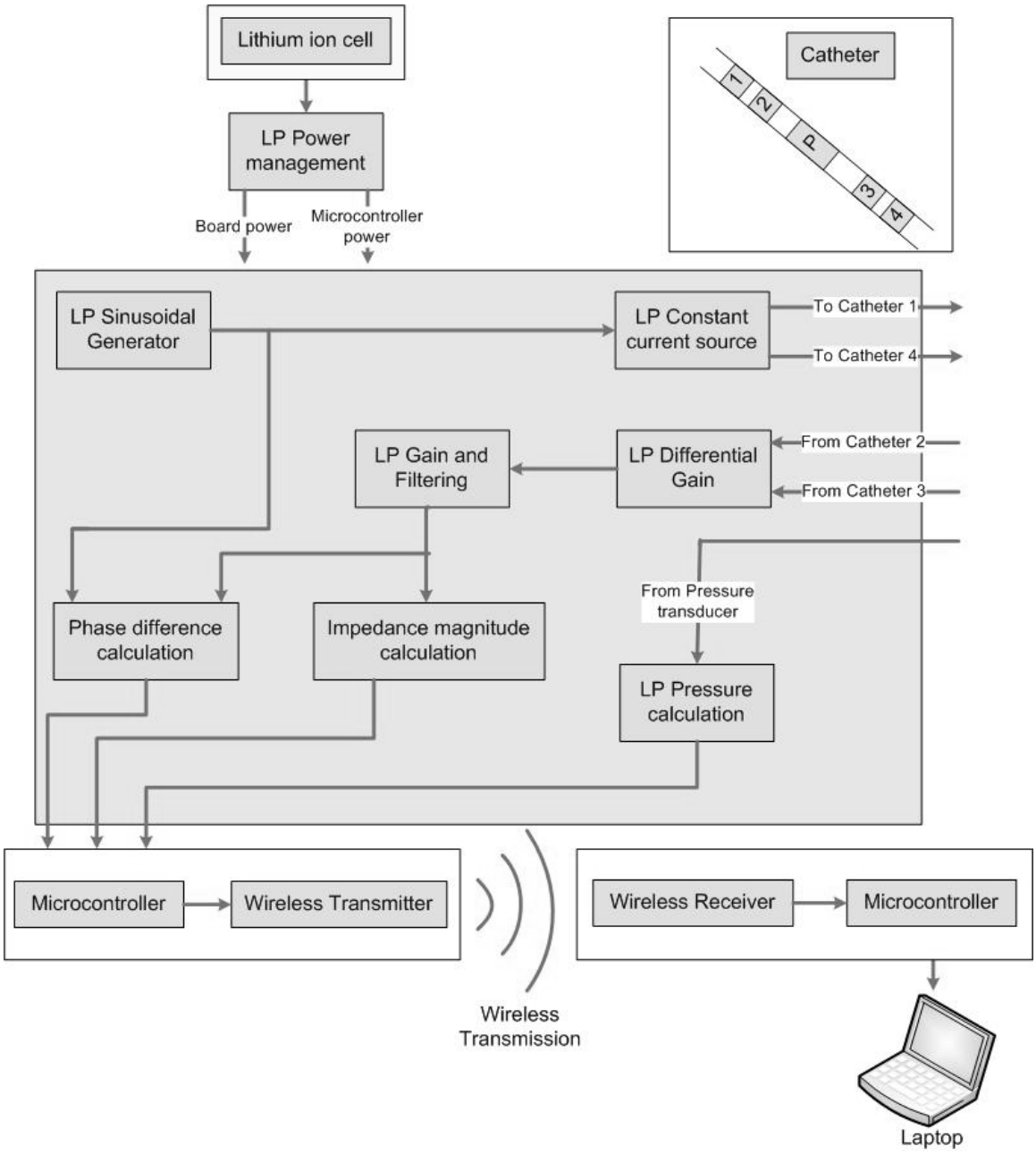

Figure 5-1: Overall block diagram of the backpack.

The instrumentation was interfaced with the tetrapolar P-V catheter and the microcontroller / transceiver block. The instrumentation PCB consisted of a low power (LP) 20-kHz sinusoid generator, followed by a LP voltage-to-current converter. This

generated a 10μA rms current, which fed to the outer two electrodes of the catheter (Electrodes 1 and 4). The voltage resulting from the inner 2 electrodes (Electrodes 2 and 3) was then differentially sensed, followed by a gain and filtering stage. This was used to generate a DC signal corresponding to the impedance magnitude signal. In parallel, a phase detection chip was used to determine the phase difference between the original reference signal and the resulting output signal. A separate signal path was employed to process the pressure signal arising from the pressure transducer.

The resulting magnitude, phase and pressure signals were fed to the inputs of three 10-bit ADCs respectively (part of the LP microcontroller). A low power, low bit-rate protocol was used to transmit the signals over an RF link to the other transceiver. The receiver was placed less than 6 feet away connected to a laptop. Data were collected and stored on this laptop for post-processing analysis and display.

The backpack shape and structure itself was determined based on the desire for it to be strong yet comfortable and light-weight. Initially, a light-weight enclosure was used to house the backpack. However, it was determined that this nearly doubled the weight of the backpack. Also, this was relatively inflexible and was easily removed by the rat because of the flexible nature of the rat's back. A simple and effective solution was to use a bubble wrap pocket to store the backpack contents. This was effective because the circuit was protected from external fluids/influences and the wrap itself was comfortable and very light-weight.

5.2.2 Block level design description

5.2.2.1 Power management block

The entire circuit was powered of a single 3.7V, 625 mAh lithium – ion cell. The instrumentation was designed to run off a single power supply (3.6V). Therefore, apart from the actual ground (0V), there was an additional virtual ground set at 1.8V, the signal reference node. Fig. 5-2 is the setup of the power management circuit. All resistors used are precision metal–film resistors (1% tolerance) and all capacitors are ceramic capacitors (10% tolerance).

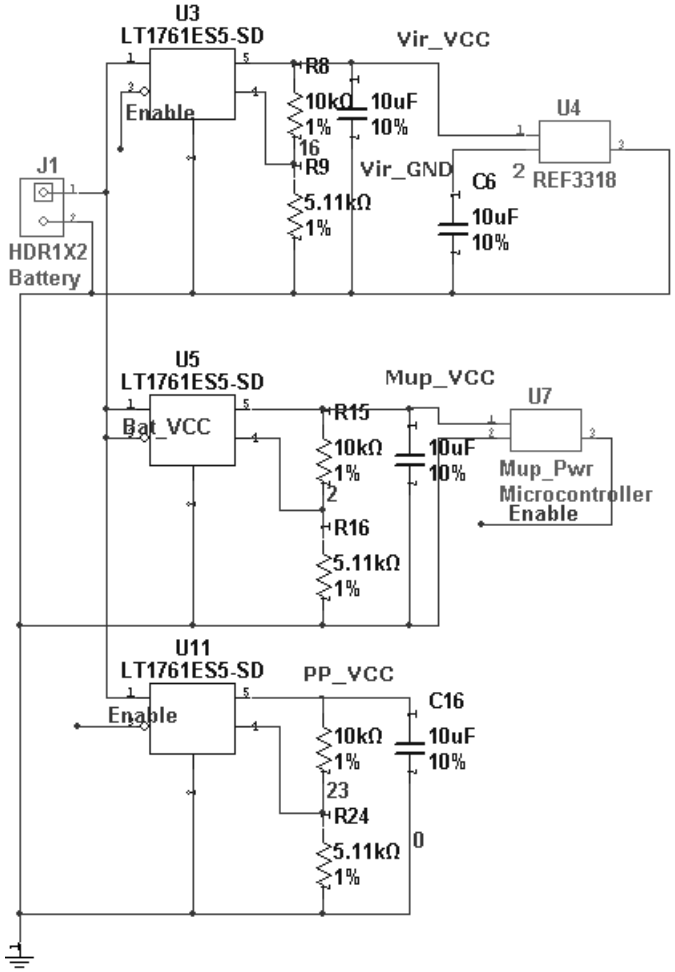

Figure 5-2: Power management blocks

Three different LP voltage regulators (LT1761ES5-SD) were used to power different parts of the backpack. All of them were set at a 3.6V level. The regulator U5 (Fig. 5-2) powers the microcontroller/transmitter. This was always ON. This way the microcontroller would always receive power, regardless of whether the instrumentation is collecting data or in an "idle" state. Regulator U11 powers the phase detector chip and also serves as the voltage difference applied across the bridge that is part of the pressure sensing network. Regulator U3 powers the rest of the instrumentation (LP clock, LP operational amplifiers and LP differential amplifiers). Both U11 and U3 are controlled by an enable signal, which is connected to the microcontroller. It is ON for the time frame when the instrumentation is actively sending data to the microcontroller (about 12 seconds every 2 minutes). It is OFF for the rest of the 2 minutes, thus, conserving power.

The virtual analog ground (1.8V) connection is provided using a LP reference chip (U4 REF3318).

5.2.2.2 Low power sinusoidal generator

Fig. 5-3 is the circuit implementation of the LP sinusoidal generator. An LP oscillator (LTC6906) was used to generate a reference square wave at 20 kHz. This was followed by a 20 kHz band pass filter implemented as 2 biquad sections with Sallen-Key Multiple Feedback architecture. The output is a 1Vp-p sine wave at 20 kHz, relative to the virtual analog ground at 1.8 V. This is used as the reference signal for the phase detector chip. The node "0" in all the circuit diagrams refers to the "real" power ground (0V). All resistors used are precision metal – film resistors (1% tolerance) and all capacitors are ceramic capacitors (10% tolerance).

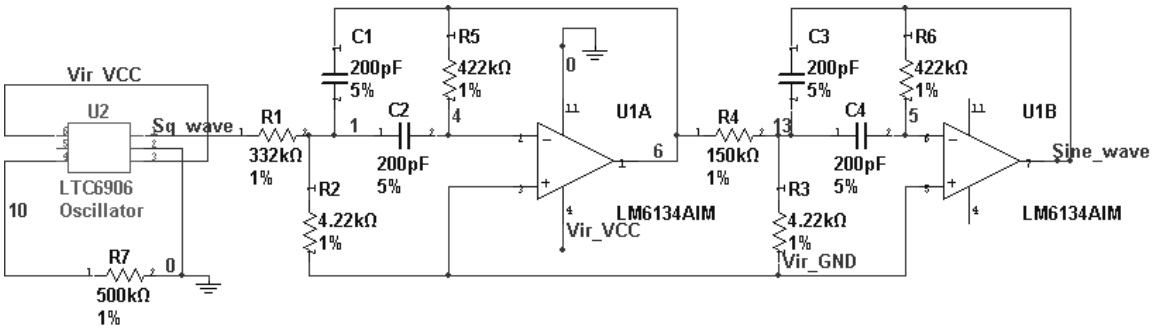

Figure 5-3: Low power sinusoidal generator

5.2.2.3 Low power constant current source

Fig. 5-4 illustrates the circuit used for the constant current source. The 1MΩ resistor in the feedback path of the operational amplifier guarantees that it never enters an open loop state. The 1μF capacitors in series with the signal path provide a means for the DC elimination from the AC sinusoidal stimulus signal entering the catheter (the heart). Additional elimination of the extremely low frequency signals (close to DC) is provided by the pass high pass pole provided by the C7-R12 combination. Node "0" in all the circuit diagrams refers to the "real" power ground (0V). All resistors used are precision metal – film resistors (1% tolerance) and all capacitors are ceramic capacitors (10% tolerance).

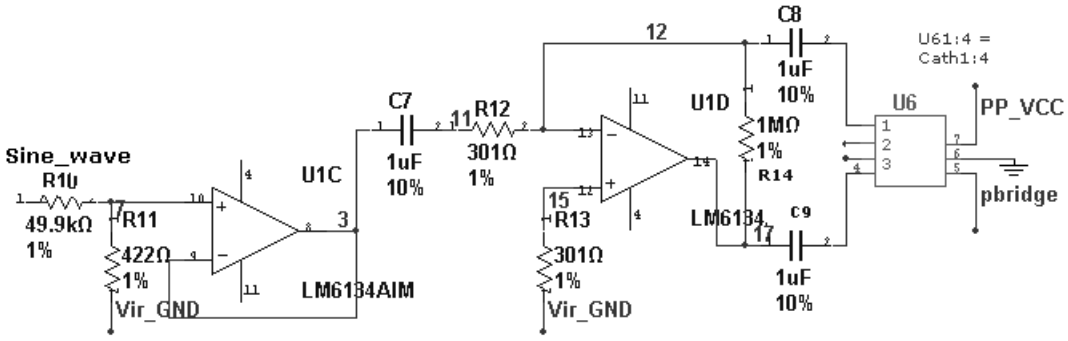

Figure 5-4: Low power constant current source

5.2.2.4 Low power post-catheter signal processing

The differential signal from the inner two electrodes (2 and 3) of the catheter is processed by a differential gain stage. A low power instrumentation amplifier (INA331IDGK) was used with a gain of 10V/V. This was followed by a 20 kHz band pass filter (Q=1, Sallen Key Multiple Feedback architecture). This is followed by a gain stage and buffering. The output is the phase-shifted, amplitude-modified signal used for impedance magnitude calculation. This also serves as the second input for the phase detector chip. The node "0" in all the circuit diagrams refers to the "real" power ground (0V). All resistors used are precision metal – film resistors (1% tolerance) and all capacitors are ceramic capacitors (10% tolerance).

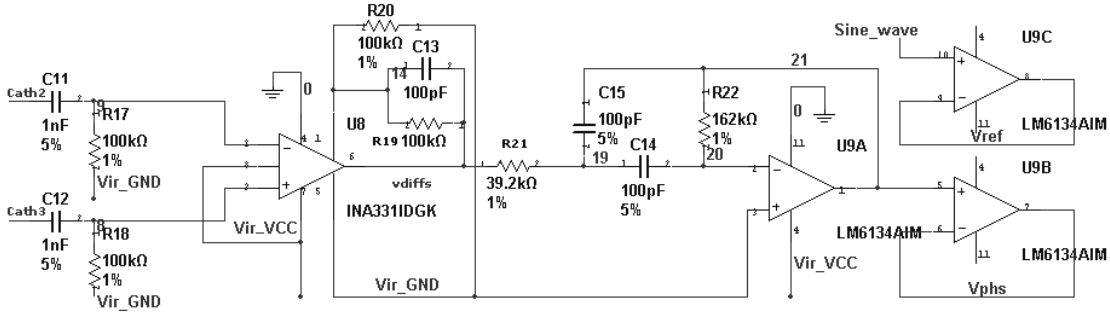

Figure 5-5: Low power post-catheter signal processing

5.2.2.5 Impedance magnitude calculation

The impedance magnitude calculation circuit is illustrated in Fig. 5-6. This essentially is a full wave rectification stage followed by a low pass filter at 25 Hz (Q=0.5803, Sallen-Key Multiple feedback architecture). U14 is a single chip package containing 2 pair of diodes. This is convenient because it was customized for rectifier circuits, thereby reducing area.

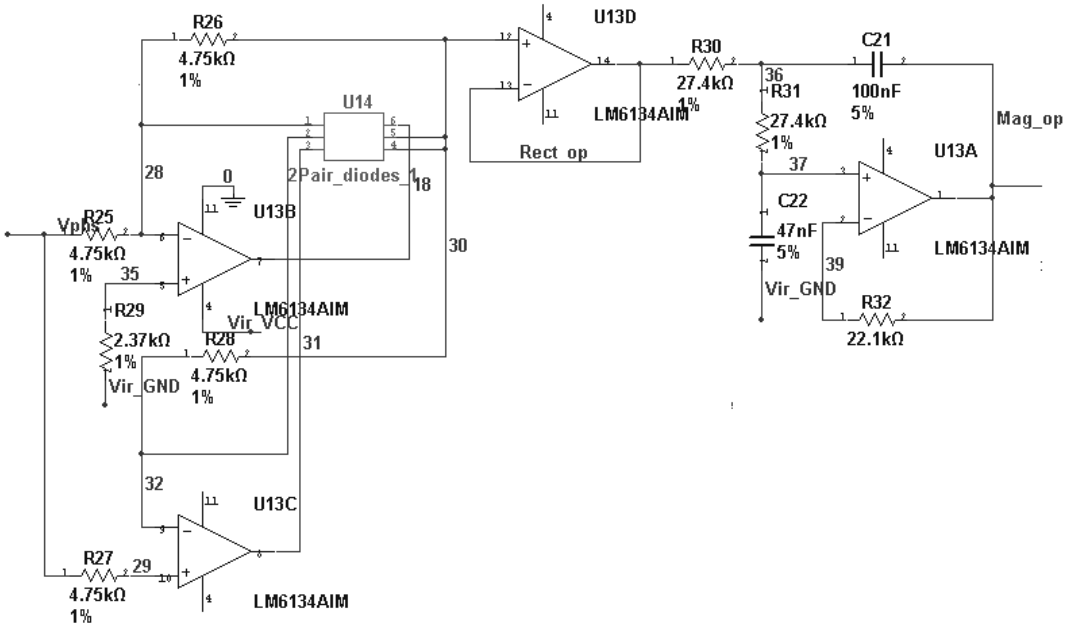

Figure 5-6: Impedance magnitude calculation

5.2.2.6 Low power phase estimation

To obtain the phase difference between the reference voltage signal and the phase-shifted post-processed signal, an RF/IF Phase detector chip (AD8302) was used in its low-frequency" topology.

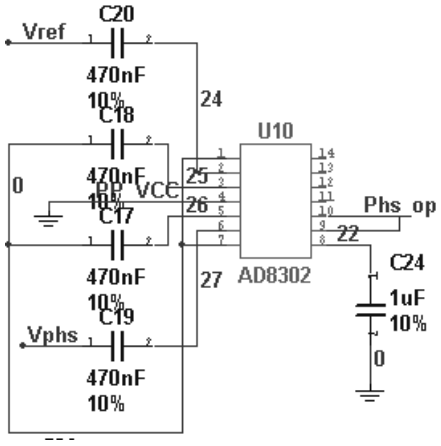

Figure 5-7: Low power phase estimation

5.2.2.7 Low power pressure calculation

Fig. 5-8 illustrates the schematic for the LP pressure calculation. Two arms of the Wheatstone bridge are part of the pressure transducer. The remaining two arms are completed using a resistor network. The regulator supplies a constant voltage (3.6V) across the bridge. The differential voltage is sensed using the LP instrumentation amplifier (INA331IDGK), followed by low pass filter (25 Hz, Q=0.52, Sallen-Key Multiple feedback architecture) and a gain stage.

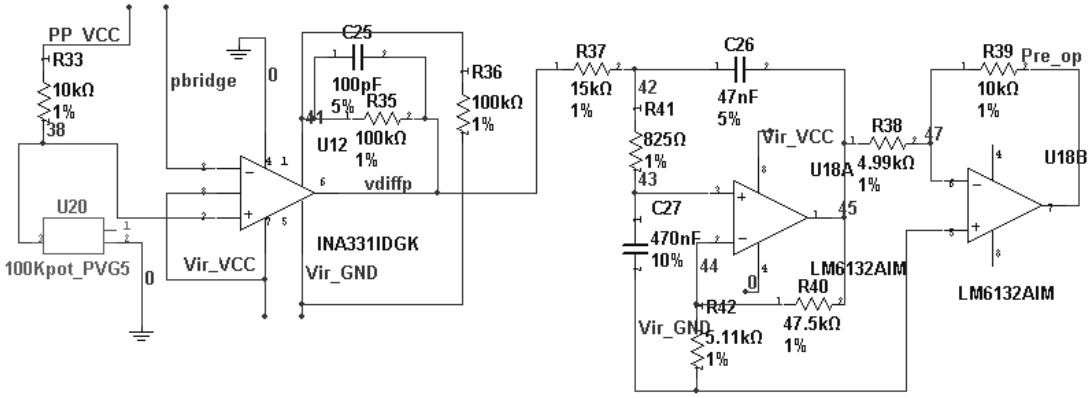

Figure 5-8: Low power pressure measurement

5.3 PCB LAYOUT

After some bench testing of the prototype, a 4-layer PCB was designed and fabricated (PCBFabExpress) using the above schematics. To save real estate, all four layers were dedicated to signals. The final PCB outline was 1.78'' x 1.54''. Fig. 5-9 is the 2-D top view of the PCB and Fig. 5-10 is a 3-D view of the PCB (generated by National Instruments Ultiboard software).

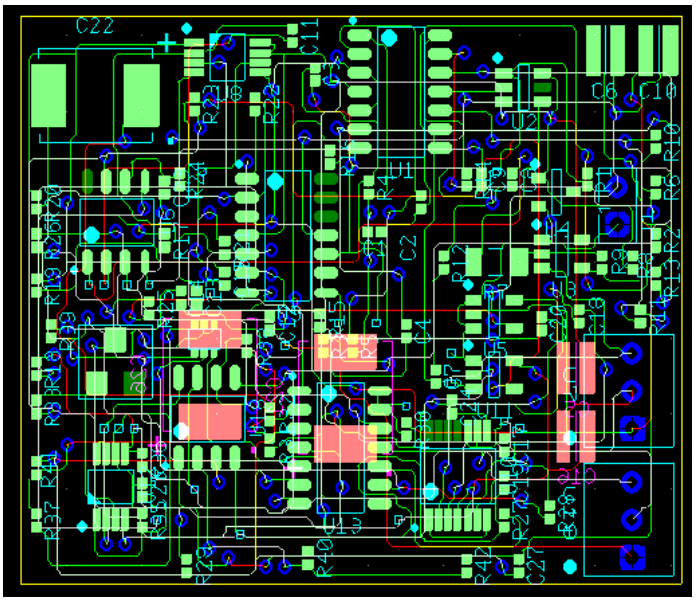

Figure 5-9: 2-D top view of PCB

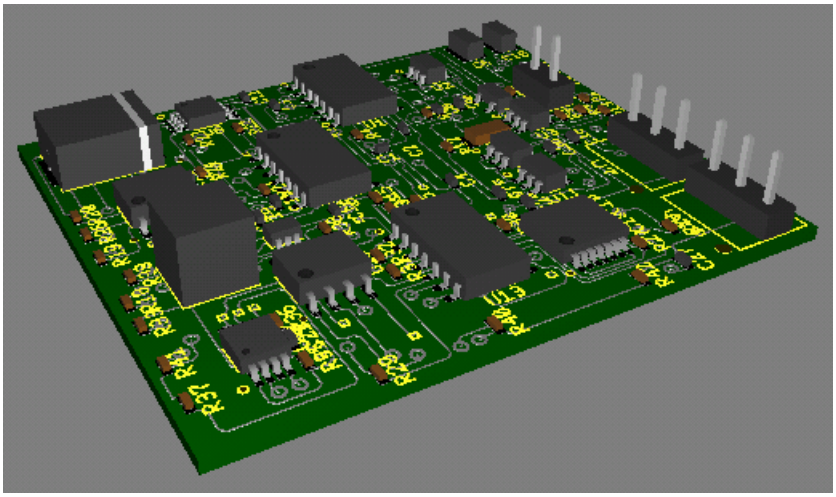

Figure 5-10: 3-D view of PCB

5.4 BENCH TESTING

5.4.1 Impedance magnitude calibration

The impedance magnitude was calibrated with four known precision resistors connected as the test load (in place of the catheter). The resistor was placed between

Electrodes 2 and 3 and Electrode 1 was shorted to Electrode 2 and similarly Electrode 4 was shorted with Electrode 3. Thus, this represented a purely resistive load. The resistors were chosen to represent the entire range of impedance magnitudes that can be expected from a rat LV P-V experiment: 500 Ω to 2 kΩ. The resistors were 1% metal-film resistors. Fig. 5-11 is a representative impedance magnitude calibration curve obtained from the rat backpack instrumentation.

5.4.2 Phase calibration

To calibrate the phase detection chip, known parallel R-C load combinations were connected as the test load (in place of the catheter); the phase difference was calculated at f=20 kHz. Fig. 5-12 is a representative phase calibration curve obtained from the rat backpack instrumentation.

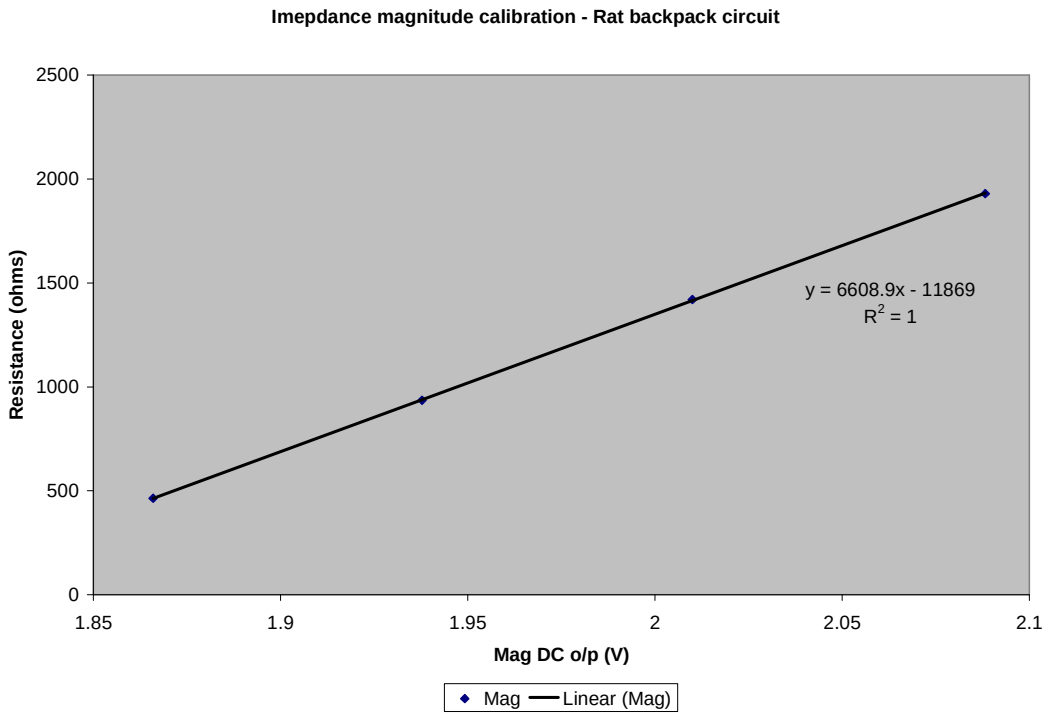

Figure 5-11: Impedance magnitude calibration curve

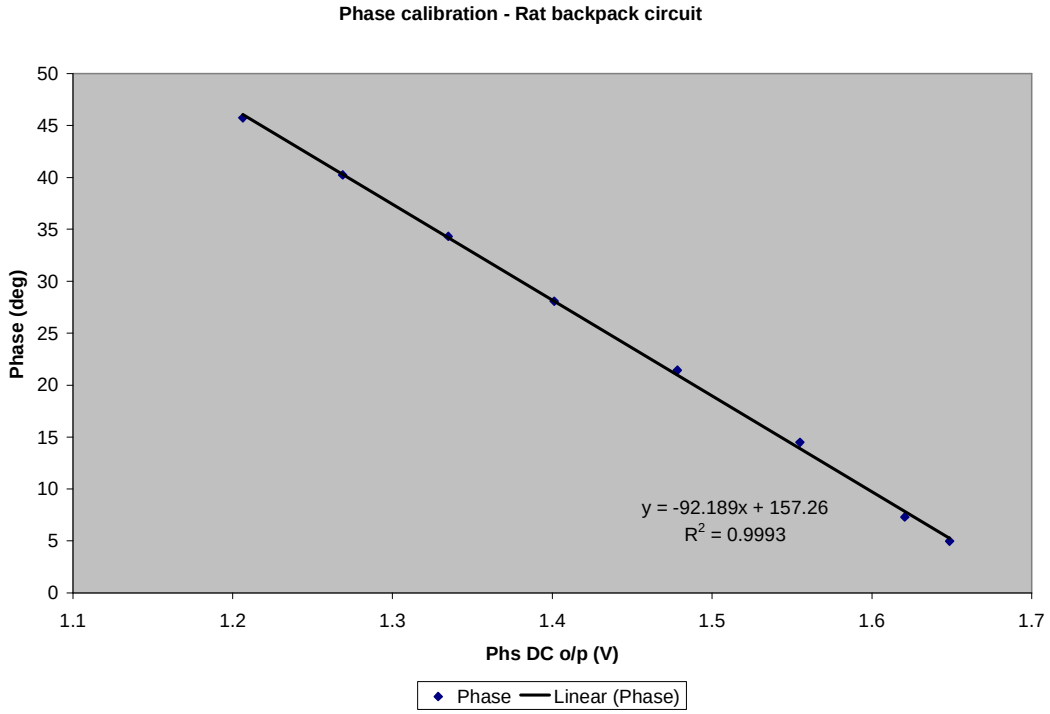

Figure 5-12: Phase calibration curve

5.4.3 Saline calibration

In order to eliminate the effects of the catheter, the catheter was connected to the circuit and the electrodes were submerged into saline solutions of known conductivity. Table 5-1 represents a typical saline calibration table.

Cond. (uS/cm)	Mag (Ω)	Phs (deg)	MagY (S)	MagY (μS)	F (cm)	F (m)	K (1/m)	K (1/cm)	ImY (μS)	ReY (μS)
1025	1620	18.0	0.000617	617	0.573	0.00573	175	1.75	191	587
1882	1341	15.8	0.000746	746	0.381	0.00381	262	2.62	204	718
2860	632	6.5	0.001582	1582	0.550	0.00550	182	1.82	180	1572
3540	610	6.1	0.001639	1639	0.460	0.00460	217	2.17	175	1630
5690	481	4.0	0.002079	2079	0.365	0.00365	274	2.74	145	2074
					Avg	0.00466	215			

Table 5-1: Saline calibration table

Where Cond. is the conductivity of the saline solution, Mag is the impedance magnitude measured using the backpack, Phs is the measured phase using the backpack, MagY is the admittance magnitude, F is the field form factor and K is the probe constant. F and K are estimated from the real part of admittance (ReY) and the conductivity of the saline solution [6]. ImY represents the imaginary component of the admittance. These table values were used in the conversion of the LV admittance data into volume using Wei's equation [6].

5.4.4 Dynamic testing

To simulate the beating of the rat heart, the backpack circuit was tested for dynamic characteristics. To simulate the changing magnitude of impedance, an amplitude – modulated (AM) signal was applied. The amplitude varied at a rate of 5 Hz (300 beats/minute) on the 20 KHz stimulus. To test the phase variation, the reference signal at 20 kHz was generated along with a phase modulated signal at a rate of 4 Hz (240 beats/minute) over the same stimulus signal at 20 kHz. These two signals were created in LabVIEW^{TM} (National Instruments (NI), Austin, TX) and output via the DAC channels of a fast sampling ADC (NI PCI-6110, 5 MS/s/channel) capable of outputting upto 2.5 MS/s on two simultaneous 16-bit, analog output channels. Fig. 5-13 shows the output of an oscilloscope tracing of the magnitude output (in yellow, top signal) and the actual AM signal (in green, bottom signal). Fig. 5-14 shows the phase output (in green, top signal) and the actual reference and PM signal (in pink and yellow, bottom signals). The same screen was zoomed in on the oscilloscope for clarity purposes and shown on Fig. 5-15.

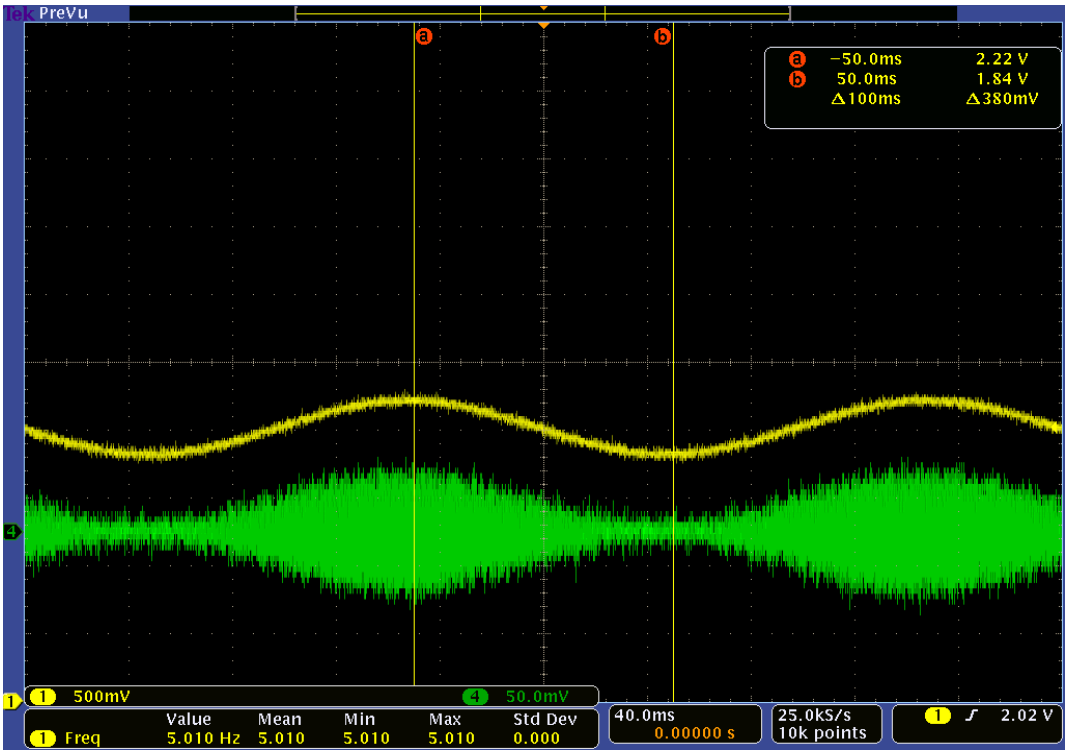

Figure 5-13: Impedance magnitude - AM modulation: 5Hz over 20kHz

5.4.5 Battery life estimation

To estimate the battery life, the 3.7V lithium – ion cell rated at 625 mAh was connected to the circuit and the circuit was allowed to run for more than 24 hours. Current data was collected using Chart during the entire time at a rate of 1 Hz. Table 5-2 summarizes the results.

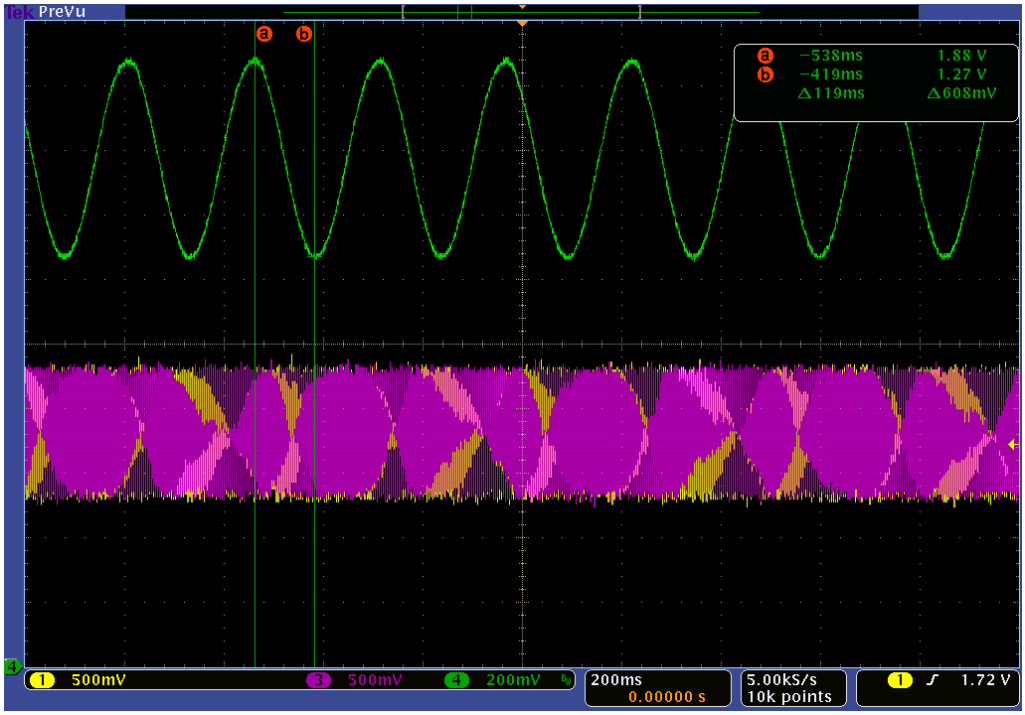

Figure 5-14: Phase – PM modulation: 4 Hz over 20 kHz

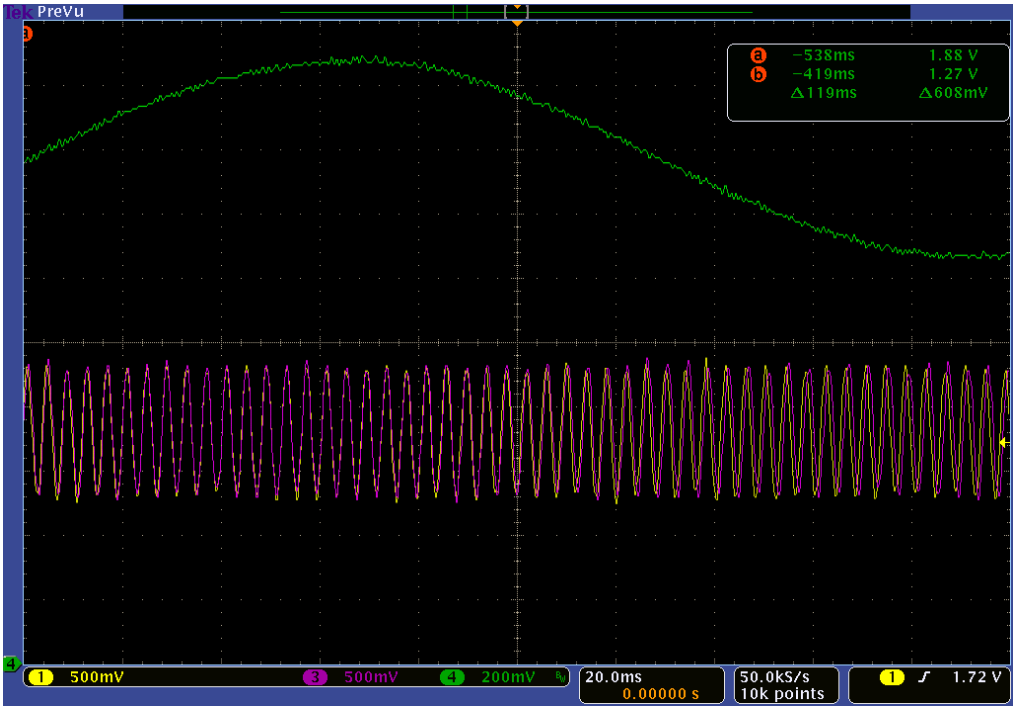

Figure 5-15: Phase – PM modulation: 4 Hz over 20 kHz (Zoomed In)

Current type	Current (mA)	Bkpk. Reg.	Bkpk.	Mic. Reg.	Mic.	Mic. State	ADC	TxRx	Duration (s)	Avg. current mA/hr.
Bkpk. ON current	41.6	ON	ON	ON	ON	LPM0	ON	ON	360	4.16
Bkpk. OFF current	22.3	OFF	OFF	ON	ON	LPM3	OFF	OFF	3240	20.07
									Total	**24.23**
									Battery life (hrs.)	**25.8**

Table 5-2: Battery life estimation

In Table 5-2, "Mic." refers to the microcontroller, "TxRx" refers to the transceiver, "LPM" refers to Low Power Mode of the microcontroller, and "Bkpk." Refers to backpack. The results show that the battery can last for 25.8 hours. Actual results also prove the same.

5.4.6 Backpack weight

Finally, Table 5-3 summarizes the weight of the individual components making up the backpack. The lithium-ion cell has been highlighted in red to indicate that the weight is dominated by the weight of the lithium – ion cell (about 66.7%).

Item	Weight (g)	% of weight
Instrumentation PCB weight	7.49	27.0
Mup + TxRx PCB weight	1.77	6.4
Total circuit weight	**9.26**	
Li ion cell weight	18.5	**66.7**
Backpack weight	**27.8**	

Table 5-3: Backpack weight distribution

5.5 WIRELESS TELEMETRY

The choice of wireless telemetry was critical because the battery needs to power the microcontroller/TX pair. Therefore, it has to be low power. Also, the rat's heart rate varies from about 150 beats/min (2.5 Hz) to about 300 beats/min (5 Hz). The signals that

have to be transmitted are of a very low frequency (<5 Hz). The required data rate is very low.

The Texas Instruments' (TI) eZ430-RF2500 kit was ideal for this application (Texas Instruments, Dallas, TX). This was a complete kit with a MSP430F2274 microcontroller and CC2500 2.4 GHz wireless transceiver. The key points which motivated this choice were:

a) The MSP430F2274 microcontroller was ultra-low power drawing a maximum active (ON) current of 390 μA. In the standby (OFF) mode, it draws a maximum current of 1.4 μA.

b) The microcontroller had 8 10-bit, 200 ksps ADCs for use.

c) The CC2500 transceiver was also of the low power type with programmable data rates from 1.2 to 500 kbps drawing a typical current of 21.2 mA during TX.

d) Ultra low power star network stack, called SimpliciTI™, protocol.

e) Easily programmable/debuggable with the convenience of USB. Sample code already was setup to transmit and receive low data rate temperature sensor data, and modified to use in these experiments.

CHAPTER 6

Acute and Chronic Animal (Rat) Studies

6.1 Objectives of Animal (Rat) Studies

The main objective of the animal (rat) studies is to prove the viability of chronic LV P-V studies in freely roaming, concious rats using the admittance technique to obtain volumes for the first time in ambulatory animals.

The animal experiments were divided into three sets. The first two sets were performed with rats on the surgical bench (acute studies). The third set of experiments was the 24-hour chronic studies performed with the rats roaming freely in the cage.

Volumes were also calculated using cuvette-based volume calibration.

All rats used for all the studies were of the WKY strain (white (albino) color).

Special acknowledgement: I would like to thank Mr. Danny Escobedo, chief animal surgeon, UTHSCSA for his expertise with the animal surgery. All animal surgeries were performed by him.

6.2 Study 1: Surface Probe Study

The first study involved the estimation of myocardial electrical properties (σ and ε) using the epicardial surface probe. This study was also used to estimate the baseline electrical conductivity of rat blood. The following protocol was used for this acute study with the rat placed on a temperature controlled surgical bench. (N=4 rats)

a) Rats were anesthetized using an isoflurane container.
b) The body weight and sex were recorded.
c) After the rats were placed on the surgical bench, the anesthesia was maintained using isoflurane delivered via a respirator (Harvard Rodent

Ventilator Model 683, Harvard Apparatus, Holliston, MA) at a rate of 70 breaths/min.

d) The chest was opened via median sternotomy.
e) The epicardial surface probe was placed on the top of the LV using a micro-manipulator.
f) The impedance magnitude and phase were measured using the backpack instrumentation and recorded using the Chart Software (AD Instruments, Bella Vista, NSW, Australia).
g) After the impedance measurements, 4-5 cc. of blood was extracted from the LV using a 23-gauge needle and placed into a vial. This vial was placed in a 37^{o}C water bath (Precision water bath, Thermo Fisher Scientific, Waltham, MA). Using the surface probe, admittance measurements were made to estimate the electrical conductivity of blood.
h) Finally, the rat was euthanized. The heart weight and LV weight were measured.

6.3 STUDY 2: HYPERTONIC SALINE, 2D ECHO AND FLOW STUDIES

The second study was a critical study. This study is used to calibrate the admittance technique with standards for volume measurement using 2-D echocardiography and ultrasonic flow probe. It also compares admittance-derived volumes with volumes derived from previously used techniques such as conductance (magnitude–only) derived volume, which involves myocardial contribution estimation using a hypertonic saline bolus administration. [7] Again, this was an acute study with the rat placed on the temperature controlled surgical bench. (N=7 rats).

a) Rats were anesthetized using an isoflurane container.
b) The body weight and sex were recorded.

c) After the rats were placed on the surgical bench, the anesthesia was maintained using isoflurane delivered via a respirator at a rate of 70 breaths/min.

d) The jugular vein was accessed. A small neck incision was made to expose the jugular vein.

e) An IV catheter was placed into the jugular vein for later administration of IV hypertonic saline.

f) A similar incision was made to expose the right carotid artery.

g) The catheter was guided into the LV via the carotid artery.

h) The impedance magnitude and phase were measured using the backpack instrumentation and recorded using the Chart Software. LV Pressure was also measured in parallel using a Scisense Pressure Control Unit, FP891B (Scisense Inc., London, ON, Canada). This serves as the baseline measurement.

i) After the measurements, the rats were placed on their back. The chest was shaved and gel (Parker Aquasonic 100 Ultrasound Transmission Gel, Parker Laboratories Inc., Fairfield, NJ) was applied on the chest.

j) The 2-D echocardiogram (Philips HDI 5000CV) probe was placed on the top of the beating heart.

k) A 2-D echocardiogram was performed through a closed chest (CC Echo). A short-axis M-mode picture was taken so that the LV EDV, LV ESV, and SV can be determined from it. A long-axis picture was also taken for catheter placement reference.

l) After the CC Echo, hypertonic saline boluses were injected via the incision made on the jugular vein. A total of three 0.2 mL boluses of 3%

hypertonic saline (3g of NaCl in 100mL of solution) and two 0.2 mL boluses of 10% hypertonic saline were administered in a sequence.

m) During each bolus administration, the impedance magnitude and phase data were measured (at 20 kHz) using the backpack instrument and recorded using Chart software.

n) The chest was opened via median sternotomy.

o) Using a specially designed apparatus, a plastic bag was placed on top of the open chest. Saline was poured into this bag (as an offset). The 2D echo probe was placed inside this saline filled bag on top of the beating heart.

p) A 2-D echocardiogram was performed through the open chest (OC Echo). A short-axis M-mode picture was taken so that the LV EDV, LV ESV, and SV can be determined from it.

q) After the OC echo, an ultrasonic rat-sized flow probe (Transonic flow probe, Serial # 2.5PSB1154, Transonic Systems Inc., Ithaca, NY) was placed around the ascending aorta.

r) Using a flowmeter (TS420: Transit time perivascular flowmeter, Transonic Systems Inc., Ithaca, NY), that was connected to this flow probe; the aortic blood flow was measured and recorded using Chart.

s) After the flowprobe measurements, 4-5 cc. of blood was extracted from the LV using a 23-gauge needle and placed into a vial. This vial was placed in a 37^{o}C water bath. Using the surface probe, admittance measurements were made to estimate the electrical conductivity of blood.

t) Finally, the rat was euthanized. The heart weight and LV weight were measured.

6.4 STUDY 3: CUVETTE-BASED VOLUME CALIBRATION

Another traditional approach to calibrate small volumes was to drill small cuvettes in a Plexiglas block and map the conductance measured to the actual volume of the chamber.

To perform this experiment, holes were drilled in a Plexiglas block. The holes were deep enough so that the entire catheter would submerge in it completely. 7 different holes were drilled. The diameters of the holes ranged form 2.79 mm to 10.67 mm. These holes were filled with saline solutions (two different experimental solutions: 0.4 and 0.5 S/m). The catheter was submerged in each one of these holes for each of the solutions (a total of 7*3 = 21 measurements). Impedance magnitude was measured to determine the volume calibration constant (α).

6.5 STUDY 4: CHRONIC RAT STUDIES

This was the final objective of this dissertation. This was first time a chronic (24-hour) study was performed to obtain admittance–derived volumes from conscious, freely moving rats in a cage.

Several factors/hurdles had to be surmounted to get this experiment working correctly. Battery life, weight of the backpack, the catheter placement surgery, wireless transmission, the aggressive nature of rats, sleepless nights watching the rat, and catheter breakage (due to bends) are only a few of the challenges that were met during this experiment. Six successful preps were obtained from these 24-hour chronic studies.

The following protocol was used for the 24-hour chronic studies.

a) Rats were anesthetized using an isoflurane container.
b) The body weight and sex were recorded.

c) After the rats were placed on the surgical bench, the anesthesia was maintained using isoflurane delivered via a respirator at a rate of 70 breaths/min.

d) A 2-D echocardiogram was performed through a closed chest (CC Echo). A short-axis M-mode picture was taken so that the LV EDV, LV ESV, and SV can be determined from it. This served as the baseline starting reference for the LV volume.

e) A small incision was made on the back of the rat. The catheter was passed through this.

f) The rat was flipped on the back and the catheter was passed to midline of the neck.

g) The carotid artery was exposed and the catheter was guided into the LV. A tie in was made close to the neck incision.

h) The rat was flipped to make it lie face down. The rat was then placed in a jacket (Guinea-pig jacket, Catalog # 620069, Harvard Apparatus, Holliston, MA).

i) The complete backpack (with the lithium ion cell, circuit board and TX) was placed in a bubble wrap and placed between the rat's body and the jacket.

j) The jacket was then closed and umbilical tape was used to secure the backpack inside the jacket.

k) The rat was placed in a cage for anesthesia recovery.

l) Impedance magnitude, phase and pressure was measured, once every 2 minutes, using the backpack, transmitted wirelessly and the RX converted and recorded the data on a laptop for 24 hours.

m) The rat was monitored during the entire time with periodic water and food feeding. It was made sure that the rat would not attempt to remove the backpack.

n) After 24 hours had elapsed, the rats were placed on the surgical bench, the anesthesia was maintained using isoflurane delivered via a respirator at a rate of 70 breaths/min.

o) A 2-D echocardiogram was performed through a closed chest (CC Echo). A short-axis M-mode picture was taken so that the LV EDV, LV ESV, and SV can be determined from it. This served as the end of the experiment reference for the LV volume.

p) After the CC echo measurements, the chest was open via median sternotomy.

q) 4-5 cc. of blood was extracted from the LV using a 23-gauge needle and placed into a vial. This vial was placed in a 37^{o}C water bath. Using the surface probe, admittance measurements were made to estimate the electrical conductivity of blood.

r) Finally, the rat was euthanized. The body weight was re-measured.

s) The heart weight and LV weight were measured.

6.6 ANIMAL STUDIES

All experiments were approved by the IACUC (The Institutional Animal Care and Use Committee).

Fig. 6-1 is a picture of the rat placed on the experiment surgical bench. This bench is temperature controlled (maintained at 37^{0}C). Also pictured is the respirator that has controlled flow of oxygen and isoflurane.

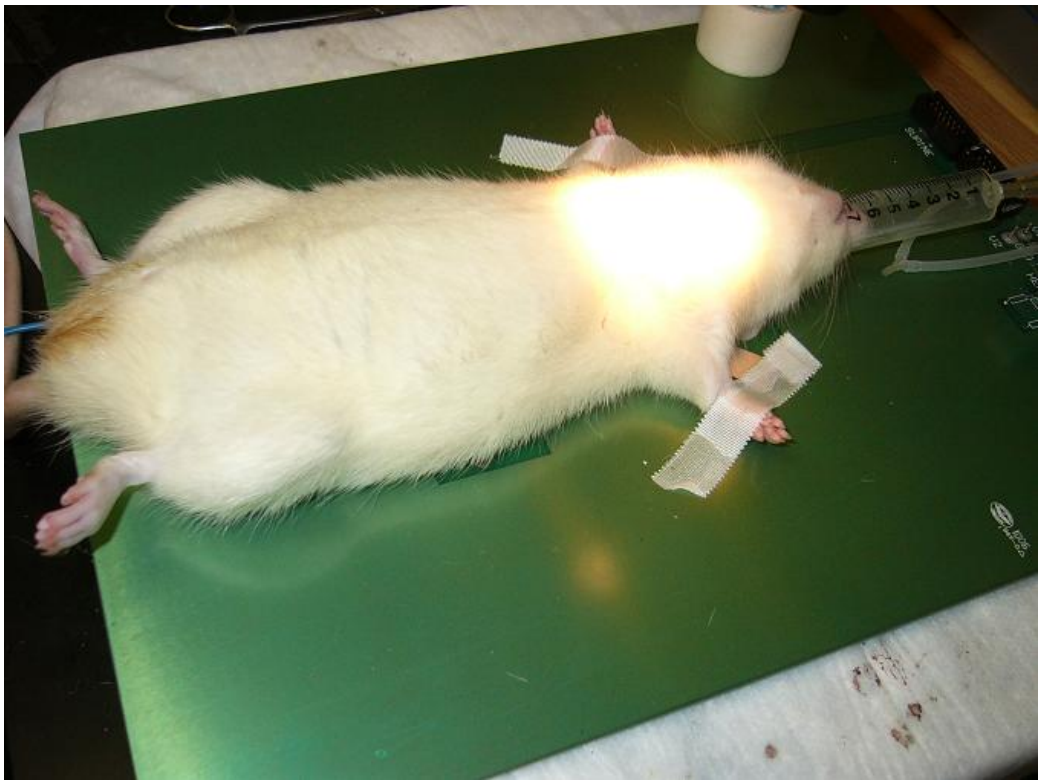

Figure 6-1: Rat placed on the surgical bench

Fig. 6-2 shows the placement of the rat-sized epicardial surface probe (using a micro manipulator) on the open-chest LV. This was used for the estimation of the myocardial electrical properties measurement.

Fig. 6-3 shows the placement of the 2-D echo probe on top of the ultrasound gel for the closed chest (CC) echo measurements. This 2-D echo was used as the standard of comparison for the closed chest admittance derived volumes (EDV, ESV and SV).

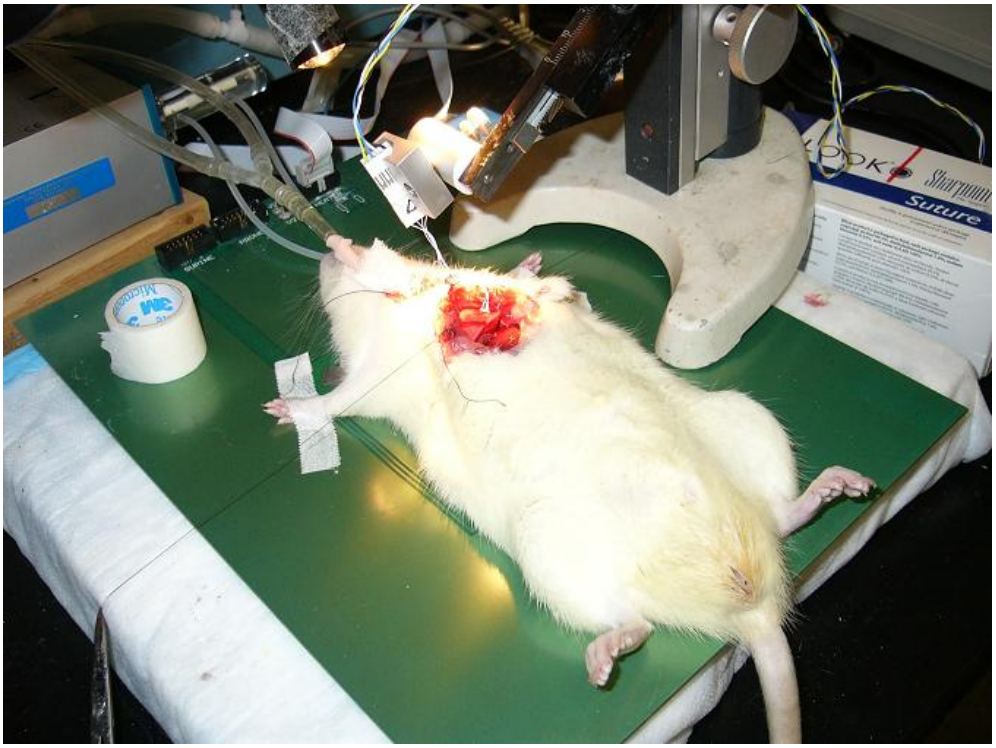

Figure 6-2: Placement of the epicardial surface probe on the LV

Fig. 6-4 is the similar setup of 2-D echo for the open chest conditions. The saline offset plastic bag can be seen in this picture into which the 2-D echo probe was placed. In addition to the flow meter, the OC echo provides a standard of comparison for the admittance derived OC volumes.

Fig. 6-5 is the picture of the ultrasonic flow meter placed in the ascending aorta for the measurement of aortic blood flow.

Fig. 6-6 and Fig. 6-7 are pictures of the process of putting a jacket onto the rat for the chronic studies. The backpack circuit was then placed in between the jacket and the rat and secured using umbilical tape.

Fig. 6-8 and Fig. 6-9 are pictures of the rat in the cage after the anesthesia wore off in the chronic studies. Not pictured is the laptop placed 4 feet away gathering

impedance magnitude, phase and pressure data. The rats were monitored for a 24-hour period within this cage.

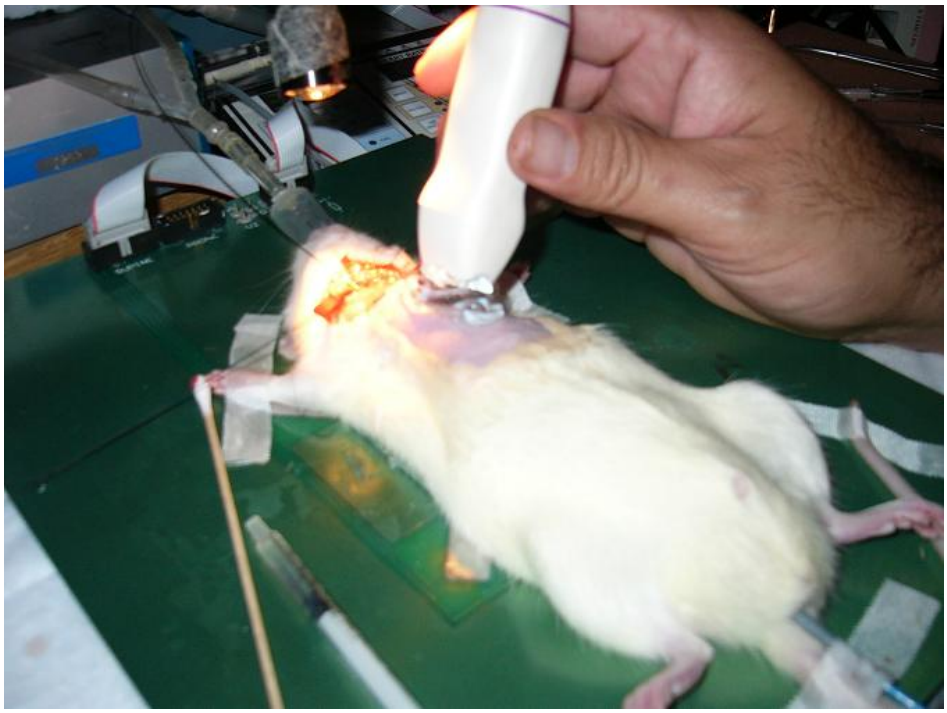

Figure 6-3: Placement of the 2-D echo probe for the closed chest (CC) echo

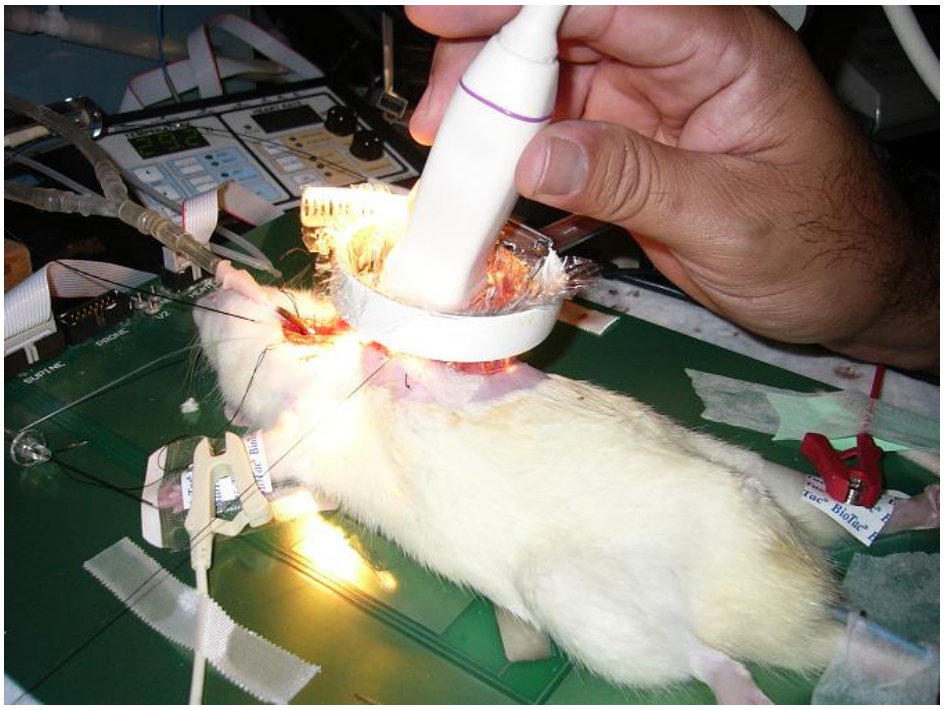

Figure 6-4 Placement of the 2-D echo probe for the open chest (OC) echo

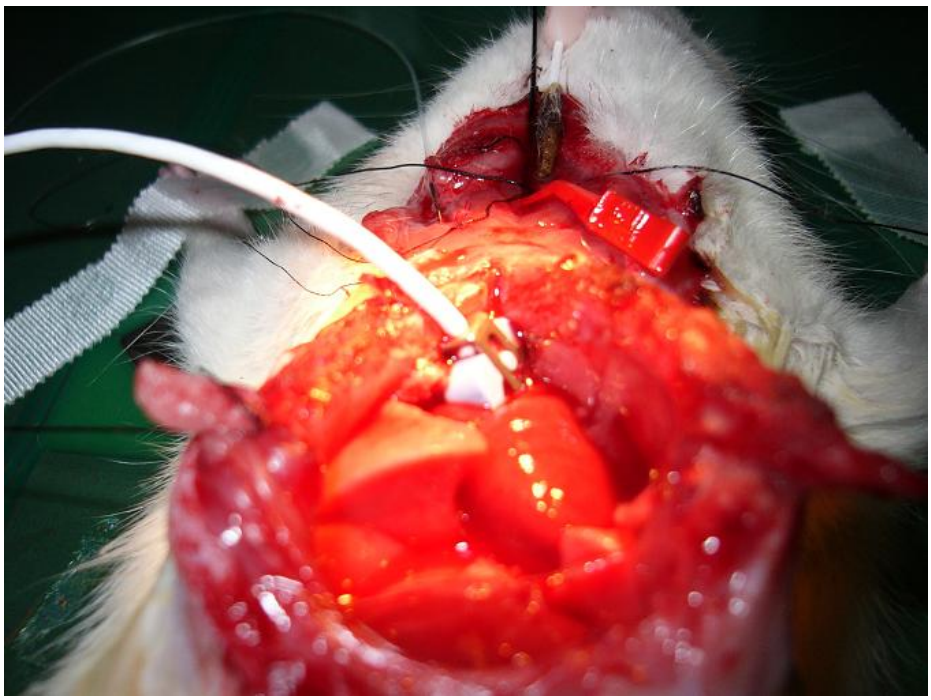

Figure 6-5 Placement of the flow probe on the ascending aorta

Figure 6-6 Ambulatory, concious rat in cage for chronic study

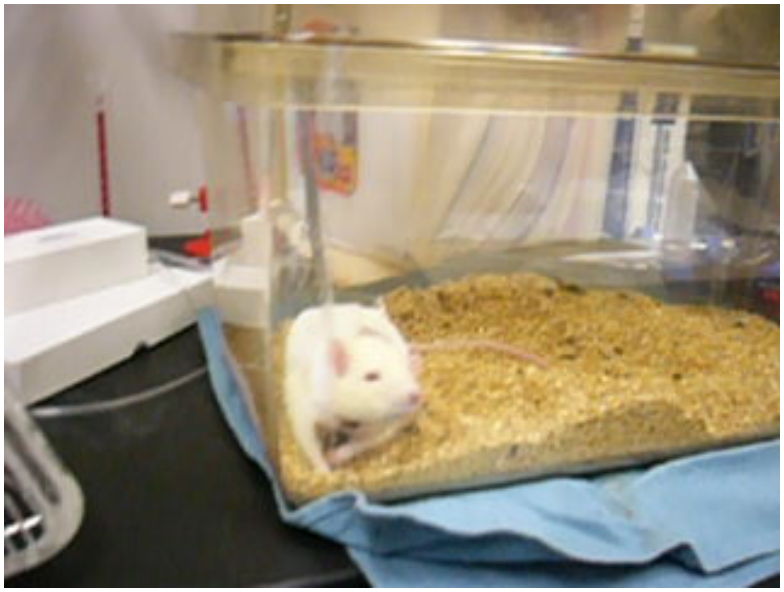

Figure 6-7 Rat freely moving in cage during chronic study

CHAPTER 7

Results and findings from animal studies

7.1 STUDY 1: SURFACE PROBE STUDY

In this study, the electrical properties of the blood and myocardium are measured. Table 7-1 summarizes the details of the rats used for this study. Here HW refers to the heart weight and LVW refers to the LV weight. Table 7-2 summarizes the results of the estimates of the myocardial and blood electrical properties. The procedure for this estimation is described in Chapter 2 and by Raghavan *et al*. [6]

Rat #	Sex	Weight (g)	HW (mg)	LVW (mg)
1	M	318	994	747
2	M	338	1001	780
3	M	325	1010	802
4	M	308	815	650
Mean		322	955	745
SD		12.6	93.6	67.1

Table 7-1: Details of rats used for Study 1

Rat #	σ_b(S/m)	σ_m(S/m)	ε_r
1	0.525	0.184	16670
2	0.581	0.164	17578
3	0.563	0.210	12538
4	0.558	0.190	13530
Mean	0.557	0.187	15079
SD	0.023	0.019	2424
SD%	4	10	16

Table 7-2: Myocardial and blood electrical properties: Results summary

In the above table, σ_b is the blood electrical conductivity (S/m) and σ_m is the myocardial electrical conductivity (S/m) and ε_m is the myocardial relative permittivity.

7.2 STUDY 2-A: CLOSED – CHEST (CC) 2D ECHO, ADMITTANCE, HYPERTONIC SALINE, AND CUVETTE STUDIES

a) In this part of the study, CC LV volume is obtained using the admittance technique (Wei's equation, Equation (2)). This will be termed as "Admittance P-V SV Adj." volume.

b) Using previously established techniques, parallel conductance (G_p) is estimated. In this technique, the end-systolic conductance (G_{ES}) and end – diastolic conductance (G_{ED}) are determined during the hypertonic saline administration. Assuming a linear relationship, the slope and intercept of the equation describing G_{ED} and G_{ES} can be found. The G_p is then estimated as the conductance where it intersects the line of identity ($G_{ED} = G_{ES}$). The assumption being at this point, the complete contribution to the signal arises from the myocardium [7]. G_p was estimated using the average of 2 different hypertonic saline concentration (3% and 10 %) boluses. The calibration factor α is obtained using the ratio of the derived stroke volume (using Baan's equation (1) with a first pass assumption of $\alpha = 1$) to the actual stroke volume (obtained using 2-D echo). Once α and G_p are obtained, volume is re-estimated using Baan's equation (1). This will be termed as "Cond P-V SV Adj." volume.

c) As a third measure of volume, α and V_p (parallel volume) are obtained from the cuvette experiment. A slight modification of Baan's equation (1) leads to the equation

$$\alpha Volume + \alpha Vp = \rho L^2 G \qquad (5)$$

Thus, plotting $\rho L^2 G$ on the Y –axis vs. Volume (cuvette volume) on the X-axis, one can derive the V_p (parallel volume) and α. Using this V_p and α and Baan's equation (1), the cuvette – derived volume is obtained. This will be termed as "Cuv. Der. Vol.".

d) All the above derived volumes are compared to CC Echo (End diastolic volume (EDV), End – systolic volume (ESV) and stroke volume (SV)). The M-mode 2-D echo images were taken and the LV volume was traced using software. Then the inside LV wall distances were used to obtain the estimates of ESV, EDV and SV. This was considered as the standard for comparison.

Table 7-3 summarizes the details of the rats used for this study (and the follow-on open-chest (OC) study).

Rat #	Sex	Weight (g)	HW (mg)	LVW (mg)	Notation
1	M	278	765	643	Ex4, R1
2	M	272	802	628	Ex4, R2
3	M	214	811	688	Ex6, R1
4	M	235	770	590	Ex6, R2
5	M	232	735	545	Ex7, R1
6	M	257	806	640	Ex7, R2
7	M	235	711	568	Ex7, R3
8	M	247	747	594	Ex8, R2
9	M	315	944	736	Ex8, R3
Mean		254	788	626	Exper #
SD		30.6	67.7	59.9	Rat #

Table 7-3: Details of rats used for Study #2 (acute studies)

Table 7 – 4 summarizes the estimation of Gp (parallel conductance) using the two different hypertonic saline (HS) concentrations (3% HS and 10% HS).

		Gp (uS)	
Expt	**Rat**	**3%-10% Avg**	**3%-10% SD**
4	1	873	100
	2	489	-
6	1	766	440
7	1	907	19.4
	2	520	42.8
	3	1022	32.2
8	2	589	427

Table 7-4: Hypertonic saline studies: Gp estimation

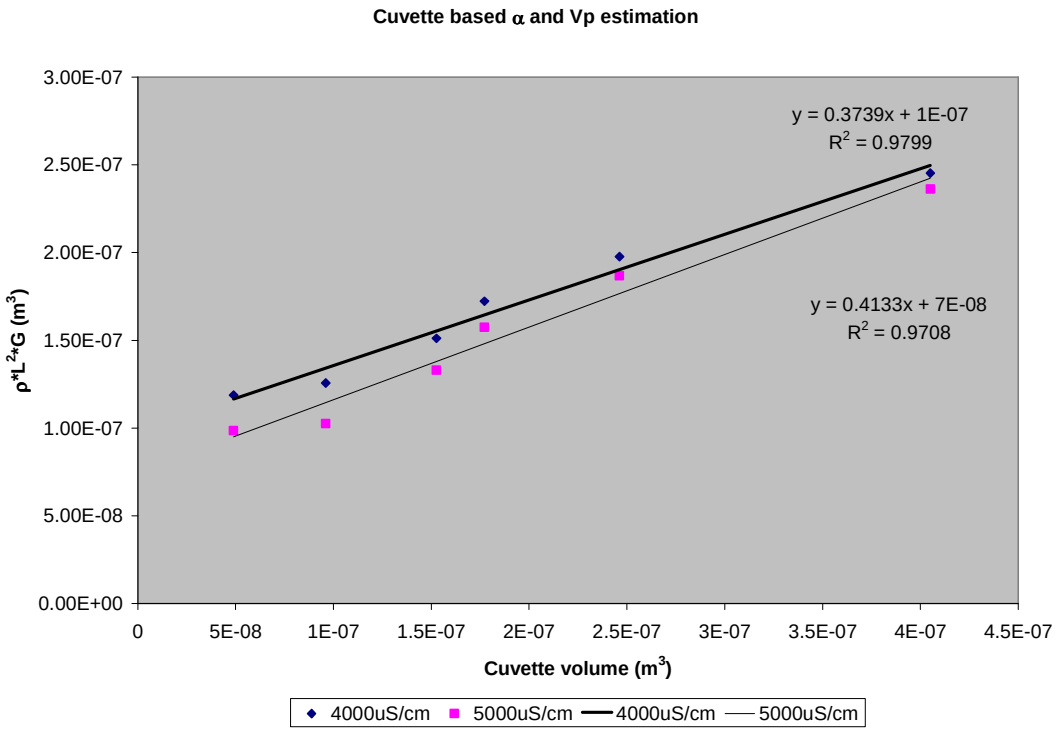

Figure 7-1: Slope-intercept based α and V_p using cuvettes

Fig. 7-1 shows the graphs of cuvette based estimation of α and V_p. Two different saline conductivity solutions were chosen (0.4 S/m and 0.5 S/m). The final α and V_p was the average of the two estimates. Using the above graph and Equation (5) α was estimated to be 0.394 and Vp was estimated as 218 μL.

Table 7-5 is a summary of the 2-D echo EDV, ESV, SV and ejection fraction (EF) mean estimates and a comparison of this versus admittance, conductance and cuvette based mean volume estimations.

Expt	Rat	Echo CC EDV Mean (uL)	Echo CC ESV Mean (uL)	Echo CC SV Mean (uL)	Echo CC EF Mean (%)	Admittance CC EDV Mean (uL)	Admittance CC ESV Mean (uL)	Admittance CC EF Mean (%)	Conductance (HS) CC EDV Mean (uL)	Conductance (HS) CC ESV Mean (uL)	Conductance (HS) CC EF Mean (%)	Cuvette CC EDV Mean (uL)	Cuvette CC ESV Mean (uL)	Cuvette CC EF Mean (%)
4	1	423	63.1	360	85.3	391	31	92.1	553	193	65.1	207	77.6	62.4
	2	185	35.7	149	80.6	181	32	82.4	1510	1361	9.88	301	268	11.10
6	1	209	37.3	172	82.0	242	70	71.2	950	778	18.1	315	263	16.4
7	1	282	62.7	219	77.7	301	82	72.9	523	304	41.4	442	297	32.8
	2	196	39.5	156	79.9	274	118	57.0	630	474	25.0	342	248	27.4
	3	149	30.4	118	79.8	235	117	50.3	227	109	52.0	383	229	40.4
8	2	254	45.8	208	81.8	301	93	69.2	611	403	34.1	251	146	42.0

Table 7-5: CC Head to head comparison: 2-D Echo vs admittance vs conductance (HS) vs Cuvette derived mean volumes

Figures 7-2 to 7-8 (total of N=7 rats) are representative P-V loops (only one loop shown for clarity). Table 7-5 estimates are based on the average of 4 such loops.

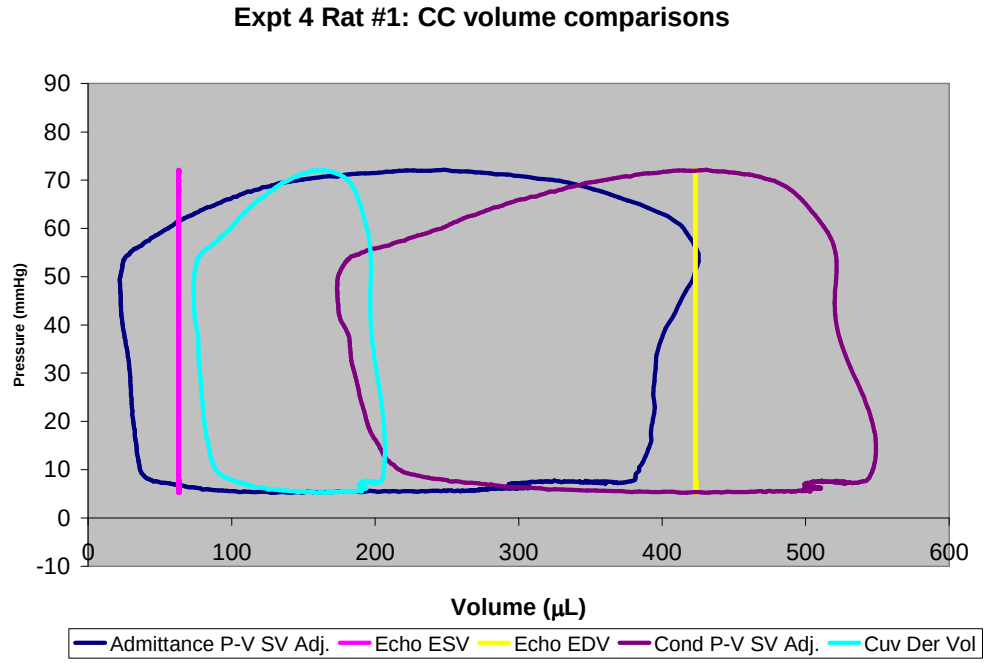

Figure 7-2: CC Volume comparisons-P-V Loop: Expt 4, Rat #1

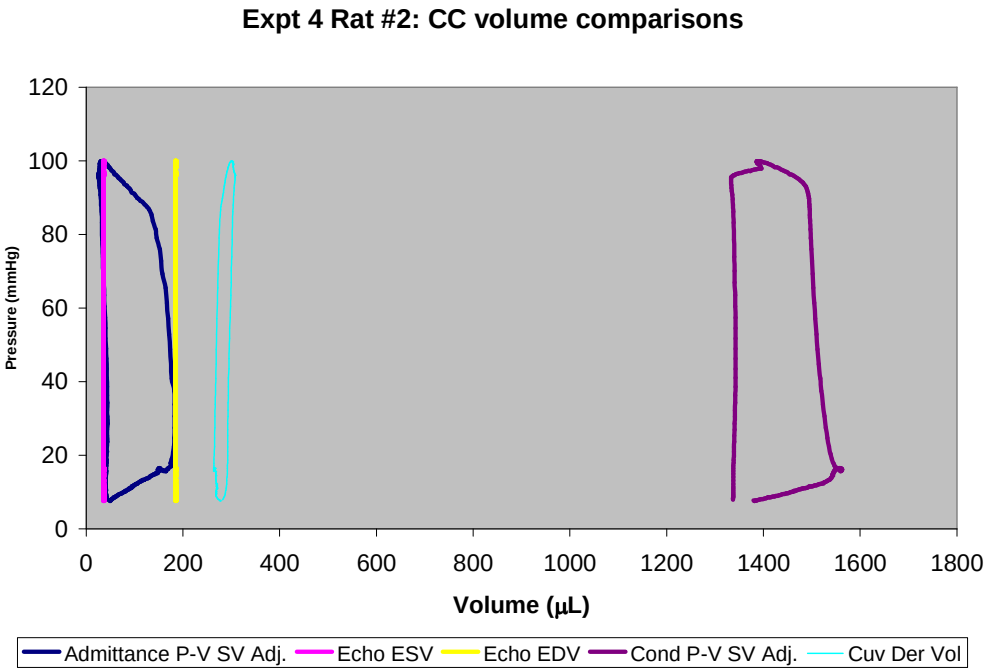

Figure 7-3: CC Volume comparisons-P-V Loop: Expt 4, Rat #2

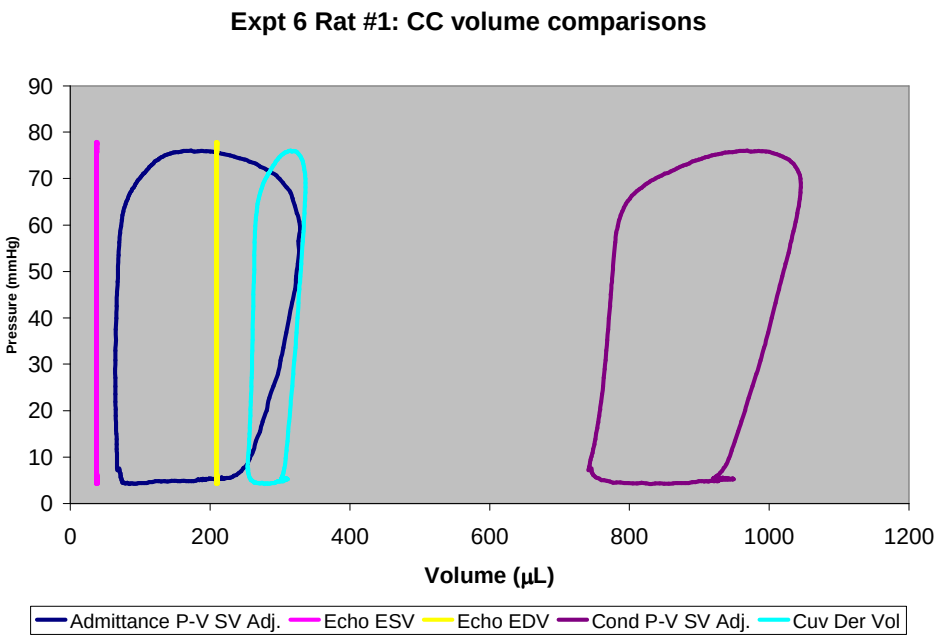

Figure 7-4: CC Volume comparisons-P-V Loop: Expt 6, Rat #1

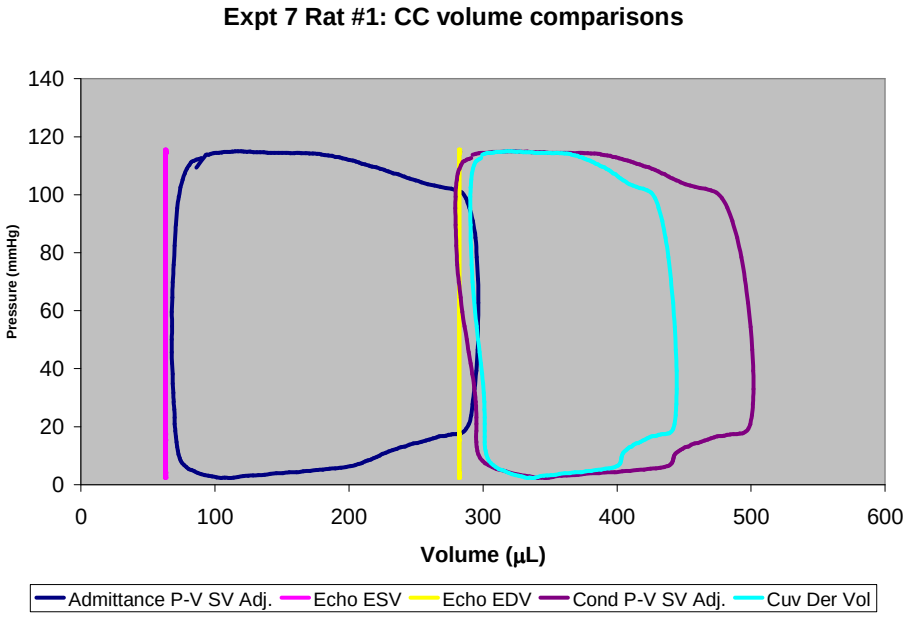

Figure 7-5: CC Volume comparisons-P-V Loop: Expt 7, Rat #1

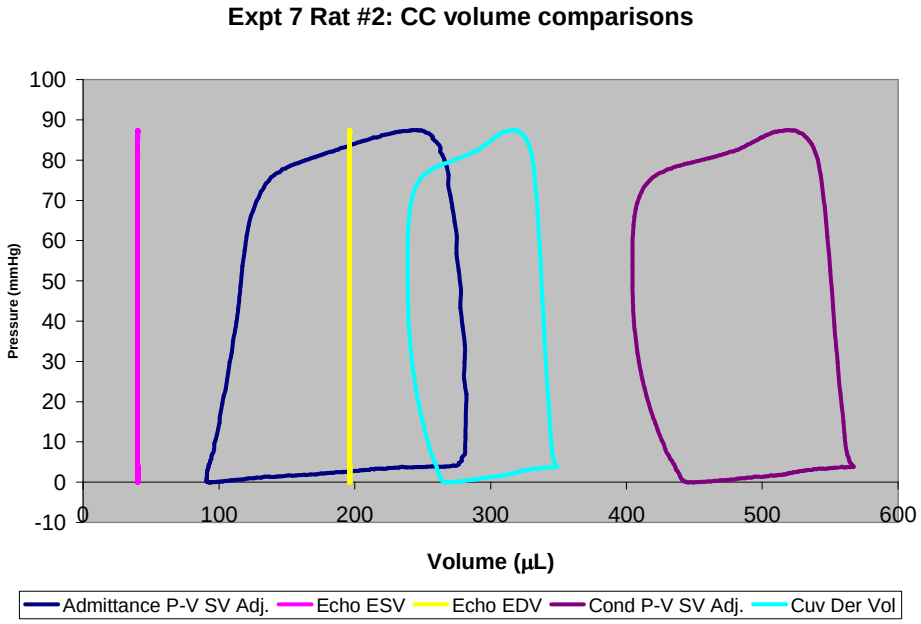

Figure 7-6: CC Volume comparisons-P-V Loop: Expt 7, Rat #2

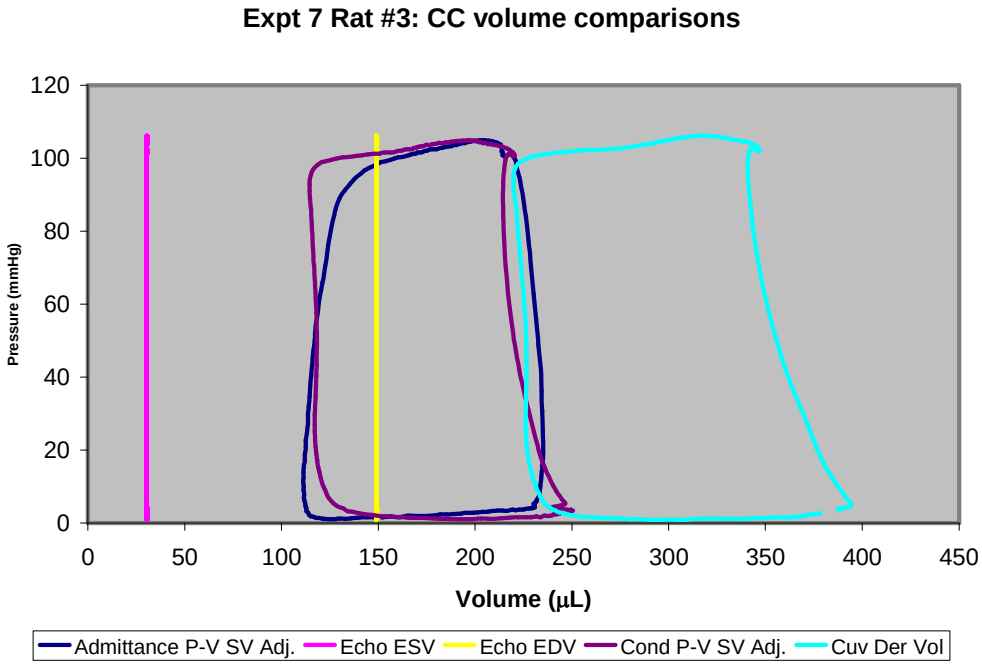

Figure 7-7: CC Volume comparisons-P-V Loop: Expt 7, Rat #3

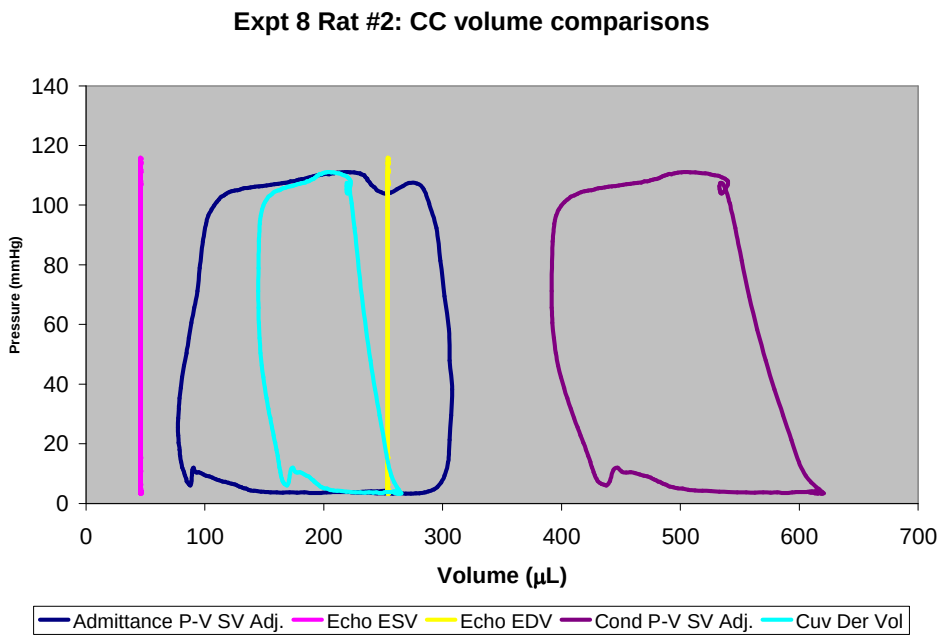

Figure 7-8: CC Volume comparisons-P-V Loop: Expt 7, Rat #3

Statistical tests were done on the means of the different techniques. Specifically, repeated ANOVA analysis (p=0.05) with three different post-hoc tests (Tukey HSD, LSD and Bonferroni) were performed. Table 7-6 shows the results of the statistical analysis.

EDV				ESV			
Post-hoc method	**Compare 1**	**Compare 2**	**p**	**Post-hoc method**	**Compare 1**	**Compare 2**	**p**
Tukey HSD	2-D Echo	Admittance	0.992	Tukey HSD	2-D Echo	Admittance	0.993
LSD	2-D Echo	Admittance	0.785	LSD	2-D Echo	Admittance	0.778
Bonferroni	2-D Echo	Admittance	1	Bonferroni	2-D Echo	Admittance	1
Tukey HSD	2-D Echo	Conductance (HS)	0.003	Tukey HSD	2-D Echo	Conductance (HS)	0.003
LSD	2-D Echo	Conductance (HS)	0.001	LSD	2-D Echo	Conductance (HS)	0.001
Bonferroni	2-D Echo	Conductance (HS)	0.003	Bonferroni	2-D Echo	Conductance (HS)	0.003
Tukey HSD	2-D Echo	Cuvette	0.906	Tukey HSD	2-D Echo	Cuvette	0.47
LSD	2-D Echo	Cuvette	0.506	LSD	2-D Echo	Cuvette	0.154
Bonferroni	2-D Echo	Cuvette	1	Bonferroni	2-D Echo	Cuvette	0.926

Table 7-6: Repeated ANOVA analysis comparing EDV and ESV of 2-D Echo vs. admittance vs. Conductance (HS) vs. Cuvette

It can be clearly seen that the Conductance (Hypertonic Saline (HS)) based approach was statistically different from 2-D echo (from the very low p ($p<0.05$) values), both for EDV as well as for ESV.

However, for the cuvette based approach, the results are not that straightforward. Therefore, in order to make a better judgment on the cuvette data, a separate statistical analysis was performed. This time the 2-D echo data was compared only to admittance and cuvette. Table 7-7 shows the results of the statistical analysis.

EDV				ESV			
Post-hoc method	**Compare 1**	**Compare 2**	**p**	**Post-hoc method**	**Compare 1**	**Compare 2**	**p**
Tukey HSD	2-D Echo	Admittance	0.736	Tukey HSD	2-D Echo	Admittance	0.472
LSD	2-D Echo	Admittance	0.461	LSD	2-D Echo	Admittance	0.248
Bonferroni	2-D Echo	Admittance	1	Bonferroni	2-D Echo	Admittance	0.744
Tukey HSD	2-D Echo	Cuvette	0.185	Tukey HSD	2-D Echo	Cuvette	<0.0001
LSD	2-D Echo	Cuvette	0.082	LSD	2-D Echo	Cuvette	<0.0001
Bonferroni	2-D Echo	Cuvette	0.247	Bonferroni	2-D Echo	Cuvette	<0.0001

Table 7-7: Repeated ANOVA analysis comparing EDV and ESV of 2-D Echo vs. admittance vs. Cuvette

This test clearly shows that the Cuvette ESV means are statistically different from 2-D echo ($p<0.05$). Also, the test shows that the Cuvette EDV has lower numbers than the admittance counterpart. This indicates that the admittance data agrees more with the 2-D echo data than the cuvette derived volumes.

Both the tests prove that the admittance data is statistically not different from the 2-D echo data, both for EDV and ESV.

7.3 STUDY 2-B: OPEN – CHEST (OC) ECHO, FLOW AND ADMITTANCE STUDIES

As a means to further solidify the concept of admittance and that it truly does scale from mice to rats, 2-D echo was compared to admittance. Also, as a means to validate 2-D echo itself as a standard of comparison, SV estimated from 2-D echo was

compared to SV estimated from flow meter, which is considered by many as the standard for blood flow measurements. Table 7-8 summarizes the head to head comparison of OC 2-D echo SV measurement with OC flow SV measurement. The Echo OC Mean is calculated over an average of 3 heart cycles. The Flow OC is estimated from averaging 10 heart cycles. The results show that they differ from each other on an average by about 15%. Here echo-flow mean refers to the mean SV estimated from OC echo and OC flowmeter. SD refers to standard deviation.

Expt	Rat	Echo OC SV Mean (uL)	Flow OC SV Mean (uL)	Echo-Flow Mean (uL)	Echo-Flow SD (uL)	SD % of mean
6	1	121	100	111	14.8	13.4
	2	172	114	143	41.0	28.7
7	1	214	164	189	35.4	18.7
	2	286	309	298	16.3	5.47
8	2	242	205	224	26.2	11.7
	3	302	378	340	53.7	15.8
					Average	**15.6**

Table 7-8: Head to head comparison of OC echo SV vs. flow SV

Table 7-9 summarizes the 2-D OC Echo EDV, ESV and EF means vs. admittance derived volume means.

Expt	Rat	Echo OC EDV Mean (uL)	Echo OC ESV Mean (uL)	Echo OC SV Mean (uL)	Echo OC EF Mean (%)	Admittance OC EDV Mean (uL)	Admittance OC ESV Mean (uL)	Admittance OC EF Mean (%)
6	1	148	26.8	121	81.8	210	89	57.6
	2	197	25.0	172	87.3	219	47	78.5
7	1	235	21.0	214	90.9	271	57	79.1
	2	305	18.8	286	93.8	380	94	73.7
8	2	276	33.7	242	87.8	300	58	80.7
	3	331	27.6	302	91.3	331	29	91.2

Table 7-9: Head to head comparison of OC echo volumes vs. OC admittance volumes

Figures 7-9 to 7-14 (total of N=6 rats) are representative P-V loops (only one loop shown for clarity). Table 7-9 estimates are based on the average of 4 such loops.

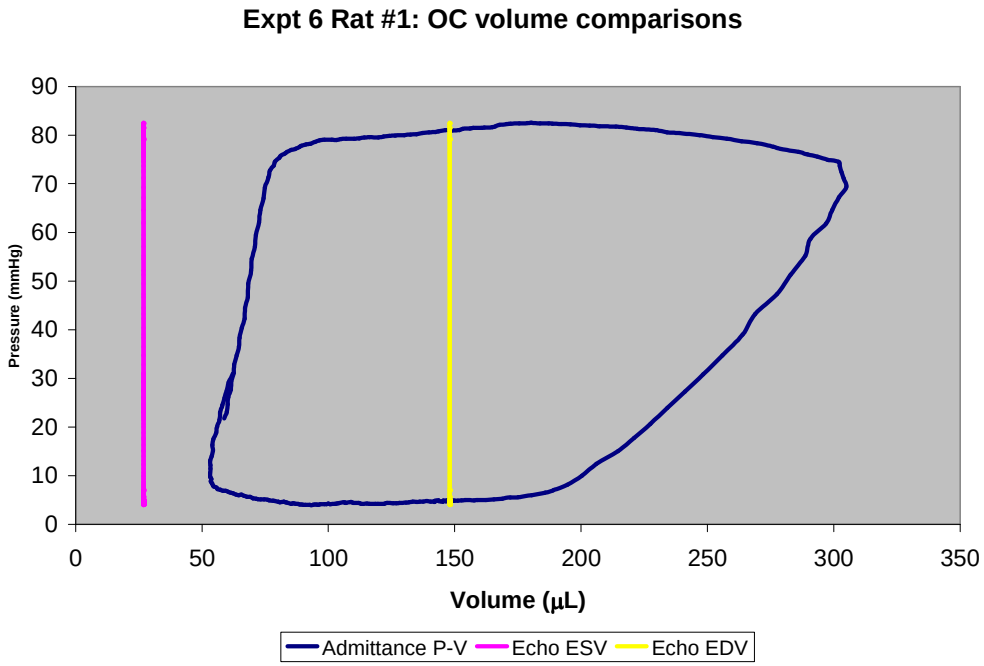

Figure 7-9: OC Volume comparisons-P-V Loop: Expt 6, Rat #1

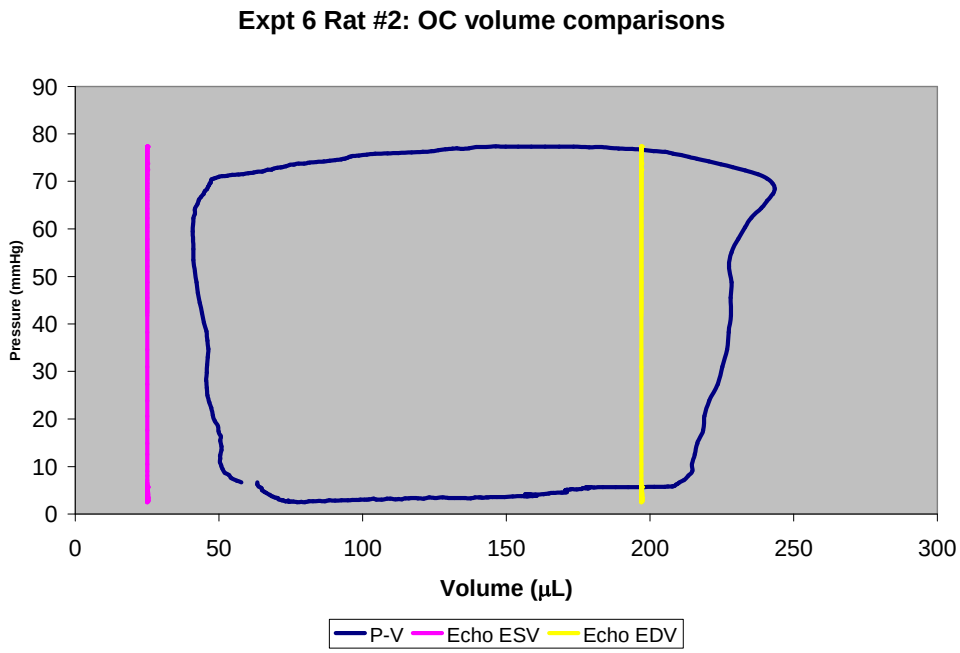

Figure 7-10: OC Volume comparisons-P-V Loop: Expt 6, Rat #2

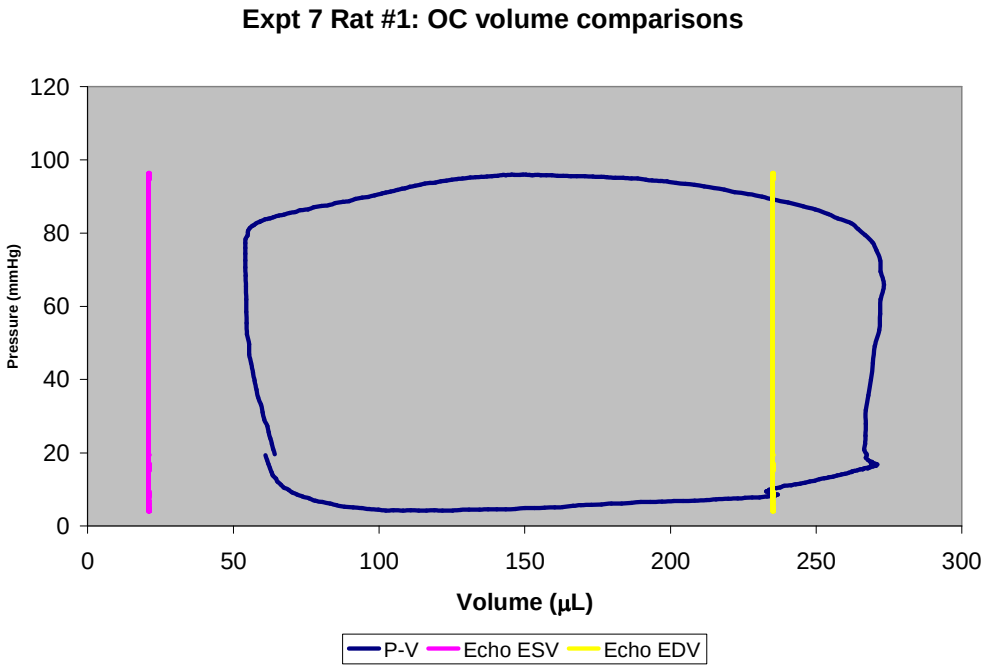

Figure 7-11: OC Volume comparisons-P-V Loop: Expt 7, Rat #1

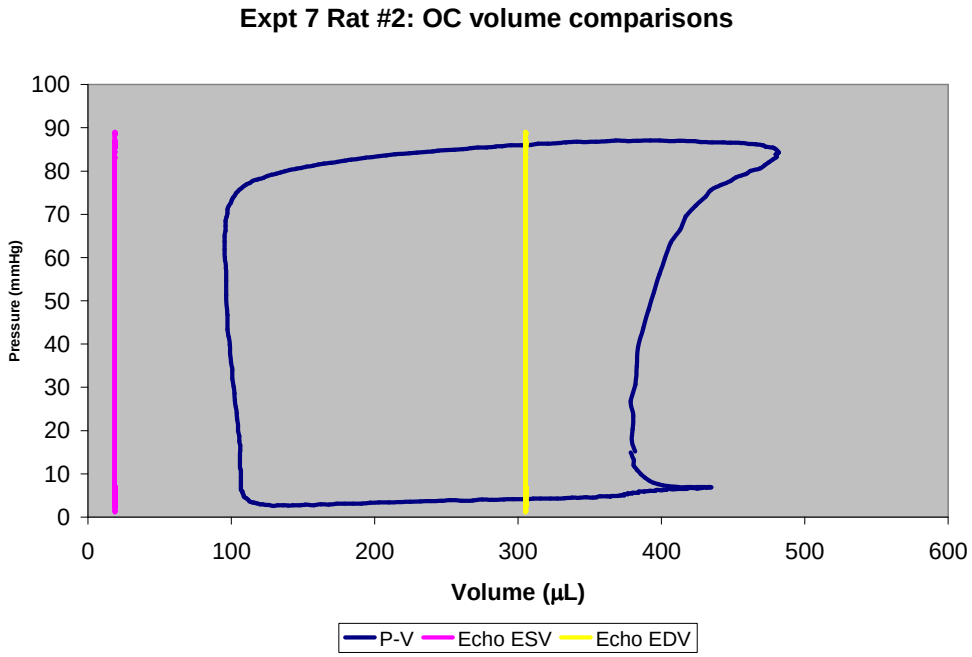

Figure 7-12: OC Volume comparisons-P-V Loop: Expt 7, Rat #2

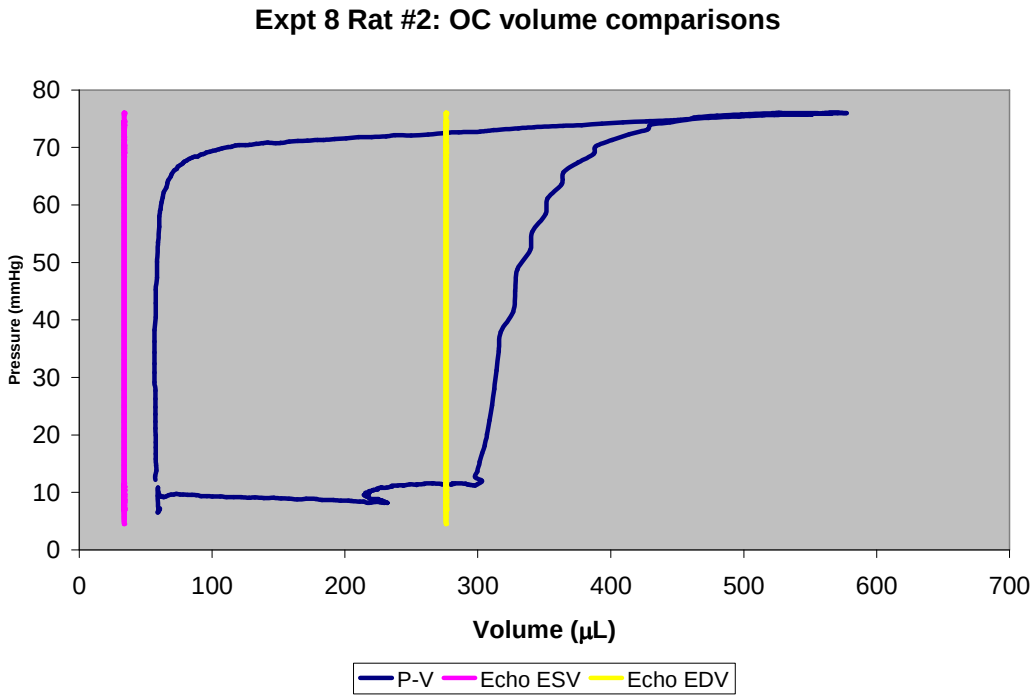

Figure 7-13: OC Volume comparisons-P-V Loop: Expt 8, Rat #2

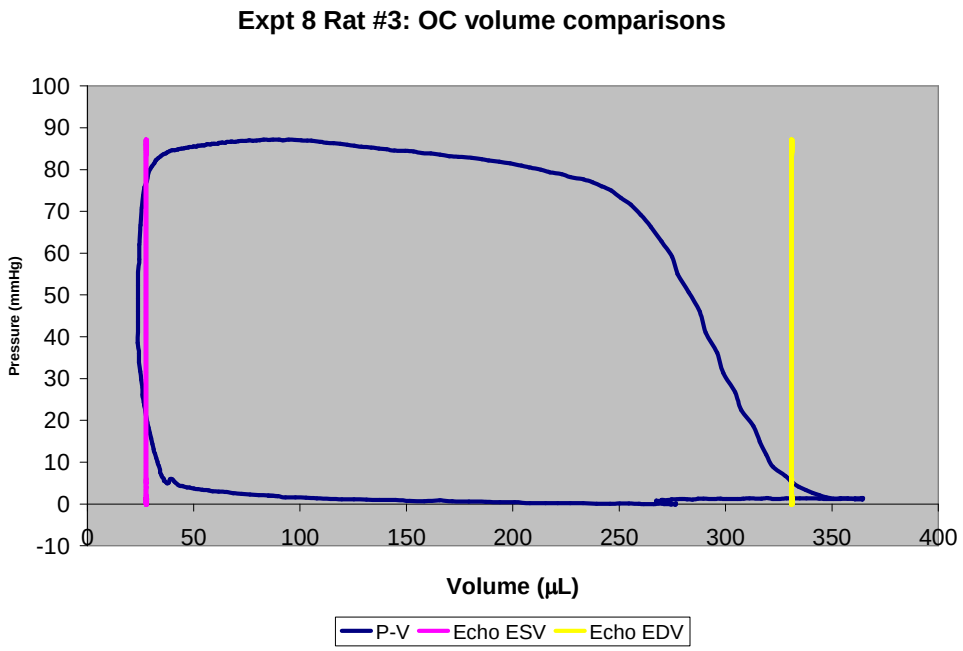

Figure 7-14: OC Volume comparisons-P-V Loop: Expt 8, Rat #3

7.4 STUDY 4: CHRONIC STUDIES

Table 7-10 is a summary of the details of the rats used in the chronic studies (N=6 rats). The body weights shown are at the start of the experiment and at the end of the experiment (after 24 hours).

Rat #	Sex	Weight (g)	Weight 24h (g)	Weight loss (%)	HW (mg)	LVW (mg)	Notation
1	M	201	180	10.4	692	480	Ex9, R3
2	M	208	197	5.29	645	477	Ex10, R1
3	M	229	210	8.30	711	525	Ex10, R2
4	M	247	225	8.91	795	615	Ex11, R2
5	M	295	279	5.42	882	660	Ex11, R3
6	M	307	287	6.51	912	700	Ex11, R4
Mean		248	230	7.48	773	576	Exp #
SD		44.4	44.0	2.07	108	95.5	Rat #

Table 7-10: Details of rats used for Study #4 (chronic studies)

Figures 7-15 to 7-20 are representative P-V loops obtained from the chronic studies using the admittance techniques (N=6 rats). Each of the rat loops has been divided into 3 groups, based on a 24-hour time line scale. This was done to improve the clarity of the loops. P-V loops represented here are at Baseline (0 hours), 3, 6, 9, 12, 15, 18, 21 and 24 hours.

The 2-D echo ESV and EDV shown are taken at the beginning and the end of the experiment. For calibration purposes, the echo SV taken at the beginning of the experiment was used for the Baseline, 0, 3, 6, 9 and 12 hour loops. The echo SV taken at the end of the experiment was used for the 15, 18, 21 and 24 hour loops.

Loops look different in morphology, pressure etc., because these were obtained from a conscious rat in a cage, moving, crouching, eating, sleeping etc., amidst other natural activities of a rat.

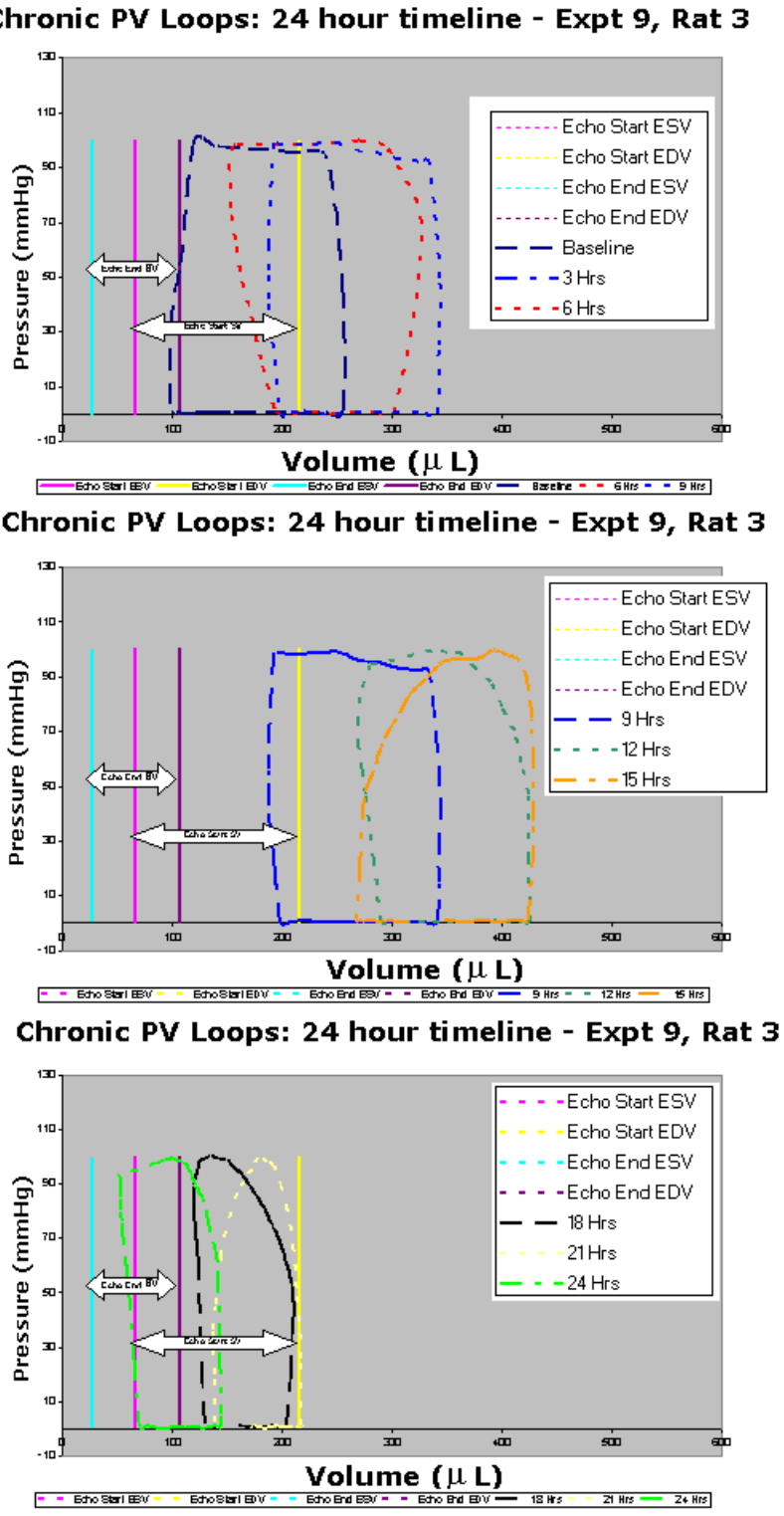

Figure 7-15: Chronic Experiments – 3hr P-V Loops: Expt 9, Rat #3

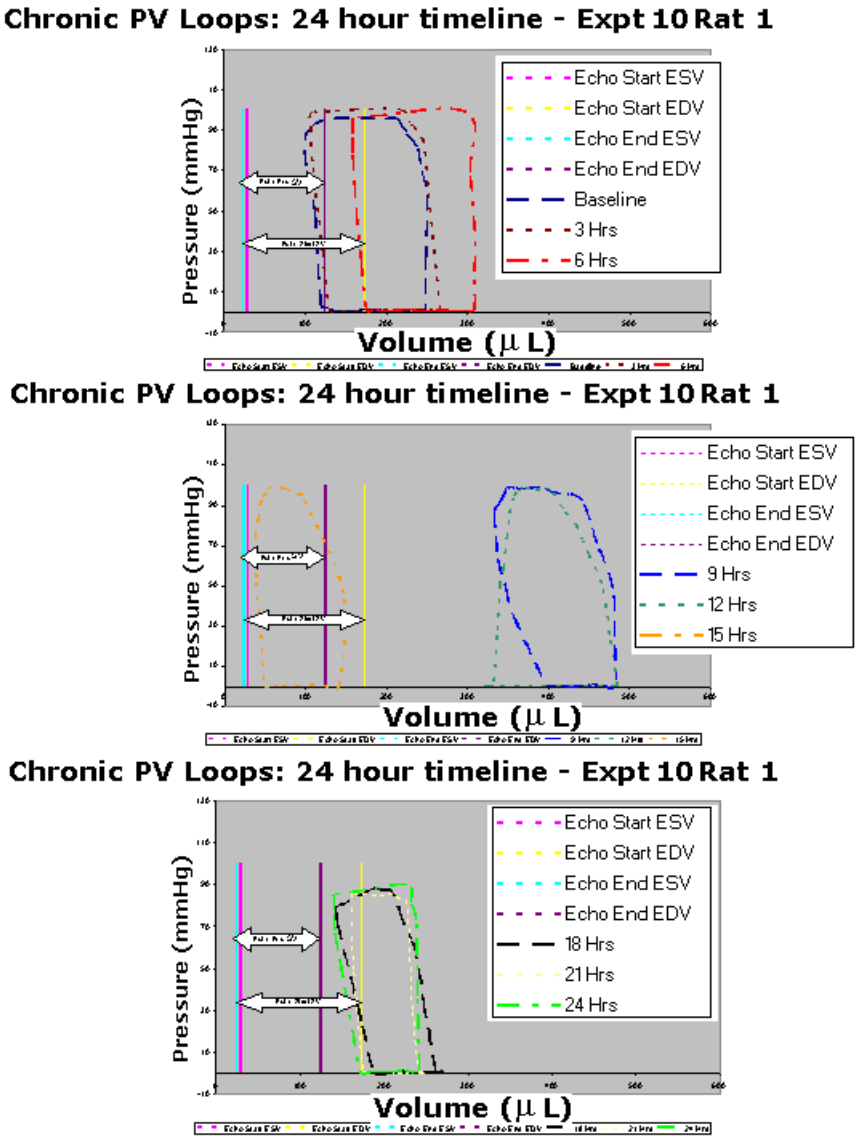

Figure 7-16: Chronic Experiments – 3hr P-V Loops: Expt 10, Rat #1

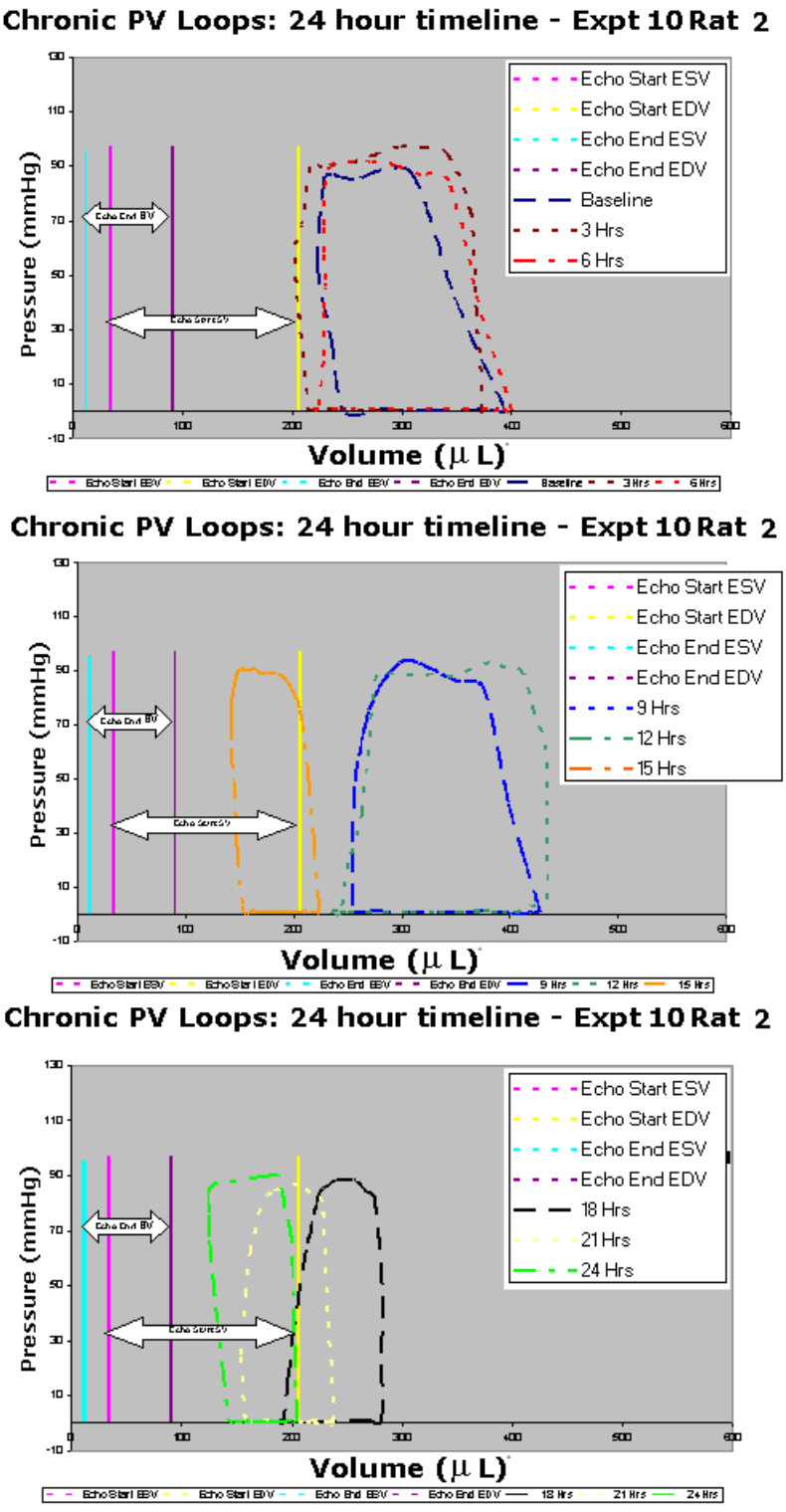

Figure 7-17: Chronic Experiments – 3hr P-V Loops: Expt 10, Rat #2

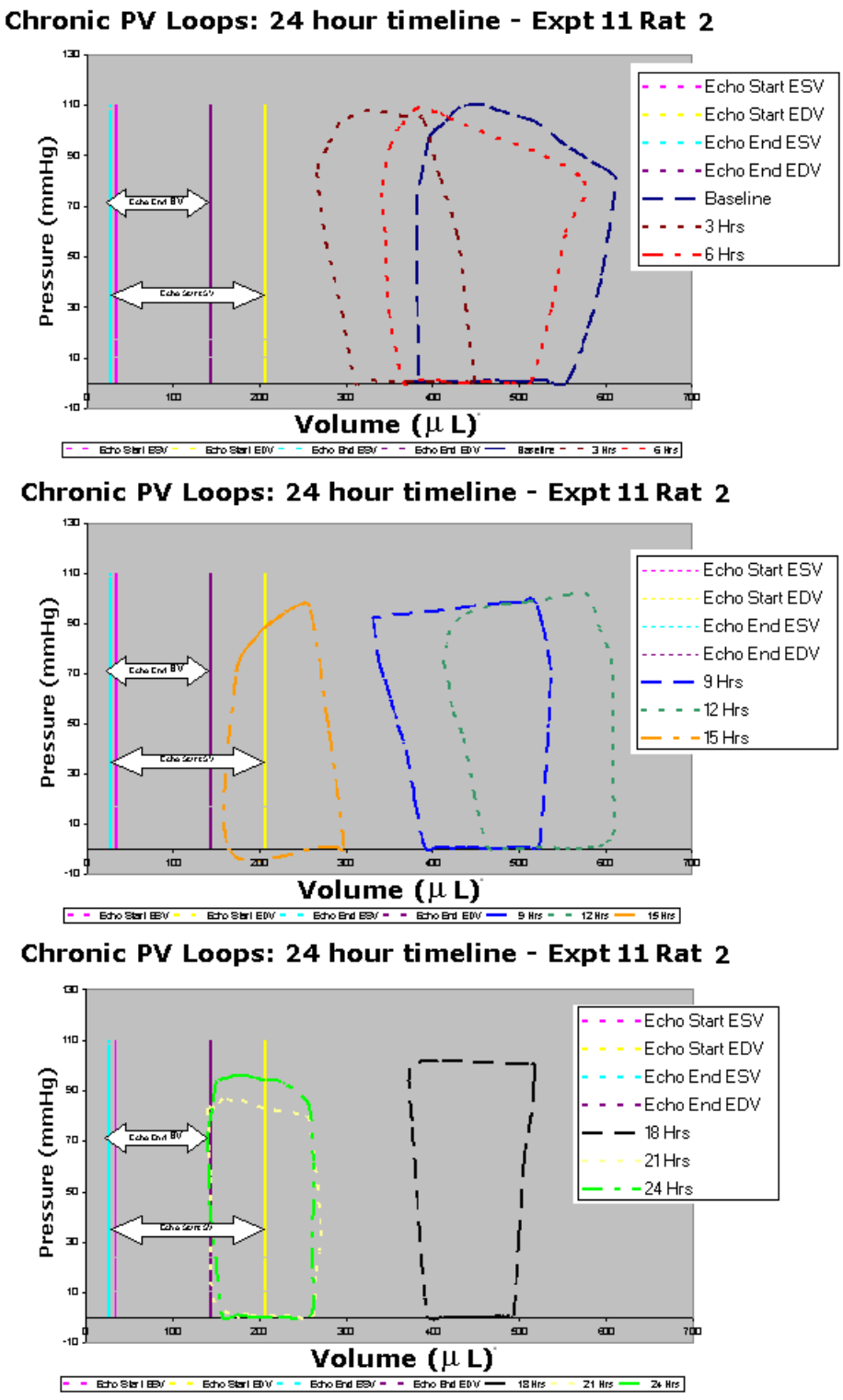

Figure 7-18: Chronic Experiments – 3hr P-V Loops: Expt 11, Rat #2

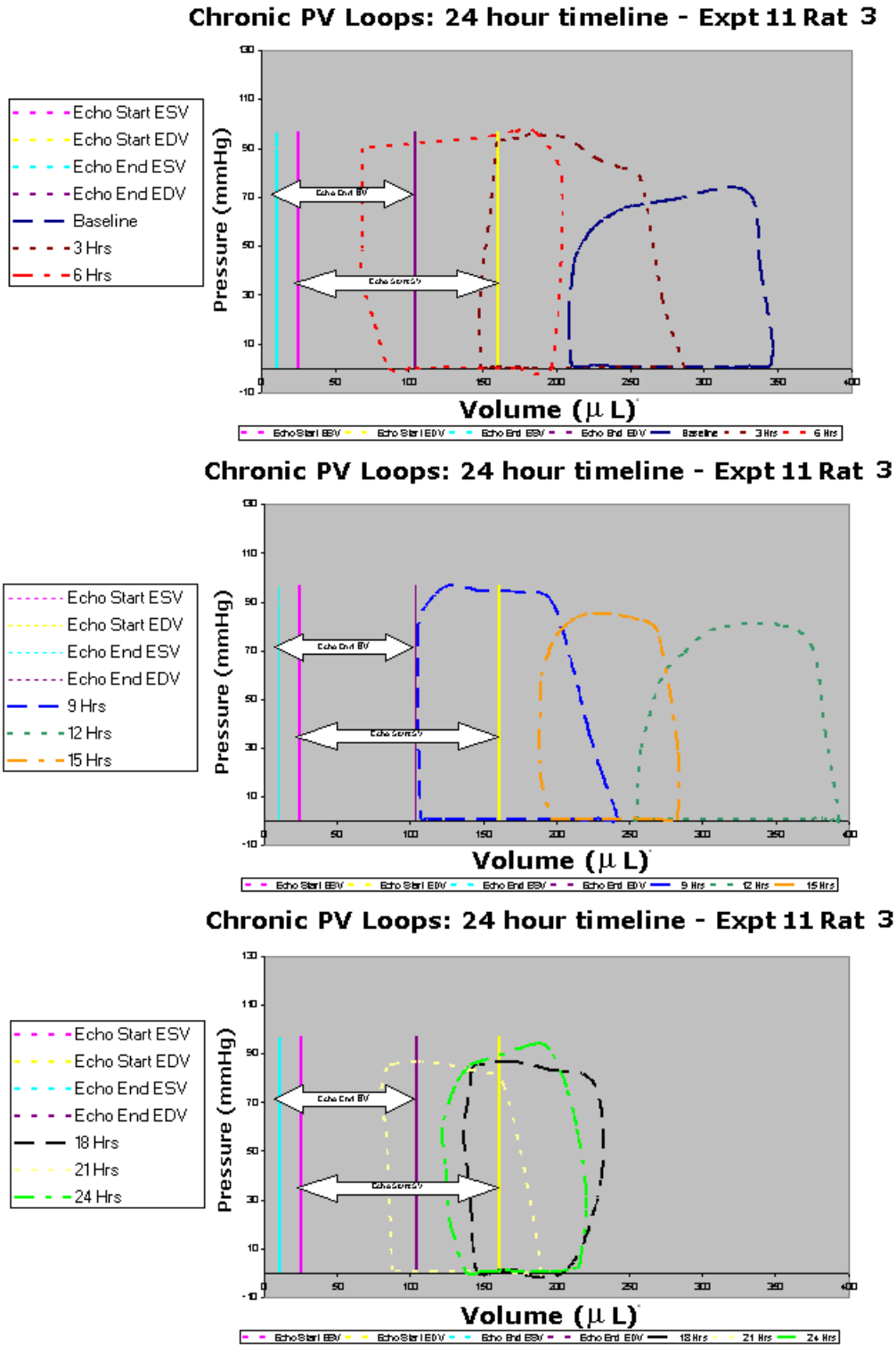

Figure 7-19: Chronic Experiments – 3hr P-V Loops: Expt 11, Rat #3

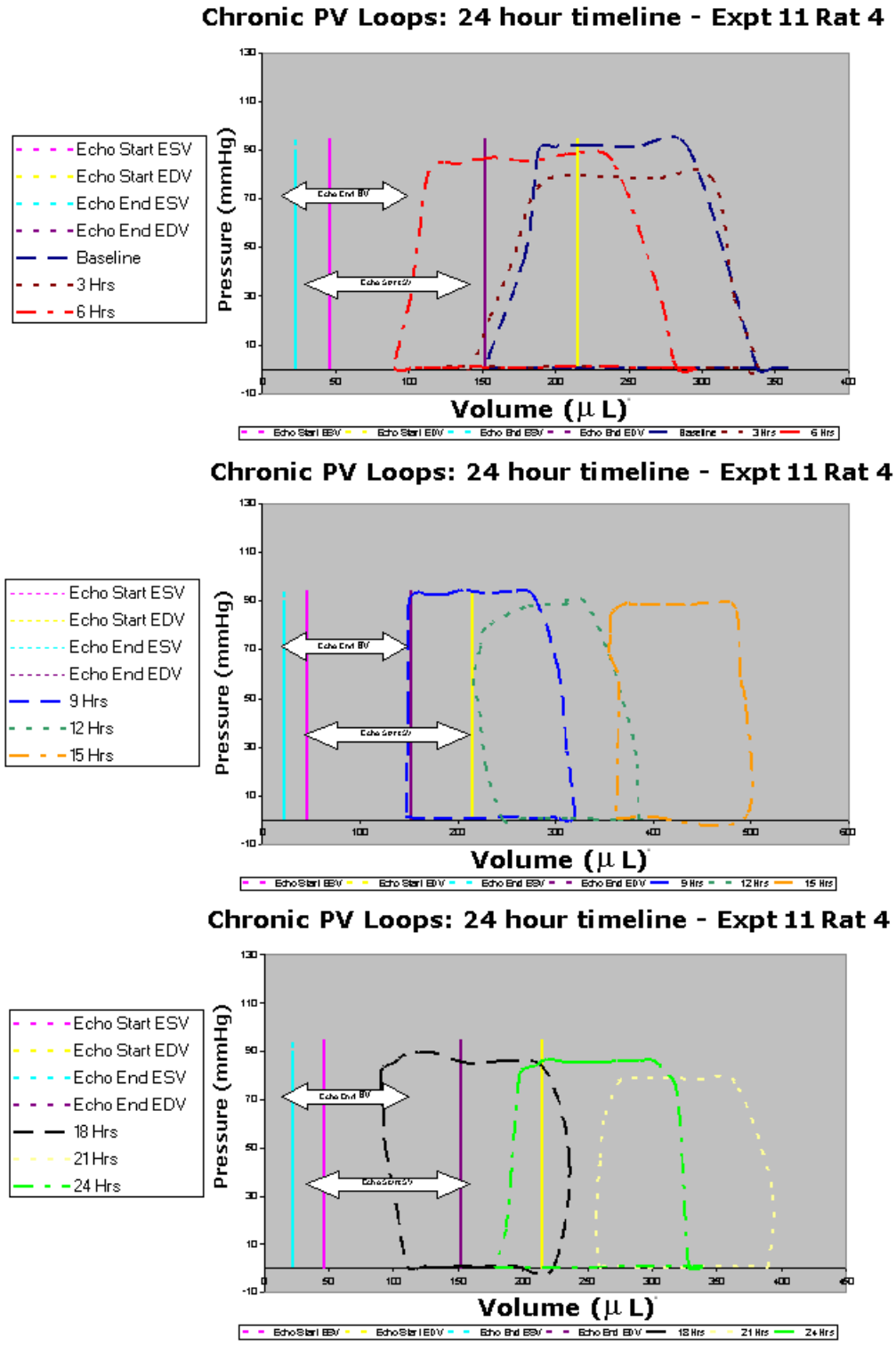

Figure 7-20: Chronic Experiments – 3hr P-V Loops: Expt 11, Rat #4

CHAPTER 8

Discussions/Conclusions

8.1 RE-REFER SPECIFIC AIMS

Chapter 1 highlighted the specific aims of this dissertation. For the reader's convenience, it has been repeated here.

Specific Aim 1: Design and build instrumentation capable of measuring impedance magnitude, phase and pressure with low power and low area; Instrument should be interfacable with a tetrapolar LV catheter.

Specific Aim 2: Design and build a backpack complete with above low power instrument, low power microcontroller, low power transmitter and lithium ion cell. Measure, sample and transmit data wirelessly to a receiver nearby. Receiver collects data and post-processes it to obtain pressure, admittance magnitude and phase data which will later be converted to volume. The backpack must sample at a sampling frequency of fs=100 Hz and transmit at least 5 heart cycles of data every 2 minutes. The battery must last at least 24 hours.

Specific Aim 3: Perform chronic LV P-V studies on rats. Rats must be concious and freely moving in a cage. Rats should have the tetrapolar LV catheter surgically placed into their LV and must be devoid of anesthesia (fully concious) during the experiment.

8.2 INNOVATIONS/FINDINGS

This dissertation explored new techniques in the field of LV P-V analysis. Here are some of the innovations/findings:

1) For the first time, a wireless telemetry device was designed and built capable of measuring impedance magnitude, phase and pressure. Using this device, LV volume was estimated using the admittance technique from concious, ambulatory rats moving freely in a cage.

2) As far as I know, this was the first time an open chest 2-D echo was performed on rats. This provided a way to validate the echo's SV using SV standards such as ultrasonic flowmeter. In turn, the echo was used to validate the admittance based volume measurements.

3) This study further validates the fact that admittance does scale from mice to rats. Rat based studies were used to obtain admittance based volumes in the LV and were validated against standards such as 2-D echo.

4) In the acute studies, the conductance method of estimating volume (using hypertonic saline calibration for parallel conductance) was statistically different from the 2-D echo obtained both at ESV and EDV.

5) The cuvette based volume estimations were not statistically different from the 2-D echo at EDV, while the ESV estimations were statistically different from the 2-D echo.

6) The admittance derived volumes were statistically not different from the 2-D echo volumes both at ESV and at EDV.

8.3 FUTURE WORK

While the surface mounted PCB design laid the foundation for a proof of concept for wireless telemetry studies, a system on a chip (SOC) with the impedance and pressure

measurement system in it would prove much more useful. This work developed some ideas for the building of the SOC. This would greatly reduce the size (area/volume) and the weight of the backpack. Ideally, the circuit could go underneath the skin (subcutaneous), right behind the neck. A lighter backpack would also ensure that the rat would be able to stand up and reach for water as they would normally do. The rats lost an average of 7.5% of their body weight during the course of a 24-hour study.

Also, in parallel, a backpack device could be built and used to perform saline calibration periodically (during the course of the study). This would ensure that the estimation of volumes would be more accurate.

The current active current (ON current) of the entire backpack circuit was about 42 mA and the standby current (OFF current) was about 22 mA. Some careful planning could further reduce the OFF current, thereby, increasing the longevity of the battery.

8.4 CONCLUSIONS

Rats were studied in both acute and chronic studies for LV P-V estimations. The acute studies compared admittance derived volumes with standards such as 2-D echo in both closed – chest (CC) and open-chest (OC) conditions. Also, admittance-derived volumes were compared against previously established techniques such as conductance techniques (with hypertonic saline calibration) and cuvette-based estimations. Also, OC SV was compared from two different techniques – 2-D echo vs. ultrasonic flowmeter. In the chronic studies, admittance derived volumes were obtained from wirelessly transmitted data from concious, ambulatory rats freely moving in their cages for a period of 24 hours each.

APPENDIX A

The following code was used in the transmitter (TX). It samples the 3 ADC channels (impedance magnitude, phase and pressure) at a sampling rate of f_s = 100 Hz every 2 seconds. This code was obtained by modifying the TI Demo - ez430-RF2500 Temperature Sensor End Device v1.02, written by L. Westlund, Texas Instruments Inc., Nov 2007.

Two different timers are used to achieve the timing. Timer A's ISR wakes up the microcontroller every 2 minutes. At this point, all the flags are reset and the ADC enabled. Also the enable bit (Port 4, Bit3) is set to high. This enable bit is connected to the enable pin of the regulator which powers the backpack instrumentation. Timer B's ISR samples the three channels of the ADC, in a sequential fashion. Timer B is set at 0.01s which translates to a sampling rate of 100 Hz.

```
#include "bsp.h"
#include "mrfi.h"
#include "nwk_types.h"
#include "nwk_api.h"
#include "bsp_leds.h"
#include "bsp_buttons.h"
#include "vlo_rand.h"

//////////////////Function prototypes///////////////

void linkTo(void);
void MCU_Init(void);
void createRandomAddress();

////////////////////////////////////////////////////

//////////////////Factory settings//////////////////

// Temperature offset set at production
__no_init volatile int tempOffset @ 0x10F4;
// Flash address set randomly
__no_init volatile char Flash_Addr[4] @ 0x10F0;

////////////////////////////////////////////////////

//////////////////Semaphores////////////////////////

//sSendData is set when data is ready to be TX
static uint8_t sSendData=0;
//sWakeUpSem is set to wake up end device (ED or TX) every 120 seconds
static uint8_t sWakeUpSem=1;
```

```
//sSamplesReqReached is set when the reqd # of samples has been collected
static uint8_t sSamplesReqReached=0;
//sMultipleOf40sec is the multiplication factor multiplied to the 40sec which
//brings up the waking up interrupt into the minutes range (currently 2 minutes)
static uint8_t sMultipleOf40sec=0;

//////////////////////////////////////////////////

/////////////////Data and data pointers//////////////

//3 "int" data sampled from ADC (Mag, Phs and Pre). Only 10 bits are filled
//out of the 16 bits because it is a 10-bit ADC
int dADCSamples[3]={0,0,0};
//Read and Write pointers to access the data
int *pReadPtr, *pWritePtr;
//Data converted to bytes, ready to TX
uint8_t  dTXMsg[6];

//////////////////////////////////////////////////

/////////////////Other variables/////////////////////

//# of samples collected
int cSamplesCollected=0;
//Link ID for the ED (TX)
linkID_t linkID1;

//////////////////////////////////////////////////

void main (void)
{
  addr_t lAddr;

  //Point both the read and write pointers to the first ADC Sample
  pReadPtr=&dADCSamples[0];
  pWritePtr=&dADCSamples[0];

  WDTCTL = WDTPW + WDTHOLD;                 // Stop WDT
  {
  // delay loop to ensure proper startup before SimpliciTI increases DCO
  // This is typically tailored to the power supply used, and in this case
  // is overkill for safety due to wide distribution.
    volatile int i;
    for(i = 0; i < 0xFFFF; i++){}
  }
  if( CALBC1_8MHZ == 0xFF )             // Do not run if cal values are erased
  {
    volatile int i;
    P1DIR |= 0x03;
    while(1)
    {
      for(i = 0; i < 0x5FFF; i++){}
    }
  }

  // SimpliciTI will change port pin settings as well
  P1DIR = 0xFF;
  P1OUT = 0x00;
  P2DIR = 0x27;
  P2OUT = 0x00;
  P3DIR = 0xC0;
  P3OUT = 0x00;
  P4DIR = 0xFF;
  P4OUT = 0x08; //Enable bit set high to power ON the backpack

  BSP_Init();
```

```
  if( Flash_Addr[0] == 0xFF &&
      Flash_Addr[1] == 0xFF &&
      Flash_Addr[2] == 0xFF &&
      Flash_Addr[3] == 0xFF )
  {
    createRandomAddress();       // set Random device address at initial startup
  }
  lAddr.addr[0]=Flash_Addr[0];
  lAddr.addr[1]=Flash_Addr[1];
  lAddr.addr[2]=Flash_Addr[2];
  lAddr.addr[3]=Flash_Addr[3];
  SMPL_Ioctl(IOCTL_OBJ_ADDR, IOCTL_ACT_SET, &lAddr);
  BCSCTL1 = CALBC1_8MHZ;                    // Set DCO after random function
  DCOCTL = CALDCO_8MHZ;

  BCSCTL3 |= LFXT1S_2;                      // LFXT1 = VLO
  TACCTL0 = CCIE;                           // TACCR0 interrupt enabled
  TACCR0 = 60000;                           // ~5 seconds
  TACTL = TASSEL_1 + MC_1+ID_3;             // ACLK, upmode; ID_3 makes it
                                            // 5*8=40 seconds

  TBCCTL0 = CCIE;                           // TBCCR0 interrupt enabled
  TBCCR0 = 120;                             // 0.01s = 10msec -> fs=100 Hz
  TBCTL = TBSSEL_1 + MC_1;                  // ACLK, upmode

  ADC10AE0 |= 0x07;                         // Configure multiplexed pin to
                                            // to Analog IN

  // Set sample and hold time, turn on the ADC, enable ADC interrupts
  ADC10CTL0 = ADC10SHT_3 + ADC10ON + ADC10IE;

  // keep trying to join until successful.
  while (SMPL_NO_JOIN == SMPL_Init((uint8_t (*)(linkID_t))0))
  {
    __bis_SR_register(LPM3_bits + GIE);     // LPM3 with interrupts enabled
  }

  // unconditional link to AP which is listening due to successful join.
  linkTo();
}

void createRandomAddress()
{
  unsigned int rand, rand2;
  do
  {
    rand = TI_getRandomIntegerFromVLO();   // first byte can not be 0x00 of 0xFF
  }
  while( (rand & 0xFF00)==0xFF00 || (rand & 0xFF00)==0x0000 );
  rand2 = TI_getRandomIntegerFromVLO();

  BCSCTL1 = CALBC1_1MHZ;                    // Set DCO to 1MHz
  DCOCTL = CALDCO_1MHZ;
  FCTL2 = FWKEY + FSSEL0 + FN1;             // MCLK/3 for Flash Timing Generator
  FCTL3 = FWKEY + LOCKA;                    // Clear LOCK & LOCKA bits
  FCTL1 = FWKEY + WRT;                      // Set WRT bit for write operation

  Flash_Addr[0]=(rand>>8) & 0xFF;
  Flash_Addr[1]=rand & 0xFF;
  Flash_Addr[2]=(rand2>>8) & 0xFF;
  Flash_Addr[3]=rand2 & 0xFF;

  FCTL1 = FWKEY;                            // Clear WRT bit
  FCTL3 = FWKEY + LOCKA + LOCK;             // Set LOCK & LOCKA bit
}
```

```
void linkTo()
{
  // keep trying to link...
  while (SMPL_SUCCESS != SMPL_Link(&linkID1))
  {
    __bis_SR_register(LPM3_bits + GIE);     // LPM3 with interrupts enabled
  }

  //Infinite loop (foreground task)
  while (1)
  {
    //When device is "awake" and it is ready to send data (TX)
   if(sWakeUpSem==1 && sSendData==1)
   {
    SMPL_Ioctl( IOCTL_OBJ_RADIO, IOCTL_ACT_RADIO_SLEEP, "" );
    __bis_SR_register(LPM3_bits+GIE);       // LPM3 with interrupts enabled

    SMPL_Ioctl( IOCTL_OBJ_RADIO, IOCTL_ACT_RADIO_AWAKE, "" );

    //Create data packets
    dTXMsg[0] = (*pReadPtr) & 0xFF;
    dTXMsg[1] = ((*pReadPtr)>>8) & 0xFF;pReadPtr+=sizeof(int);

    dTXMsg[2] = (*pReadPtr) & 0xFF;
    dTXMsg[3] = ((*pReadPtr)>>8) & 0xFF;pReadPtr+=sizeof(int);

    dTXMsg[4] = (*pReadPtr) & 0xFF;
    dTXMsg[5] = ((*pReadPtr)>>8) & 0xFF;

    // Transmit!!
    while (SMPL_SUCCESS != SMPL_Send(linkID1, dTXMsg, sizeof(dTXMsg)));

    //Now, point read pointer back to begining of data set.
    //Also reset sSendData to as ACK that the data has been sent and we are
    //ready for the next set of ADC samples.
    pReadPtr=&dADCSamples[0];sSendData=0;

    //Once we have enough samples, stop collecting!
    if(cSamplesCollected++ == 600)
    {
      sSamplesReqReached=1;
      sWakeUpSem=0;
      ADC10CTL0 &= ~ADC10ON;        // turn off A/D to save power
      P4DIR = 0xF7; P4OUT = 0x00;   // Reset Enable bit to turn OFF bkpk power
    }
  }
 }
}

/*-------------------------------------------------------------------------------
* ADC10 interrupt service routine
-------------------------------------------------------------------------------*/
#pragma vector=ADC10_VECTOR
__interrupt void ADC10_ISR(void)
{
  __bic_SR_register_on_exit(CPUOFF);        // Clear CPUOFF bit from 0(SR)
}

/*-------------------------------------------------------------------------------
* Timer A0 interrupt service routine
-------------------------------------------------------------------------------*/
#pragma vector=TIMERA0_VECTOR
__interrupt void Timer_A (void)
{
  __bic_SR_register_on_exit(LPM3_bits);        // Clear LPM3 bit from 0(SR)
```

```
  sMultipleOf40sec++;

  //Wakeup system every 40*3=120 seconds. Reset all flags
  //Enable ADC and set the enable flag to turn ON the backpack power
  if(sMultipleOf40sec==3)
  {
    sMultipleOf40sec=0;
    sWakeUpSem=1;sSamplesReqReached=0;sSendData=0;cSamplesCollected=0;
    ADC10CTL0 = ADC10SHT_3 + ADC10ON + ADC10IE;
    P4DIR = 0xFF; P4OUT = 0x08;
  }
}

/*-------------------------------------------------------------------------
* Timer B0 interrupt service routine
-------------------------------------------------------------------------*/
#pragma vector=TIMERB0_VECTOR
__interrupt void Timer_B (void)
{
  //Check if the device is "awake"
  if(sWakeUpSem==1)
  {
    __bic_SR_register_on_exit(LPM3_bits);   // Clear LPM3 bit from 0(SR)

    //Once the device is "awake" and we need more samples and the device is
    //not currently TX data, then reset Write pointer and sample all 3 channels
    if(sSamplesReqReached==0 && sSendData==0)
    {
      pWritePtr=&dADCSamples[0];

      ADC10CTL1 = INCH_2;
      ADC10CTL0 |= ENC + ADC10SC;           // Sampling and conversion start
      __bis_SR_register(CPUOFF + GIE);      // LPM0 with interrupts enabled
      *pWritePtr=ADC10MEM;pWritePtr+=sizeof(int);
      ADC10CTL0 &= ~ENC;                    // End sampling

      ADC10CTL1 = INCH_1;
      ADC10CTL0 |= ENC + ADC10SC;           // Sampling and conversion start
      __bis_SR_register(CPUOFF + GIE);      // LPM0 with interrupts enabled
      *pWritePtr=ADC10MEM;pWritePtr+=sizeof(int);
      ADC10CTL0 &= ~ENC;                    // End sampling

      ADC10CTL1 = INCH_0;
      ADC10CTL0 |= ENC + ADC10SC;           // Sampling and conversion start
      __bis_SR_register(CPUOFF + GIE);      // LPM0 with interrupts enabled
      *pWritePtr=ADC10MEM;
      ADC10CTL0 &= ~ENC;                    // End sampling

      //Once sampled, it is ready to be TX
      sSendData=1;
    }
  }
}
```

APPENDIX B

The following code was used in the receiver (RX). It collects the 3 channels of data (from each packet of data) and transmits this as a string to be output through the Serial Interface. This code was obtained by modifying the TI Demo - ez430-RF2500 Temperature Sensor Access Point v1.02, written by L. Westlund, Texas Instruments Inc., Nov 2007.

```
#include "bsp.h"
#include "mrfi.h"
#include "bsp_leds.h"
#include "bsp_buttons.h"
#include "nwk_types.h"
#include "nwk_api.h"
#include "nwk_frame.h"
#include "nwk.h"

#include "msp430x22x4.h"
#include "vlo_rand.h"

//Define the message length in bytes
#define MESSAGE_LENGTH 6

//////////////////Function prototypes///////////////

void TXString( char* string, int length );
void MCU_Init(void);
void transmitData(int addr, signed char rssi,  char msg[MESSAGE_LENGTH] );
void transmitDataString(char addr[4],char rssi[3], char msg[MESSAGE_LENGTH]);
void createRandomAddress();

////////////////////////////////////////////////////

//data for terminal output
const  char  splash[]  =  {"\r\n-------------------------------------------------
\r\n       ****\r\n       ****               eZ430-RF2500\r\n       ******o****
Temperature   Sensor   Network\r\n********_///_****         Copyright   2007\r\n
******/_//_/*****   Texas  Instruments  Incorporated\r\n   **  ***(__/*****    All
rights reserved.\r\n        *********       Version 1.02\r\n         *****\r\n
***\r\n-------------------------------------------------\r\n"};

//////////////////Factory settings//////////////////

// Temperature offset set at production
__no_init volatile int tempOffset @ 0x10F4;
// Flash address set randomly
__no_init volatile char Flash_Addr[4] @ 0x10F0;

// reserve space for the maximum possible peer Link IDs
static linkID_t sLID[NUM_CONNECTIONS];
static uint8_t  sNumCurrentPeers;

// callback handler
static uint8_t sCB(linkID_t);
```

```
// work loop semaphores
static uint8_t sPeerFrameSem;
static uint8_t sJoinSem;
static uint8_t sSelfMeasureSem;

// mode data verbose = default, deg F = default
char verboseMode = 0;
char degCMode = 0;
char junk[6]={1,2,3,4,5,6};
////////////////////////////////////////////////

void main (void)
{
  addr_t lAddr;
  bspIState_t intState;

  WDTCTL = WDTPW + WDTHOLD;           // Stop WDT
  {
  // delay loop to ensure proper startup before SimpliciTI increases DCO
  // This is typically tailored to the power supply used, and in this case
  // is overkill for safety due to wide distribution.
    volatile int i;
    for(i = 0; i < 0xFFFF; i++){}
  }
  if( CALBC1_8MHZ == 0xFF )           // Do not run if cal values are erased
  {
    volatile int i;
    P1DIR |= 0x03;

    while(1)
    {
      for(i = 0; i < 0x5FFF; i++){}
    }
  }

  //Initialize BSP
  BSP_Init();

  if( Flash_Addr[0] == 0xFF &&
      Flash_Addr[1] == 0xFF &&
      Flash_Addr[2] == 0xFF &&
      Flash_Addr[3] == 0xFF )
  {
    createRandomAddress();      // set Random device address at initial startup
  }
  lAddr.addr[0]=Flash_Addr[0];
  lAddr.addr[1]=Flash_Addr[1];
  lAddr.addr[2]=Flash_Addr[2];
  lAddr.addr[3]=Flash_Addr[3];
  SMPL_Ioctl(IOCTL_OBJ_ADDR, IOCTL_ACT_SET, &lAddr);

  //Initialize MCU
  MCU_Init();
  //Transmit splash screen and network init notification
  TXString( (char*)splash, sizeof splash);
  TXString( "\r\nInitializing Network....", 26 );

  //Initialize network
  SMPL_Init(sCB);

  // network initialized
  TXString( "Done\r\n", 6);

  // main work loop
  while (1)
  {
```

```
  // Wait for the Join semaphore to be set by the receipt of a Join frame from a
    // device that supports and End Device.
    if (sJoinSem && (sNumCurrentPeers < NUM_CONNECTIONS))
    {
      // listen for a new connection
      SMPL_LinkListen(&sLID[sNumCurrentPeers]);
      sNumCurrentPeers++;
      BSP_ENTER_CRITICAL_SECTION(intState);
      if (sJoinSem)
      {
        sJoinSem--;
      }
      BSP_EXIT_CRITICAL_SECTION(intState);
    }

    // Approximate one second marker
    if(sSelfMeasureSem)
    {
       sSelfMeasureSem = 0;
       //transmitData( 0,0,junk );
    }

    // Have we received a frame on one of the ED connections?
    // No critical section -- it doesn't really matter much if we miss a poll
    if (sPeerFrameSem)
    {
      uint8_t     msg[MAX_APP_PAYLOAD], len, i;

      // process all frames waiting
      for (i=0; i<sNumCurrentPeers; ++i)
      {
        if (SMPL_Receive(sLID[i], msg, &len) == SMPL_SUCCESS)
        {
          ioctlRadioSiginfo_t sigInfo;
          sigInfo.lid = sLID[i];
          SMPL_Ioctl(IOCTL_OBJ_RADIO,IOCTL_ACT_RADIO_SIGINFO, (void *)&sigInfo);
          transmitData( i, (signed char)sigInfo.sigInfo[0], (char*)msg );
          BSP_ENTER_CRITICAL_SECTION(intState);
          sPeerFrameSem--;
          BSP_EXIT_CRITICAL_SECTION(intState);
        }
      }
    }
  }
}

/*-------------------------------------------------------------------------
*
-------------------------------------------------------------------------*/
void createRandomAddress()
{
  unsigned int rand, rand2;
  do
  {
    // first byte can not be 0x00 of 0xFF
    rand = TI_getRandomIntegerFromVLO();
  } while( (rand & 0xFF00)==0xFF00 || (rand & 0xFF00)==0x0000 );
  rand2 = TI_getRandomIntegerFromVLO();

  BCSCTL1 = CALBC1_1MHZ;                    // Set DCO to 1MHz
  DCOCTL = CALDCO_1MHZ;
  FCTL2 = FWKEY + FSSEL0 + FN1;             // MCLK/3 for Flash Timing Generator
  FCTL3 = FWKEY + LOCKA;                    // Clear LOCK & LOCKA bits
  FCTL1 = FWKEY + WRT;                      // Set WRT bit for write operation
```

```
  Flash_Addr[0]=(rand>>8) & 0xFF;
  Flash_Addr[1]=rand & 0xFF;
  Flash_Addr[2]=(rand2>>8) & 0xFF;
  Flash_Addr[3]=rand2 & 0xFF;

  FCTL1 = FWKEY;                            // Clear WRT bit
  FCTL3 = FWKEY + LOCKA + LOCK;             // Set LOCK & LOCKA bit
}

/*-------------------------------------------------------------------------
*
-------------------------------------------------------------------------*/
void transmitData(int addr, signed char rssi,  char msg[MESSAGE_LENGTH] )
{
  char addrString[4];
  char rssiString[3];
  volatile signed int rssi_int;

  addrString[0] = '0';
  addrString[1] = '0';
  addrString[2] = '0'+(((addr+1)/10)%10);
  addrString[3] = '0'+((addr+1)%10);
  rssi_int = (signed int) rssi;
  rssi_int = rssi_int+128;
  rssi_int = (rssi_int*100)/256;
  rssiString[0] = '0'+(rssi_int%10);
  rssiString[1] = '0'+((rssi_int/10)%10);
  rssiString[2] = '0'+((rssi_int/100)%10);

  transmitDataString( addrString, rssiString, msg );
}

/*-------------------------------------------------------------------------
*
-------------------------------------------------------------------------*/
void transmitDataString(char addr[4],char rssi[3], char msg[MESSAGE_LENGTH] )
{
  char output[]={"\r\n3210,3210,3210"};
  int data1,data2,data3,temp;
  char out[4];

  data1= msg[0] + (msg[1]<<8);
  data2= msg[2] + (msg[3]<<8);
  data3= msg[4] + (msg[5]<<8);

  temp=(data1/1000);
  out[3]='0'+temp;
  data1=data1-(temp*1000);
  temp=(data1/100);
  out[2]='0'+temp;
  data1=data1-(temp*100);
  temp=(data1/10);
  out[1]='0'+temp;
  out[0]='0'+(data1-(temp*10));

  output[2]=out[3];
  output[3]=out[2];
  output[4]=out[1];
  output[5]=out[0];

  temp=(data2/1000);
  out[3]='0'+temp;
  data2=data2-(temp*1000);
  temp=(data2/100);
  out[2]='0'+temp;
  data2=data2-(temp*100);
```

```
  temp=(data2/10);
  out[1]='0'+temp;
  out[0]='0'+(data2-(temp*10));

  output[7]=out[3];
  output[8]=out[2];
  output[9]=out[1];
  output[10]=out[0];

  temp=(data3/1000);
  out[3]='0'+temp;
  data3=data3-(temp*1000);
  temp=(data3/100);
  out[2]='0'+temp;
  data3=data3-(temp*100);
  temp=(data3/10);
  out[1]='0'+temp;
  out[0]='0'+(data3-(temp*10));

  output[12]=out[3];
  output[13]=out[2];
  output[14]=out[1];
  output[15]=out[0];

  TXString(output, sizeof output);
}

/*------------------------------------------------------------------------------
*
------------------------------------------------------------------------------*/
void TXString( char* string, int length )
{
  int pointer;
  for( pointer = 0; pointer < length; pointer++)
  {
    volatile int i;
    UCA0TXBUF = string[pointer];
    while (!(IFG2&UCA0TXIFG));              // USCI_A0 TX buffer ready?
  }
}
/*------------------------------------------------------------------------------
*
------------------------------------------------------------------------------*/
void MCU_Init()
{
  BCSCTL1 = CALBC1_8MHZ;                    // Set DCO
  DCOCTL = CALDCO_8MHZ;

  BCSCTL3 |= LFXT1S_2;                      // LFXT1 = VLO
  TACCTL0 = CCIE;                           // TACCR0 interrupt enabled
  TACCR0 = 12000;                           // ~ 1 second
  TACTL = TASSEL_1 + MC_1;                  // ACLK, upmode.
  P3SEL |= 0x30;                            // P3.4,5 = USCI_A0 TXD/RXD
  UCA0CTL1 = UCSSEL_2;                      // SMCLK
  UCA0BR0 = 0x41;                           // 9600 from 8Mhz
  UCA0BR1 = 0x3;
  UCA0MCTL = UCBRS_2;
  UCA0CTL1 &= ~UCSWRST;                     // **Initialize USCI state machine**
  IE2 |= UCA0RXIE;                          // Enable USCI_A0 RX interrupt
  __enable_interrupt();
}

/*------------------------------------------------------------------------------
* Runs in ISR context. Reading the frame should be done in the
* application thread not in the ISR thread.
------------------------------------------------------------------------------*/
```

```
static uint8_t sCB(linkID_t lid)
{
  if (lid)
  {
    sPeerFrameSem++;
  }
  else
  {
    sJoinSem++;
  }
  // leave frame to be read by application.
  return 0;
}

/*-------------------------------------------------------------------------
* ADC10 interrupt service routine
-------------------------------------------------------------------------*/
#pragma vector=ADC10_VECTOR
__interrupt void ADC10_ISR(void)
{
  __bic_SR_register_on_exit(CPUOFF);        // Clear CPUOFF bit from 0(SR)
}

/*-------------------------------------------------------------------------
* Timer A0 interrupt service routine
-------------------------------------------------------------------------*/
#pragma vector=TIMERA0_VECTOR
__interrupt void Timer_A (void)
{
  sSelfMeasureSem = 1;
}

/*-------------------------------------------------------------------------
* USCIA interrupt service routine
-------------------------------------------------------------------------*/
#pragma vector=USCIAB0RX_VECTOR
__interrupt void USCI0RX_ISR(void)
{
  char rx = UCA0RXBUF;
  if ( rx == 'V' || rx == 'v' )
  {
    verboseMode = 1;
  }
  else if ( rx == 'M' || rx == 'm' )
  {
    verboseMode = 0;
  }
  else if ( rx == 'F' || rx == 'f' )
  {
    degCMode = 0;
  }
  else if ( rx == 'C' || rx == 'c' )
  {
    degCMode = 1;
  }
}
```

REFERENCES

1. Raghavan, Karthik. *A real-time approach towards in vivo phase measurements for the determination of volume in the murine heart*. Master's Thesis, University of Texas at Austin. Dec 2004.

2. Wei, C. L., Valvano J.W., Feldman, M., and Pearce, J. A., *Nonlinear conductance – volume relationship for murine conductance catheter measurement system*, IEEE Transactions in Biomedical Engineering, Vol. 52, No. 10, Pages 1654 – 1661, Oct 2005.

3. Rosamond, W., Flegal, K., Friday, G., Furie, K., *et al*., for the American Heart Association Statistics Committee and Stroke Statistics Subcommittee, *Heart Disease and Stroke Statistics-2007 Update: A Report From the American Heart Association Statistics Committee and Stroke Statistics Subcommittee*. Circulation. 115:E69-E171, Feb 2007.

4. Fuster, V., Alexander R. W., O' Rourke R. A., *et al*., "*Hurst's The Heart*", 11th Edition, The McGraw – Hill Companies Inc., Chapters 24 and 25.

5. Uemura, K., Kawada, T., Sugimachi, M., Zheng, C., Kashihara, K., Sato, T., and Sunagawa, K., *A self-calibrating telemetry system for measurement of ventricular pressure-volume relations in conscious, freely moving rats*. Am J Physiol Heart Circ Physiol, 287(6):H2906–H2913, Dec 2004.

6. Raghavan, K., Porterfield, J. E., Kottam A. T. G., Feldman, M. D., Escobedo, D., Valvano, J, W., and Pearce, J. A., *Electrical conductivity and permittivity of murine myocardium*. IEEE Trans Biomed Eng, (Accepted, In Press), 2009.

7. Porterfield, J. E., Kottam A. T. G., Raghavan, K., Escobedo, D., Trevino, R. J., Valvano, J. W., Pearce, J. A., and Feldman, M. D., *Dynamic correction of parallel conductance, Gp, and gain factor, α, in invasive murine left ventricular volume measurements*., Jour. Of Applied Phys., Submitted for review.

8. Baan, J., Van der Velde, E. T., Kerkof, P., *et al*., *Continuous stroke volume and cardiac output from intraventricular dimensions obtained with impedance catheter*., Cardiovasc. Res. vol. 15, pp. 320-334, 1981.

9. Sagawa, K., Maughan, W. L., Suga, H., and Sunagawa, K., *Cardiac Contraction and the Pressure-Volume Relationship*. New York: Oxford University Press, 1988.

10. Esposito, G., Santana, L. F., Dilly, K., Santos Cruz, J. D., Mao, L., Lederer, W. J., and Rockman, H. A., *Cellular and functional defects in a mouse model of heart failure,* Am J Physiol: Heart Circ Physiol vol. 279, pp. H3101-H3112, 2000.

11. Franco, F., Dubois, S., Peschock, R. M., and Shohet, R.V., *Magnetic resonance imaging accurately estimates LV mass in a transgenic mouse model of cardiac hypertrophy*, Am J Physiol: Heart Circ Physiol vol. 274, pp. H679-H683, 1998.

12. Franco, F., Thomas, G. D., Giror, B., Bryant, D., Bullock, M. C., Chwialkowski, M. C., Victor, R. G., and Peschock, R. M., *Magnetic resonance imaging and invasive evaluation of development of heart failure in transgenic mice with myocardial expression of tumor necrosis factor-α*, Circulation vol. 99, pp. 449-454, 1999.

13. Feldman, M. D., Erikson, J. M., Mao, Y., Korcarz, C. E., Lang, R. M., and Freeman, G. L., *Validation of a mouse conductance system to determine LV volume: comparison to echocardiography and crystals*, Am J Physiol: Heart Circ Physiol vol. 274, pp. H1698-H1707, 2000.

14. Baan, J., Van der Velde, E. T., Kerkof, P., *et al*., *Continuous stroke volume and cardiac output from intraventricular dimensions obtained with impedance catheter*., Cardiovasc. Res. vol. 15, pp. 320-334, 1981.

15. Georgakopoulos, G., Mitzner, W. A., Chen, C. H., Byrne, B. J., Millar, H. D., Hare, J. M., and Kass, D. A., *In vivo murine left ventricular pressure-volume relations by miniaturized conductance micromanometry*, Am J Physiol: Heart Circ Physiol vol. 274, pp. H1416-H1422, 1998.

16. Yang, B., Beishchel, J., Larson, D. F., Kelley, R., Shi, J., and Watson, R. R., *Validation of conductance catheter system for quantification of murine pressure-volume loops*, J. of Investigative Surgery vol. 14, pp. 341-355, 2001.

17. Lankford, E. B., Kass, D. A., Maughan, W. L., *et al*., *Does volume catheter parallel conductance vary during a cardiac cycle?*, Am J Physiol: Heart Circ Physiol vol. 258, pp. H1933-H1942, 1990.

18. White, P. A., Brooks, C. I. O., Ravn, H. B., Stenbøg, E. E., Christensen, T. D., Chaturvedi, R. R., Sorensen, K., Hjortdal, V. E., Redington, A. N., *The effect of changing excitation frequency on parallel conductance in different sized hearts*, Cardiovascular Research vol. 38, pp. 668-675, 1998.

19. Gawne, T. J., Gray, K. S., and Goldstein, R. E., *Estimated left ventricular offset volume using dual-frequency conductance technology*, J. of Applied Physiology vol. 63, pp. 872-876, 1987.

20. Georgakopoulos, D., and Kass, D. A., *Estimation of parallel conductance by dual-frequency conductance catheter in mice*, Am J Physiol: Heart Circ Physiol vol. 279, pp. H443-H450, 2000.

21. Gabriel, S., Lau, R. W., and Gabriel, C., *The dielectric properties of biological tissues: II. Measurements in the frequency range 10 Hz to 20 GHz*, Physics in Medicine and Biology vol. 41, no. 11, pp. 2251-69, 1996.

22. Gabriel, S., Lau, R. W., and Gabriel, C., *The dielectric properties of biological tissues: III. Parametric models for the dielectric spectrum of tissues*, Physics in Medicine and Biology, vol. 41, no. 11, pp. 2271-93, 1996.

23. Steendijk, P., Mur, G., Van der Velde, E., and Baan, J., *The four-electrode resistivity technique in anisotropic media: theoretical analysis and application on myocardial tissue in vivo*, IEEE Trans Biomed Engr., vol. 40, no. 11, pp. 1138-1148, 1993.

24. Rush, S., Abildskov, J. A., and McFee, R., *Resistivity of body tissues at low frequencies*, Circulation Research, vol. 12, pp. 40-50, 1963.

25. Schwan, H. P., and Kay, C. F., *Specific resistance of body tissues*, Circulation Research, vol. 4, pp. 664-670, 1956.

26. Sperelakis, N., and Sfyris, G., *Impedance analysis applicable to cardiac muscle and smooth muscle bundles*, IEEE Trans Biomed Engr. vol. 38, no. 10, pp. 1010-1022, 1991.

27. Steendijk, P., Van der Velde, E., Bann, J., *Dependence of anisotropic myocardial electrical resistivity on cardiac phase and excitation frequency*, Basic Research in Cardiology vol. 89, pp. 411-426, 1994.

28. Tsai, J. Z., Will, J. A., Hubard-van Stelle, S., Cao, H., Tungjitkusolmun, S., Choy, Y. B., Haemmerich, D., Vorperian, V. R and Webster, J. G., *In vivo measurement of swine myocardial resistivity*, IEEE Trans. Biomed. Engr., vol. 49, no. 5, pp. 472-483, 2002.

29. Tsai, J. Z., Will, J. A., Hubard-van Stelle, S., Cao, H., Tungjitkusolmun, S., Choy, Y. B., Haemmerich, D., Vorperian, V. R and Webster, J. G., *Error analysis of tissue resistivity measurement*, IEEE Trans. Biomed. Engr., vol. 49, no. 5, pp. 484-494, 2002.

30. Edic, P. M., Saulnier, G. J., Newell J. C., and Isaacson, D., *A real-time electrical impedance tomography*, IEEE Trans. Biomed. Engr. vol. 42, no. 9, pp. 849-859, 1995.

31. Borcea, L., *Electrical impedance tomography*, Inverse Problems vol. 18, R99-R136, 2002.

32. Reyes, M., Steinhelper, M., Alvarez, J., Escobedo, D., Pearce, J. A., Valvano, J. W., Pollock, B., Wei, C, L., Kottam, A. T. G., Altman, D., Lee, S., Bailey, S.,

Thomsen, S. L., Freeman, G., and Feldman, M. D., *Impact of physiologic variables and genetic background on myocardial frequency-resistivity relations in the intact beating murine heart*, Am J Physiol: Heart Circ Physiol 2006 Oct;291(4):H1659-69.

33. Kottam, A., and Pearce, J., *Electric field penetration depth of myocardial surface catheters and the measurement of myocardial resistivity*, Biomed Sci Instrum. 40:155-160, 2004.

34. Kottam, A., *Determination of parasitic circuit elements in cardiac conductance catheters*, M. S. thesis, Dept. Biomed. Eng., The University of Texas at Austin, Austin, TX, 2003

35. Raghavan, K., *A real – time approach towards in vivo phase measurements for the determination of volume in the murine heart*, M. S. thesis, Dept. Elec. and Comp. Eng., The University of Texas at Austin, Austin, TX, 2004.

36. Raghavan, K., Wei, C. L., Kottam, A., Altman, D. G., Fernandez, D. J., Reyes, M., Valvano, J. W., Feldman, M. D., and Pearce, J. A., *Design of instrumentation and data-acquisition system for complex admittance measurement*, Biomed Sci Instrum. 2004;40:453-7.

37. Kottam, A., *Measurement of Electrical Admittance to Study the Onset and Progression of Myocardial Ischemia*, Ph. D. dissertation, Dept. Biomed. Eng., The University of Texas at Austin, Austin, TX, 2007.

38. Streeter, D. D., Spotnitz, S. M., Patel, D. P., Ross Jr., J., and Sonnenblick, E. H., *Fiber orientation in the canine left ventricle during diastole and systole*, Circ. Res. 24: 339-347, 1969.

39. Streeter D. D., and Hanna, W. T., *Engineering mechanics for successive states in canine left ventricular myocardium*, Circ. Res. 33: 656-664, 1973.

40. Salazar, Y., Bragos, R., Casas, O., Cinca, J., and Rosell, J., *Transmural versus nontransmural in situ electrical impedance spectrum for healthy, ischemic, and healed myocardium*, IEEE Trans. on Biomed. Engr., vol. 51, no. 8, pp. 1421 – 1427, Aug 2004.

41. Epstein, R., and Foster, K. R., *Anisotropy in the dielectric properties of skeletal muscle*, Med. & Biol. Eng. & Comput. 21: 51-55, Jan 1983.

42. Wei, C. L., Valvano, J. W., Feldman, M. D., Nahrendorf, M., Peshock, R., and Pearce, J. A., *Volume Catheter Parallel Conductance Varies Between End-Systole and End-Diastole*, IEEE Trans. on Biomed. Engr., vol. 54, no. 8, pp. 1480 – 1489, Aug 2007

43. Holberg, D. R, and Allen P. E., "*CMOS Analog Circuit Design*", 2nd Edition, Oxford University Press Inc., 2002

44. Johns, D. A., and Martin, K., "*Analog Integrated Circuit Design*", John Wiley & Sons Inc., 1997

Vita

Karthik Raghavan was born in Chennai, India on the 9th of May, 1981. He is the son of Mr. Raghavan Venkataraman and Mrs. Hema Raghavan. He completed his higher secondary education at Padma Seshadri Bala Bhavan Senior Secondary School, Chennai, India. Following this, he obtained a bachelors degree in electronics and instrumentation engineering from the Birla Institute of Technology and Science in Pilani, India in June, 2002. After this, he entered the graduate school at the University of Texas at Austin, Austin, TX in the Spring of 2003, where he received his master's degree in 2004 and doctoral degree in 2009.

Permanent address: 48 Flatfield Terrace
Scarborough, ON
M1B6C4
Canada

This dissertation was typed by Karthik Raghavan.